MANIPULATION OF THE HOST CELL CYCLE: HOW *TOXOPLASMA GONDII* FORCES HOST GENOME REPLICATION

by

EDWIN PIERRE LOUIS

(Under the Direction of Ronald Drew Etheridge)

ABSTRACT

Parasites of the genera *Plasmodium and Toxoplasma* represent a substantial source of often-deadly global human parasitic infections. *Toxoplasma gondii* infects over two billion people worldwide, resulting in life-long chronic infection, and has a profound impact on host health, and disease manifests primarily in immunocompromised individuals. An exceptional and important aspect of this protozoan is its widespread ability to infect any nucleated warmed-blooded animal. The life cycle of the parasite in a host causes rounds of host cell lysis, resulting in tissue damage. Sequential discharge of micronemes, rhoptries and dense granules, which form a unique triad of secretory endomembranes, contributes to the extraordinarily success of this parasite to invade and propagate within its infected cells. Upon and after cell invasion, *Toxoplasma* releases a myriad of host modulating effectors to promote its survival and dissemination. Of the many host-manipulating proteins, the dense granules effectors (GRAs) are responsible for structural modification of the parasitophorous vacuole in which the parasite develops within the cell. Several GRAs have also been identified as controlling multiple host cell biological processes, including manipulation of signaling events, alteration of host transcription, apoptosis, immune function, and the cell cycle program. This dissertation explores how *Toxoplasma* manipulates the host cell cycle to force its genome replication. We characterized a GRA effector HCE1 by determining its role in

the induction of the host cell cycle via the upregulation of cyclin E to stimulate G1/S-phase transition and reveal a block in S-phase progression and DNA synthesis in the host. Moreover, we demonstrated that this S-phase block was dependent on the host cell. Notably, we illustrated that removal of host cell contact inhibition promotes DNA synthesis and this S-phase block was dependent on the host cell background. These data offer the first evidence of a *Toxoplasma* effector capable of modulating host cell cycle phases and answers a long-standing question in the field of *Toxoplasma* biology with regards to manipulating its infected host. This dissertation also examines other aspects of *Toxoplasma* biology, including our investigation into the roles of Secretory Effector Binding protein 1 (SEB1), an essential Golgi-resident protein, in parasite survival and replication.

INDEX WORDS: *Toxoplasma gondii*, host cell cycle, Cyclin E, FUCCI, S-phase, HCE1/TEEGR, host-parasite interaction, parasite effectors, dense granules, parasite Golgi apparatus, lytic cycle and parasite replication.

MANIPULATION OF THE HOST CELL CYCLE: HOW *TOXOPLASMA GONDII* FORCES HOST GENOME REPLICATION

by

EDWIN PIERRE LOUIS

B.S., The University of Florida, 2014

A Dissertation Submitted to the Graduate Faculty of The University of Georgia in Partial Fulfillment of the Requirements for the Degree

DOCTOR OF PHILOSOPHY

ATHENS, GEORGIA

2022

MANIPULATION OF THE HOST CELL CYCLE: HOW *TOXOPLASMA GONDII* FORCES HOST GENOME REPLICATION

by

EDWIN PIERRE LOUIS

Major Professor:	Ronald Drew Etheridge
Committee:	Dennis Kyle
	Sylvia N. J. Moreno
	Christopher M. West

Electronic Version Approved:

Ron Walcott
Vice Provost for Graduate Education and Dean of the Graduate School
The University of Georgia
May 2022

DEDICATION

To my wife:

I dedicate this work to my beloved wife Alexandria Pierre Louis.

To my family and friends for their endless love, support and inspiration:

Jean Renel Pierre Louis, Mencie Thomas, Edna Pierre Louis, Luis Candelario, Maria Candelario, Ann Shelly Pierre Louis, Ridge Pierre Louis, Rousseau Charles, Bedeline Charles, Christina Mayah Deravil, Medgina Armand, Evens Dorcelus Pierre, Diderot Pierre Louis, Yveto Thomas, Johnsky Oveny, Brehemy Pierre, Georgy-Nior E. Daccarett, Herve Bruneus, Grebert Estime, Michelle A. Monthervil, Rose Codada, Josias Ouedraogo, Steve Noutong.

ACKNOWLEDGEMENTS

I am beyond thrilled with all the work we did along with all the mentorship and support that I have received from many individuals. I want to start by thanking Dr. Ronald Drew Etheridge for serving as my primary advisor, accepting me as his first graduate student, guiding me throughout this process and inspiring me in many ways and on many occasions. His enthusiasm for science and discernment regarding life as a whole were what attracted me to his lab; which has been evident and well reflected throughout his mentorship. The work presented in this dissertation would not have been possible without his trust and his upkeep to ensure my professional growth. His patience is incredibly enthralling to stand by me over the past five years through all my ups and downs. I am honored to have accomplished this work under his supervision.

I also extend my sincere gratitude to my thesis committee members Dr. Silvia Moreno, Dr. Dennis Kyle and Dr. Christopher West for their guidance, expertise, input and comments. They have been extraordinarily supportive to my professional growth and my career aspiration(s).

I would like to thank Menna Etheridge for her joyous, hospitable and wonderful personality to make my time in the lab an undeniably wonderful experience. I admire her kind heart, her mentorship, her training, her help with my projects. She has impeccable organizational skills that she constantly reflects to make the lab overall a highly efficient environment. She also has the eyes of an artist. I greatly appreciate Dr. Nathan Chasen for always being there to provide numerous amounts of feedback on my projects and discussing multiple projects in the lab. Nathan is very curious, enthusiastic and is very good with his hands. He loves building and using a variety of 3D

printed gadgets while wrapping his head around new technologies. I would also like to thank Dr. Justin Wiedeman for his help, support and astute advice.

In addition, I thank our collaborators Dr. Rodrigo Baptista and Dr. Asis Khan for their contributions in my first manuscript. I would like to thank Kimberly Esther Oliva in Kimberly Klonowski lab for helping me with some mice work, and I am extremely grateful for her friendship. Hug e thanks to the members of Moreno and Docampo labs, especially to my great friends Stephen Vella, Beejan Asady, Sabrina E. Cline and Abigail Calixto, for all the help and encouragement through the graduate school life. Last but not least, I thank all the members of the CTEGD for making the center an inspiring and hospitable scientific community to work. A huge thank you to Dr. Steven Maher for his help and sage advice throughout the last few years. Notably, I would like to thank Dr. Muthugapatti Kandasamy and Mrs. Julie Nelson for their help with microscopy and flow cytometry, respectively. A special word of appreciation and thanks to Dr. Vassant Muralidharan who has been an inspiring scientist to me. He has been very hospitable, ready to listen as his answers always soothed one's mind.

With utmost reverence, this journey really started a year prior to entering graduate school with the trust of Julie Moore who believed in me and granted me the opportunity to join the post-baccalaureate program at University of Georgia Athens (UGA). My sincerest thanks to Julie Moore and Julie Range. Many glorious thanks to Dr. Michael Terns for sparking my curiosity for pathogens biology. Yunzhou Wei deserves a special note of gratitude for being my first mentor during my time in the Terns lab and has prepared me to embark the graduate school chapter. He helped me throughout the entire process and was always there for me.

I am immensely fortunate to have my wife, Alexandria Pierre Louis, who has stood by me throughout this journey. I am thankful for her endless support, patience, calmness and love,

without her this experience would have been lonely and miserable. A very special note of gratitude for my dog Maximus Pierre Louis (I love you buddy). Finally, I would like to complete this note of gratitude to express my heartfelt thanks and love to my parents, my siblings and the rest of my family members and friends who have supported and helped me be the man I turn out to be today inside and outside of the lab.

TABLE OF CONTENTS

Page

LIST OF TABLES

Page

LIST OF FIGURES

Page

CHAPTER 1

LITERATURE REVIEW OF *TOXOPLASMA GONDII*

INTRODUCTION

Toxoplasma gondii is an obligate intracellular parasite found in a wide range of hosts. This pathogen is able to infect almost any nucleated cell in warm-blooded animals and is considered one of the most successful protozoan parasites [1, 2]. This single-cell eukaryote belongs to the apicomplexan phylum which comprises several protozoan parasites contributing to significant global health burden in humans and livestock. Common examples of apicomplexan species of medical importance include *Plasmodium spp.,* which causes malaria, *Cryptosporidium spp.*, which causes waterborne diarrhea; and *Babesia spp.* and *Eimeria spp.*, which cause babesiosis in cattle and coccidiosis in poultry, respectively. It is reported that *Toxoplasma gondii,* a predominantly opportunistic coccidia pathogen, infects approximately one-third of the world's human population and carries with it the potential to cause severe disease [3]. Although death is uncommon in healthy infected individuals, immunocompromised patients are at risk of greater morbidity and mortality. Among the apicomplexans, *Toxoplasma gondii* has been the model parasite to be studied for its exceptional importance as a causative agent of a zoonosis; however, many aspects of its biology still remain relatively unclear. An understanding of the biology of *Toxoplasma gondii* will help contribute to the development of efficient therapies to combat the global infection of toxoplasmosis as well as provide insight into the biological mechanisms of related Apicomplexan parasites.

Toxoplasma was first identified in 1908 by Charles Nicolle and Louis Manceaux at the Pasteur Institute in Tunis. It was isolated in the tissues of the rodent *Ctenodactylus gundi*, in use as an animal model to study leishmaniasis, leading to the incorrect conclusion their isolate was a *Leishmania* species [4]. Concomitantly, the same organism was identified in Brazil by Alfonso Splendore in rabbits [5]. It was soon recognized to be a new parasite and was named based on its morphology *Toxoplasma* (Toxo=arc or Toxon 'from Greek'=bow and plasma=life) and its host in which it was discovered (*Ctenodactylus gundi=gondii*, an incorrect naming of the species), hence deriving the name *Toxoplasma gondii* (Its correct name would have been *Toxoplasma gundi* for the identification of the host *C. gundi*). For over a century, *Toxoplasma* research has experienced a splendid and immense period of growth in the field of apicomplexans. Its extraordinary ability to successfully infect virtually any nucleated cell and warm-blooded animal has been attributed to "reprogramming" the infected host by manipulating a myriad of cellular biological pathways. This, parasite also serves as an excellent model organism for the study of other medically-important parasites within this phylum, such as *Plasmodium spp*. and *Cryptosporidium spp.* In addition, *Toxoplasma* represents a public health and welfare issue for its hosts, which should not be underestimated. This thesis explores how *Toxoplasma* manipulates the host cell cycle to force the replication of its genome. Specifically, this research investigates the role of a secreted *T. gondii* host-nuclear-targeted protein that modulates the infected host cell cycle for its advantage. We also probed the effect of the loss of a new Golgi apparatus-resident protein of *Toxoplasma* on the parasite's development cycle and how its loss affects the parasite's endomembranes.

1.1. TOXOPLASMOSIS: PREVALENCE IN HUMANS

Toxoplasmosis, the disease caused by *Toxoplasma* within its intermediate and accidental hosts, is of great veterinary and medical importance, and yet this parasite is highly prevalent in most areas of the world. Many infected hosts show a balanced and near-commensal relationship with the parasite, often leading to a complete co-existence with the parasite and a lifelong infection [6]. The first biological and immunological evidence of *T. gondii* infection in humans was described in the late 1930s in several samples from animals and from an encephalopathic human infant who passed away shortly after birth [7, 8]. An additional human infection was also reported in the early 1940s [9]. A famous example of this was a 6-year-old boy in the US (Cincinnati, Ohio) whose brain tissue was homogenized and was used to inoculate mice. Parasites were later isolated from these mice by Albert B. Sabin who named *T. gondii* strain 'RH' after the initials of the 6 year old child [9]. This strain, commonly referred as Type I, became the most common strain used within research laboratories. Type II and Type III are two additional clonal lineages, which have emerged from a minor genetic polymorphism [10-12]. Together, as these types are the most globally prevalent strains, they are also the three most predominant lab strains of *T. gondii*. They vary in their virulence in mice and humans, with the highest observed in the Type I and the lowest in the Types II and III [13, 14]. They also differ in their growth rate and how frequently they convert into bradyzoites/tissue cyst. The regularly used Type I strain has a faster replicative rate and a low conversion rate to bradyzoites form than the Types II and III [15] .

In humans, the global frequency of *Toxoplasma* infection ranges between 30-50% [15-17]. A substantial geographical variation of the prevalence is reported to be as low as 10% seroprevalence in some areas and as high as 95% in others [18-22]. Severally highly variable factors, such as climate, socio-economic status, and dietary habits can be used as reasonable factors

explaining this uneven geographical distribution. For instance, while the prevalence of toxoplasmosis in Northern Europe and South East Asia is low, it is reported to be extremely high in other countries [18-20] (e.g. France, Argentina, Brazil, Cameroon, Gabon and Togo) [18, 21, 22]. However, the United States is reported to possess an approximate 15% seroprevalence [20]. In immunocompetent hosts, *T. gondii* infection may be mild or asymptomatic, while infection in immune-compromised or suppressed hosts (e.g. HIV patients) can become fulminant, causing severe disease, including ocular toxoplasmosis, seizures, and cognitive dysfunction, or death. A common example of *T. gondii* as an important opportunistic pathogen is often displayed in AIDS patients, of which up to 40% can suffer from severe encephalitis [23]. Another mode of infection is congenital transmission which can cause potentially fatal cerebral toxoplasmosis (e.g. encephalitis) in the fetuses of pregnant women resulting in developmental delays, blindness, epilepsy and even pregnancy loss [16]. In sum, toxoplasmosis remains one of the most common global parasitic zoonosis, albeit with clear clinical manifestation mainly restrained to high-risk individuals.

1.2. TOXOPLASMOSIS: DIAGNOSIS AND TREATMENT

Multiple methods have been used to diagnose *Toxoplasma* infection. The first successful diagnostic assay was the Sabin-Feldman dye test (a serologic test) that was established in 1948 by Albert Sabin and Harry Feldman [24]. Other methods for detection of *T. gondii* infection include polymerase chain reaction (PCR), histological examinations using immunoperoxidase staining, antigen detection in body fluids, antigen specific-lymphocyte transformation assays, skin tests and serologic tests [25, 26]. Additional strategies for detection of *T. gondii* infection in humans include

enzyme linked immune sorbent assay (ELISA), indirect hemagglutination assay (IHA) Western Blotting, and detection of specific immunoglubulins such as IgA, IgE, IgG, and IgM [18, 27].

Thus far, drug therapy and chemotherapy are the only treatments undertaken to combat toxoplasmosis. The arsenal of drugs available for treatment include compounds such as pyrimethamine, sulfadiazine, leucovorin, clindamycin (cleocin), and spiramycin. These compounds control acute infection and are often recommended to be administered in combination based upon the condition of the patients. These treatments are indicated for use in HIV/AIDS patients, pregnant woman, and individuals with cerebral or ocular toxoplasmosis [28-34]. With the discovery of effective drug treatments for HIV patients, the incidence of toxoplasmic encephalitis, which is the most common disease manifested in these individuals, has declined significantly as reported in the early 2000s [35]. Depending on the time of infection, congenital toxoplasmosis is treated with spiramycin and an alternating regimen of pyrimethamine, sulfadiazine and folic acid. For instance, during the first trimester, a pregnant woman is usually prescribed spiramycin to avoid teratogenic risks in the fetus as this drug is unable to cross the placental barrier. Then, either pyrimethamine alone or a combination of pyrimethamine, sulfadiazine, and folic acid are recommended at the time of pregnancy [36]. Unfortunately, the current antiparasitic treatment regimens cause undesirable and often extreme toxic side effects in immunocompromised hosts and human vaccines are not available [28]. Likewise, reactivation of a dormant tissue infection is the main cause for toxoplasmosis in individuals with hematopoietic stem cell, bone marrow, and liver transplants, cancer patients, and HIV-infected patients because of immuno-suppressive treatment [37]. Most of these drugs target the tachyzoite form of the parasite and do not kill bradyzoites. Hence, tremendous effort to find therapies with more specific, and multiple, modes of action are

needed to improve toxoplasmosis treatment, prevention, and control in humans as well as veterinary applications.

1.3. LIFE CYCLE OF *TOXOPLASMA GONDII* & MODES OF TRANSMISSION

Toxoplasma gondii features a complex life cycle involving multiple hosts as well as sexual and asexual stages. Felines are the "definitive host" of *T. gondii,* or the host where it undergoes sexual replication. The parasite also replicates asexually in all warm-blooded animals which serve as intermediate hosts, while humans are considered to be zoonotic hosts [38, 39]. After feline ingestion of prey harboring *T. gondii*-containing cysts, the cysts rupture, releasing bradyzoites which subsequently invade and infect the feline intestinal epithelium. Bradyzoites then undergo a process called schizogony within enterocytes followed by gametogony, leading to female and male gametes, which fuse to form a zygote [18]. Notably, the majority of felines only shed oocysts during their first infection, although it is possible for them to re-shed in the environment [40-42]. Infected hosts become lifelong carriers. The pathogen is transmitted in the environment through the release of oocysts from felines and that, in turn, are taken up by other animals through contaminated food or water; in the other hand, tissues cysts are transmitted via scavenging, carnivorism and cannibalism (Figure 1.1) [43]. However, examples of three main modes of transmission in humans that are often depicted in the literature are congenital/vertical transmission, ingestion of tissue cysts, and ingestion of oocysts [23]. Most humans become infected inadvertently via ingestion of oocysts that are released in the feces from infected felines via contaminated food and water, and also via the consumption of contaminated tissue cyst from raw or undercooked food [1, 44-46]. Individuals can also become infected via vertical transmission from an infected mother to her fetus (Figure 1.1), during organ transplantation from a donor organ

or blood transfusion harboring parasites, a puncture wound from a contaminated needle, syringe or a knife (e.g., a butcher's knife, and laboratory accidents) [28, 37, 47-49]. Additionally, many other means of *T. gondii* detection have been reported and this includes detection of the parasite within the semen of humans and milk of infected animals which is a potential risk of infection if consumed in its unpasteurized state [50]. As a result, human infection with toxoplasma is frequent: this ubiquitous pathogen infects approximately one-third of the world's population [3, 15].

During acute infection of a host, the rapidly dividing tachyzoite form of *T. gondii* undergoes asexual replication [51]. In the event parasites are not cleared by the immune system after approximately 10 days, the tachyzoite form undergoes a stage differentiation into a slowly-growing bradyzoite form which has the ability to persist as a semi-dormant stage within the host [52-54]**.** These bradyzoites form tissue cysts in various organs, but most commonly in the eye, muscles, and central nervous system (CNS) [38]. Although the parasite displays a remarkable ability to invade a wide spectrum of cell types and tissues, the CNS is a prime place where its role has been suggested to be manipulative and important for the parasite life cycle. This was demonstrated in a study where *T. gondii*-infected rats appear to be attracted to the odor of cat urine, showcasing the parasite manipulating the behavior of infected rodents to cats, which are their natural predators [55-60]. That way, parasites can eventually be taken up by the definitive host to complete the life cycle. Other reports suggest that mate choice with potential venereal transmission is also possible where infected male rats are found to be more attractive to uninfected female rats, thereof displaying *T. gondii's* chances to transmit to its mammalian hosts [58, 59, 61]. Thus, it is no surprise that *Toxoplasma gondii* life cycle is habitually described as "complex" (Figure 1.1). In fact, its reproductive cycle relies on three specialized secretory organelles known as micronemes, rhoptries and dense granules that sequentially discharge an array of proteins to eventually assure

its survival, propagation, perturbation and dissemination within the infected host. This aspect will be further discussed in section the following section (1.4).

1.4. THE ROLE OF THREE SECRETORY VESICLES (MICRONEMES, RHOPTRIES AND DENSE GRANULES) AND THEIR EFFECTORS IN MODULATING THE HOST CELL.

Significant knowledge has been made available describing the three infectious forms of *T. gondii* during its life cycle. As previously described, this includes tachyzoites, which undergo rapid asexual division, bradyzoites, which divide slowly and can form cysts and enter a dormant stage, and finally, sporozoites, which are derived from sporulated oocysts within the feces of felines. The ingestion of oocysts via contaminated water or food by any warm-blooded animal including livestock and humans leads to the asexual phase of the parasite life cycle. This pathogen perpetuates its life cycle between an intermediate host (e.g. rodents) or an accidental host (e.g. human) where the asexual cycle occurs, and a definitive host (e.g. feline) where the sexual forms of the parasite are found, and mating occurs (Figure 1.1). Following ingestion of oocysts by intermediate and accidental hosts, acute infection is thought to mainly involve the replication of tachyzoites. Motility of tachyzoites is critical for finding a host, invading, multiplying inside a porous membranous structure (the parasitophorous vacuole 'PV'), and egressing to infect another host for the continuation of its lytic cycle (Figure 1.2). Multiple subsequent rounds of the *T. gondii* lytic cycle cause significant tissue damage and are the main cause of the pathogenesis associated with toxoplasmosis. Key to the ability of *T. gondii* to establish a successful infection is the coordinated secretion of proteins from three specialized secretory vesicles, termed micronemes, rhoptries and dense granules (DG) (Figure 1.3).

Micronemes

Micronemes are small vesicles located near the apical end of the cell along the cell cortex that contain "MIC" proteins and are discharged first in relation to the other secretory vesicles. Previous kinetic studies report that the secretion of the contents of the micronemes and rhoptries are highly regulated, while DG effectors can be secreted in either a regulated or constitutive manner [38, 39]. Micronemes, in particular, are predominantly important for motility and mediate the adhesion between the parasite and the membranes of the host cells [38, 39]. Secretion from these exocytic organelles is regulated in a calcium-dependent manner [62, 63]. Within a host cell, an increase in cytoplasmic calcium has been linked to tachyzoites egress, which is also associated with the secretion of MIC proteins [64]. It is no surprise for this single-celled eukaryote to employ calcium-regulated secretion, as this is a common among eukaryotes [65]. An interesting and transient feature of this organelle is the remarkable interaction of its secreted MIC proteins and the host cell receptors, which forms a transitory ring-shaped structure, called the "moving junction," which facilitates parasite invasion [66]. MIC8 is another microneme protein that is essential for the formation of the moving junction and, when depleted, inhibits the secretion of RONs [67]. During parasite motility and invasion, the interaction of MICs and host cell receptors form a moving junction that helps the parasite invasion. Parasite utilizes its actin-myosin motor complex that contributes to propelling the pathogen into the host cell [68, 69].

Rhoptries

Rhoptries are discrete secretory vesicles that are also necessary for invasion. A typical tachyzoite contains 6 to 12 of these club-shaped organelles, each measuring about ~2-3 μm long[70, 71]. They harbor two distinct groups of effectors, RON and ROP proteins, that are respectively situated in the apical rhoptry neck and the rhoptry bulb. These effectors are secreted

asynchronously, with RONs being released before ROPs [72, 73]. Contrary to the micronemes, the mechanism of rhoptry discharge remains enigmatic. Moreover, some rhoptries and micronemes proteins are occasionally found to interact with one another. One example of this is the well-described micronemal Apical Membrane Antigen protein 1 (AMA1) that anchors to the RON2 complex which has been inserted by *T. gondii* into the host cytosol and plasma membrane to form the moving junction [74-76]. The moving junction is unable to form in the absence of AMA1, but tachyzoites are still able to secrete RONs [71, 77]. Notably, RON4 was the first documented rhoptry protein associated with the moving junction [78]. Additional experiments showed that the inhibition of parasite motility by the actin microfilament-destabilizing drug Cytochalasin D was unable to block rhoptry discharge, instead causing the formation of some empty proteinaceous vacuoles, termed evacuoles [79]. However, ablation of some microneme proteins, such as AMA1 and MIC8, exhibited a reduction of rhoptry secretion, thereby reiterating parasite attachment is necessary for proper release of rhoptry contents in the host cell [67, 80].

The ROP proteins however, start being secreted inside the host cell shortly after the moving junction is formed. They are mainly involved in parasite invasion, when the parasite wraps itself in the host cell plasma membrane in a corkscrew manner to form the intracellular parasitophorous vacuole which functions as a sieve permitting nutrients and small molecule uptake from the host cytoplasm [81-83]. ROP proteins often depicted to have enzymatic characteristics such as kinases, pseudo-kinases, phosphatases and proteases that participate in altering multiple host cell processes [39, 73, 84]. At the initiation of invasion, they are released to target the parasitophorous vacuole membrane (PVM), the cytoplasm, and the nucleus of the host cell. Among the multiple functions of ROP proteins within the host cell, the modulation of immune and metabolic responses are quintessential examples of their role in the parasite lifecycle. For instance, ROP2 family effectors

and ROP5/ROP18, respectively, are involved in protecting against the degradation of the PVM by the host cell. Additionally, ROP2 involves in preventing the rupture of the PVM by the interaction of the pseudo-kinase ROP5 which activates the ROP18 kinase to phosphorylate the host immune related GTPases (IRGs) [85, 86]. ROP17, a kinase that phosphorylates IRG oligomers, was found to bind to the transmembrane protein GRA7 [87, 88]. Together, both ROP17 and GRA7 form a complex with ROP5-ROP18 to collectively target IRG system protecting the parasite against the host defense to assure its survival [89]. Interestingly, the first report about a parasite protein interacting with the host cell nucleus was the rhoptry protein phosphatase 2C, which role still remains unresolved [90]. ROP16 was later identified as a host nuclear targeted protein that phosphorylates STAT3 and STAT6, thereby activating transcription of multiple genes and downregulating proinflammatory cytokine signaling [91].

Dense granules

Dense granules are spherical and electron-dense vesicles which can be as small as 200 nm in diameter [92]. They contain effector proteins called GRA that, when released, are predominantly involved in setting up the structural modification of the PV [84, 93]. Dense granules differ in number depending on the parasite stage. These vesicles are mostly present in tachyzoite forms which contain about 15 dense granules, while merozoite stages enclose about 3 to 6 DG vesicles [94-97]. They have been demonstrated to display both regulated and constitutive secretion characteristics. Nonetheless, it is mostly-accepted that DGs constitute the default constitutive secretion pathway for soluble proteins [98, 99]. It is thought that regulated secretion may occur at the time of the PV formation, while constitutive secretion may be more pronounced during the entire intracellular cycle [100].

Notably, it has been abundantly demonstrated that an arsenal of GRAs are released within the host cell and play major roles in intracellular parasitism, thus qualifying them as virulence determinants of *Toxoplasma*. However, compared to micronemes and rhoptries, both the biogenesis and secretion process of the dense granules are poorly understood elements of *T. gondii* biology. In particular, the mechanism of GRA trafficking to the DGs is poorly understood. Unlike our understanding of MICs and ROPS [101, 102], no specific sorting mechanisms or amino acid motifs that direct GRA proteins to the dense granules have been identified. One hypothesis is that a unique GRA motif exists and serves to sort the GRAs in the Trans-Golgi Network (TGN) for transport into the DG. Work described in this thesis will attempt to provide some new knowledge on how a Golgi-resident protein might regulate GRAs transport and trafficking (final chapter/future direction).

Interestingly, it has been observed that the majority of the GRAs possess an N-terminal hydrophobic sequence [99]. Inside the DG compartments, GRAs are hydrophobic and, once mature, they bind to myosin and/or Rab11A-positive vesicles to mediate transport [103]. Most GRA effectors of *Toxoplasma* contain either a classical or non-classical N-terminal hydrophobic signal sequence of about 22-30 amino acids short which would target them to the secretory pathway (e.g. GRA3, GRA6, GRA20 etc.) [104]. A significant proportion of GRAs also contain putative transmembrane domains (TM) (e.g.: GRA7, GRA10 and GRA12), while a few are identified to lack the TM domain altogether (GRA1, GRA2 and GRA9) [104].

Over the last decade, we have begun to unravel the molecular mechanisms underlying the function(s) of GRAs, such as how they travel from dense granules to their final destination within the host cell. They mainly participate in the establishment of a favorable environment for growth within the PV by promoting the survival of the parasite and manipulating multiple host cell

processes [86]. Some of them are anchored in the PV membrane while extending into the host cytosol where they are interacting with host proteins [86]. To name a few, Figure 1.4 displays a list of GRAs depicted from a summation of multiple review articles and primary literature articles based on the localization of these effectors [86, 104-114]. Extensive efforts have been dedicated to understanding the role of the GRAs. One GRA with a characterized function is GRA15, which plays a role in modulating the host cell's cytokine production. GRA15 functions through activating Nuclear Factor Kappa-Light-Chain-Enhancer (NF-κB), a signalling molecule found in activated cells downstream of TRAF6 activation [115, 116]. GRA6 is another important DG effector that has a significant role in the stimulation of the synthesis of chemokines CXCL2 and CCL2 through the activation of the Nuclear Factor of Activated T cells 4 (NFAT4) [117]. These chemokines are known to control infection by attracting inflammatory monocytes and neutrophils to the site of infection. Additionally, GRA25, GRA28, and GRA18 have been recently reported to induce the chemokines CCL2 and CCL22, as well as the expression of a specific set of genes associated with CCL17 and CCL22 which was showed to be critical for immune tolerance in placental cells (thus, important during pregnancy) [111, 117-119]. These examples of GRA proteins primarily showcase the role of GRAs in relation to the immune response; however, other GRAs such as GRA7, GRA17/GRA23 , GRA24 and GRA35 have been found to function in the modulation of host cell signaling pathways and acquisition of host nutrients [82, 112, 118, 120, 121] .

Another interesting aspect about the group of GRAs that translocate across the PV membrane is their dependence on the MYR translocon (initially identified as MYR1, then MYR2 and MYR3, and named for the effect on host c-Myc regulation) and the rhoptry-derived kinase ROP17 [122, 123]. Additionally, the aspartyl protease 5 (ASP5) was identified to govern the export mechanism of all exported GRAs; including those that harbor the TEXEL/RRL motif, which is

proteolytically processed by ASP5 [108, 111-114, 124, 125]. This list was recently augmented to include 3 more proteins (MYR4, GRA44 and GRA45) that are essential for the translocation of GRA proteins [126]. So far, among the exported GRAs, only MAG1 is found to be secreted independent of both the MYR translocon and ASP5 cleavage; the mechanism remains unknown and needs further study [106]. In Chapter 2 of this dissertation, we will show how a host nuclear targeted GRA protein is dependent on the MYR1 translocon and the ASP5 protease.

Recently, it has become clear that during and after invasion of host cells, the parasite secretes a myriad GRA (and ROP) proteins into the PVM and cytoplasm of the host cell. These secreted effectors have been proposed to act on the host cell by dramatically regulating gene expression levels and fundamental signal transduction pathways, immune responses, and metabolism [84, 109, 112, 114]. A large group of recently-identified GRA secreted effectors, have been shown to be exported across the PVM and reach the host cell's nucleus, similar to what has been reported for rhoptry host nuclear-targeted effectors PP2Chn and ROP16 [90, 91]. Nuclear-targeted GRA proteins have been shown to function by modifying a plethora of host cell regulatory networks, including controlling the host p38 MAPK (GRA24), repressing STAT1 to downregulate IFN-γ signaling to further block immune functions (TgIST), regulating p53 tumor suppressor pathway and activating host genes that are involved in the cell cycle progression (GRA16), inducing necroptotic gene expression in bradyzoite infected cells (TgNSM), inducing the immunomodulatory chemokine CCL22 (GRA28), and controlling host cyclin E resulting in the inhibition of NF-κB signaling and the modulation of cell cycle phases (HCE1/TEEGR and Chapter 2 this work) [91, 108, 109, 112-114, 119, 127]. This latter example, which is the regulation of the host cell cycle, is a common strategy adopted by intracellular pathogens. Although multiple studies reported that *Toxoplasm*a infection results in cell cycle arrest at S-phase or G2/M checkpoints,

they have failed to identify a secreted effector responsible for this process [128-130]. Chapter 2 of this thesis will add to our knowledge providing answers to the remaining questions of this aspect of *Toxoplasma* biology and how this pathogen regulates the host cell cycle progression and DNA synthesis. These modifications and manipulations largely highlight how *T. gondii* can reprogram its host to its advantage by regulating conserved cellular pathways with secreted factors.

1.5. THE SUPPLIERS: PROTEINS AND VESICULAR TRAFFICKING IN *TOXOPLASMA GONDII.*

Canonical Eukaryotic Organelles in T. gondii: Endoplasmic Reticulum and Golgi Apparatus as suppliers.

In addition to the secretory endomembranes discussed above, canonical eukaryotic organelles such as a mitochondrion, a Golgi complex and a Endoplasmic Reticulum (ER) (enveloping its nucleus 'Fig. 3') are also found in *T. gondii* [131]. Prior to entering the secretory pathways, *T. gondii* secretory effectors must translocate from the ER (the site of protein synthesis) through the Golgi via the classical ER/Golgi route to be accurately sorted and packaged into their corresponding vesicles. Therefore, we consider that the secretory system is composed of suppliers (ER, Golgi) and accomplices (trafficking proteins and secretory effectors). A handful of molecular factors indicate that this parasite has multiple components of vesicle budding, transport, and fusion machinery. Similar to other organisms, it was found that TgSLY1 may interact with TgStx5 to mediate fusion of vesicles that shed from the ER and consequently fuse with the cis-Golgi, and TgSLY1 is moreover needed to regulate the function of the Golgi [132] . Furthermore, TgN-Sec1 and Syntaxin 1 are essential for ER to Golgi vesicular transport [132]. Additionally, in nascent daughter tachyzoites, some evidence demonstrates that new rhoptries are produced from the vesicular budding of the trans-Golgi network in a process driven by the dynamin-related protein

(DrpB), a post-Golgi network and endosomal-like compartment (ELC) resident protein [133]. The ELC is another important vesicle that obtains and transfers vesicles from the Golgi to their final compartmentalized destination, including micronemes and rhoptries [134].

The accomplices: protein trafficking in Toxoplasma.

It is imperative to highlight the increasing work of molecular elements that are involved in protein and vesicular trafficking, as these pathways are utilized throughout the lytic cycle. More importantly, studies have identified sorting motifs that govern the trafficking of RON/ROP and MIC proteins to their respective compartments. The motifs for the RON/ROP family proteins have been identified and mapped to the cytoplasmic tail of TgROP2. Additionally, it was found that the C-terminal tails of TgMIC2 and TgMIC6 contain respectively two conserved amino acid motifs and one motif that mediate the targeting of MICs to the micronemes (Figure 1.5) [101, 102]. These sorting events are followed by multiple other trafficking processes. For instance, through a clathrin/AP-1 (adaptor protein 1) complex dependent fashion, MIC and RON/ROP proteins are sorted from the Golgi and subsequently transported to Rab5/vacuolar protein sorting 9 (Vps9)-positive endosomal organelles [135]. This ELC resident protein, TgVps9, plays a major role as a facilitator using trafficking to regulate protein maturation, secretory organelle maturation, and secretion [136]. Additionally, the luminal domain sortilin-like receptor (TgSORTLR), a Golgi/endosomal-related compartment resident protein, is found to interact with MIC and RON/ROP proteins while cytosolic sorting machinery is recruited by its cytosolic tail for protein transport through a non-conventional ELC [137]. The TgSORTLR C-terminal end interacts with Sec23/24 AP-1 adapter complex, clathrin, and three vacuolar sorting proteins named Vps26, Vps35, and Vps9 [137]. Other studies have showed that Rab5A/C-positive vesicles are specifically involved in the delivery of apical MICs and ROPs to their proper vesicles while lateral

MICs are delivered via the functions of Vps11/CORVET and HOPS. Vps11/CORVET are involved in the class C core vacuole and endosome tethering while HOPS complex is involved in homotypic fusion and protein sorting [138]. In a similar manner to mammalian cells, *Toxoplasma* Rab5 and Rab7 proteins induce membrane fusion within the endolysosome pathway likely through their interaction with CORVET and HOPS complexes [133, 139]. Therefore, multiple proteins such as TgVps5, and its binding-partners TgStx1, are at play during this process. The vacuolar compartment (VAC/PLV) is similarly seen to mediate some proteins transport in *T. gondii* [140, 141]. During the vesicular transport of ROPs to the neck of the rhoptry, *Toxoplasma* Carbonic anhydrase-related proteins (TgCA_RP), which localizes to the rhoptry bulb and important for its biogenesis, could mediate the fusion of prerhoptry vesicles within this organelle [142]. Results of a recent report showed that the TgStx12 effector impacts the efficient trafficking of mature MICs and RONs/ROPs to the proper compartments and it may have an indirect effect on MICs and RONs/ROPs trafficking as it is involved in the trafficking of nuclear-encoded apicoplast resident proteins [143]. Because trafficking pathways are involved in multiple endomembranes, it is critical to discuss the biogenesis/division of the vesicles of *T. gondii* during its replication. *T. gondii* utilizes a process called endodyogeny to proliferate inside the infected host whereby two daughter parasites emerge within the mother cell. Endodyogeny normally begins with the duplication of the centrosome, followed by Golgi elongation and fission, and finally the migration and division of the apicoplast. Next, the division of the ER and nucleus occur as the daughter cells emerge [144, 145]. In contrast to this, rhoptries and micronemes form *de novo* by vesicular budding from the Golgi during cytokinesis at the apical pole [145]. It was also reported that that TNG is found to be in close proximity to the ELC, presumably ensuring the transport and processing of newly synthesized MIC/RON/RON proteins [104, 145]. Thus, the configuration of the Golgi stacks,

which extend laterally and eventually undergo binary fission in synchrony with centrosome duplication, highlights the great importance of proper polarization of secretory pathway organelles. Conventionally, protein trafficking in the anterograde pathway across all eukaryotes is well conserved [146]. Thus, secretory proteins are synthesized in the rough ER and transported to the Golgi in a COPII dependent fashion. However, a direct molecular link during parasite division connecting protein trafficking between the Golgi and the dense granules vesicles has not been identified for the secretory pathway.

Considering the manner in which *T. gondii* operates, it is evident that this unicellular parasite relies on a dynamic and abundant vesicle and protein trafficking, including important sorting motifs to transport MIC/RON/ROP proteins from the Golgi to rhoptries and micronemes. Despite the novelty of the three unique secretory organelles, *Toxoplasma* possess a relatively conserved secretory protein and vesicular trafficking system to direct different functional cargoes to their destinations. However, a specific sorting mechanism and associated sorting motifs that direct GRA proteins to the dense granules have not yet been identified. Over the last decade, our understanding has grown regarding how these GRAs function as they move from dense granules to their final destination. They participate in establishing a favorable growth environment within the PV, promote the survival of the parasite, and manipulate multiple host cell processes. Based on their localization, as previously stated above, this list includes nuclear targeted proteins, vacuolar spaces, membranous nanotubular network proteins and PV membrane proteins [104]. Furthermore, studies demonstrate Rab6 regulates protein transport between the Golgi complex and endosome and could be essential to form a putative pre-dense granule organelle [147]. As the trafficking to dense granules remains the default pathway of secretory proteins, investigating the sorting machinery necessary for GRAs to translocate from the major sorting Golgi complex, where

transport pathways intersect to reach their vesicular destination, requires further exploration to improve our understanding of this apiconmplexan. In this context, the role of a newly identified *Toxoplasma* Golgi resident protein will be unraveled in this thesis to illuminate its effect on parasite lytic cycle and potein trafficking.

1.6. REFERENCES

1. Dubey, J.P., *The history of Toxoplasma gondii--the first 100 years.* J Eukaryot Microbiol, 2008. **55**(6): p. 467-75.
2. Blader, I.J., et al., *Lytic Cycle of Toxoplasma gondii: 15 Years Later.* Annu Rev Microbiol, 2015. **69**: p. 463-85.
3. Saadatnia, G. and M. Golkar, *A review on human toxoplasmosis.* Scand J Infect Dis, 2012. **44**(11): p. 805-14.
4. Nicolle, C. and L.H. Manceaux, *On a leishman body infection (or related organisms) of the gondi. 1908.* Int J Parasitol, 2009. **39**(8): p. 863-4.
5. Splendore, A., *Sur un nouveau protozoaire parasite du lapin, deuxième note préliminaire.* Bull Soc Pathol Exot, 1909. **2**: p. 462-465.
6. Maubon, D., et al., *What are the respective host and parasite contributions to toxoplasmosis?* Trends Parasitol, 2008. **24**(7): p. 299-303.
7. Sabin, A.B. and P.K. Olitsky, *Toxoplasma and Obligate Intracellular Parasitism.* Science, 1937. **85**(2205): p. 336-338.
8. Sabin, A.B., *Biological and Immunological Identity of Toxoplasma of Animal and Human Origin.* Proceedings of the Society for Experimental Biology and Medicine, 1939. **41**(1): p. 75-80.
9. Sabin, A.B., *TOXOPLASMIC ENCEPHALITIS IN CHILDREN.* The Journal of the American Medical Association 1941. **116**(9): p. 801-807.
10. Howe, D.K. and L.D. Sibley, *Toxoplasma gondii comprises three clonal lineages: correlation of parasite genotype with human disease.* J Infect Dis, 1995. **172**(6): p. 1561-6.

11. Sibley, L.D. and J.C. Boothroyd, *Virulent strains of Toxoplasma gondii comprise a single clonal lineage.* Nature, 1992. **359**(6390): p. 82-5.

12. Tibayrenc, M., et al., *Are eukaryotic microorganisms clonal or sexual? A population genetics vantage.* Proc Natl Acad Sci U S A, 1991. **88**(12): p. 5129-33.

13. Saeij, J.P., J.P. Boyle, and J.C. Boothroyd, *Differences among the three major strains of Toxoplasma gondii and their specific interactions with the infected host.* Trends Parasitol, 2005. **21**(10): p. 476-81.

14. Dubey, J.P., *Chapter1 - The History and Life Cycle of Toxoplasma gondii, in Toxoplasma Gondii (Second Edition).* Academic Press: Boston, 2014: p. 1-17.

15. Flegr, J., et al., *Toxoplasmosis--a global threat. Correlation of latent toxoplasmosis with specific disease burden in a set of 88 countries.* PLoS One, 2014. **9**(3): p. e90203.

16. Montoya, J.G. and O. Liesenfeld, *Toxoplasmosis.* The Lancet, 2004. **363**(9425): p. 1965-1976.

17. Suss-Toby, E., J. Zimmerberg, and G.E. Ward, *Toxoplasma invasion: the parasitophorous vacuole is formed from host cell plasma membrane and pinches off via a fission pore.* Proc Natl Acad Sci U S A, 1996. **93**(16): p. 8413-8.

18. Robert-Gangneux, F. and M.L. Darde, *Epidemiology of and diagnostic strategies for toxoplasmosis.* Clin Microbiol Rev, 2012. **25**(2): p. 264-96.

19. Pappas, G., N. Roussos, and M.E. Falagas, *Toxoplasmosis snapshots: global status of Toxoplasma gondii seroprevalence and implications for pregnancy and congenital toxoplasmosis.* Int J Parasitol, 2009. **39**(12): p. 1385-94.

20. Lykins, J., et al., *Understanding Toxoplasmosis in the United States Through "Large Data" Analyses.* Clin Infect Dis, 2016. **63**(4): p. 468-75.

21. Jones, J.L., et al., *Toxoplasma gondii seroprevalence in the United States 2009-2010 and comparison with the past two decades.* Am J Trop Med Hyg, 2014. **90**(6): p. 1135-9.

22. Beckers, C.J., et al., *Inhibition of cytoplasmic and organellar protein synthesis in Toxoplasma gondii. Implications for the target of macrolide antibiotics.* J Clin Invest, 1995. **95**(1): p. 367-76.

23. Tenter, A.M., A.R. Heckeroth, and L.M. Weiss, *Toxoplasma gondii- from animals to humans.* Int J Parasitol, 2000. **30**(12-13): p. 1217-1258.

24. Sabin, A.B. and H.A. Feldman, *Dyes as Microchemical Indicators of a New Immunity Phenomenon Affecting a Protozoon Parasite (Toxoplasma).* Science, 1948. **108**(2815): p. 660-3.

25. Burg, J.L., et al., *Direct and sensitive detection of a pathogenic protozoan, Toxoplasma gondii, by polymerase chain reaction.* J Clin Microbiol, 1989. **27**(8): p. 1787-92.

26. Montoya, J.G., *Laboratory diagnosis of Toxoplasma gondii infection and toxoplasmosis.* J Infect Dis, 2002. **185 Suppl 1**: p. S73-82.

27. Remington, J.S., M.J. Miller, and I. Brownlee, *IgM antibodies in acute toxoplasmosis. I. Diagnostic significance in congenital cases and a method for their rapid demonstration.* Pediatrics, 1968. **41**(6): p. 1082-91.

28. Jongert, E., et al., *Vaccines against Toxoplasma gondii- challenges and opportunities.* Mem Inst Oswaldo Cruz, 2009. **104**: p. 252-266.

29. Sabin, A.B. and J. Warren, *Therapeutic Effectiveness of Certain Sulfonamides on Infection by an Intracellular Protozoon (Toxoplasma).* Experimental Biology and Medicine, 1942. **51**(1): p. 19-23.

30. Eyles, D. and N. Coleman, *Synergistic Effect of Sulfadiazlne and Daraprim against Experimental Toxoplasmosis in the Mouse.* Antibiotics & Chemotherapy, 1953. **3**: p. 483-490.

31. Remington, J.S. and J.O. Klein, *Infectious Diseases of the Fetus and Newborn Infant* London: WB Saunders, 2001.

32. Chodos, J.B. and H.E. Habergger-Chodos, *The Treatment of Ocular Toxoplasmosis with Spiramycin.* 1961. **65**: p. 109-117.

33. Desmonts, G. and J. Couvreur, *Toxoplasmosis in pregnancy and its transmission to the fetus.* Bulletin of the New York Academy of Medicine, 1974. **50**: p. 146.

34. Torun, N.L., A.; Hartmann, C.; Metzner, S.; Pleyer, U., *Ocular toxoplasmosis antibodies in aqueous humor and serum.* Der Ophthalmologe, 2002. **99**: p. 109–112.

35. Abgrall, S., C. Rabaud, and D. Costagliola, *Incidence and risk factors for toxoplasmic encephalitis in human immunodeficiency virus-infected patients before and during the highly active antiretroviral therapy era.* Clin Infect Dis, 2001. **33**(10): p. 1747-55.

36. Rorman, E., et al., *Congenital toxoplasmosis--prenatal aspects of Toxoplasma gondii infection.* Reprod Toxicol, 2006. **21**(4): p. 458-72.

37. Siegel, S.E., et al., *Transmission of toxoplasmosis by leukocyte transfusion.* Blood, 1971. **37**(4): p. 388-94.

38. Sullivan, W.J.J. and V. Jeffers, *Mechanisms of Toxoplasma gondii persistence and latency.* FEMS Microbiol Rev, 2012. **36**(3): p. 717-33.

39. Laliberte, J. and V.B. Carruthers, *Host cell manipulation by the human pathogen Toxoplasma gondii.* Cell Mol Life Sci, 2008. **65**(12): p. 1900-15.

40. Dubey, J.P., *Reshedding of Toxoplasma oocysts by chronically infected cats.* Nature, 1976. **262**(5565): p. 213-214.

41. Dubey, J.P., *Duration of Immunity to Shedding of Toxoplasma gondii Oocysts by Cats.* The Journal of Parasitology, 1995. **81**(3): p. 410-415.

42. Webster, J.P., *Dubey, J.P. Toxoplasmosis of Animals and Humans.* Parasites & Vectors, 2010. **3**(1).

43. Weinman, D. and A.H. Chandler, *Toxoplasmosis in swine and rodents; reciprocal oral infection and potential human hazard.* Proc Soc Exp Biol Med, 1954. **87**(1): p. 211-6.

44. McCabe, R. and J.S. Remington, *TOXOPLASMOSIS: THE TIME HAS COME.* N. Engl. J. Med., 1988. **318**: p. 313 – 315.

45. Jones, J.L. and J.P. Dubey, *Waterborne toxoplasmosis--recent developments.* Exp Parasitol, 2010. **124**(1): p. 10-25.

46. Jones, J.L. and J.P. Dubey, *Foodborne toxoplasmosis.* Clin Infect Dis, 2012. **55**(6): p. 845-51.

47. Herwaldt, B.L. and D.D. Juranek, *Laboratory-acquired malaria, leishmaniasis, trypanosomiasis, and toxoplasmosis.* Am J Trop Med Hyg, 1993. **48**(3): p. 313-23.

48. Herwaldt, B.L., *Laboratory-acquired parasitic infections from accidental exposures.* Clin Microbiol Rev, 2001. **14**(4): p. 659-88, table of contents.

49. Derouin, F. and H. Pelloux, *Prevention of toxoplasmosis in transplant patients.* Clin Microbiol Infect, 2008. **14**(12): p. 1089-101.

50. Dehkordi, F.S., et al., *Detection of Toxoplasma gondii in raw caprine, ovine, buffalo, bovine, and camel milk using cell cultivation, cat bioassay, capture ELISA, and PCR methods in Iran.* Foodborne Pathog Dis, 2013. **10**(2): p. 120-5.

51. Elmore, S.A., et al., *Toxoplasma gondii: epidemiology, feline clinical aspects, and prevention.* Trends Parasitol, 2010. **26**(4): p. 190-6.

52. Weiss, L.M. and K. Kim, *THE DEVELOPMENT AND BIOLOGY OF BRADYZOITES OF TOXOPLASMA GONDII.* FrontBiosci, 2000. **391-405**.

53. Dubey, J.P., *Oocyst shedding by cats fed isolated bradyzoites and comparison of infectivity of bradyzoites of the VEG strain Toxoplasma gondii to cats and mice.* J Parasitol, 2001. **87**(1): p. 215-9.

54. Di Cristina, M., et al., *Temporal and spatial distribution of Toxoplasma gondii differentiation into Bradyzoites and tissue cyst formation in vivo.* Infect Immun, 2008. **76**(8): p. 3491-501.

55. Berdoy, M., J.P. Webster, and D.W. Macdonald, *Parasite-altered behaviour: is the effect of Toxoplasma gondii on Rattus norvegicus specific?* Parasitology, 1995. **111 (Pt 4)**: p. 403-9.

56. Berdoy, M., J.P. Webster, and D.W. Macdonald, *Fatal attraction in rats infected with Toxoplasma gondii.* Proc Biol Sci, 2000. **267**(1452): p. 1591-4.

57. Berenreiterova, M., et al., *The distribution of Toxoplasma gondii cysts in the brain of a mouse with latent toxoplasmosis: implications for the behavioral manipulation hypothesis.* PLoS One, 2011. **6**(12): p. e28925.

58. House, P.K., A. Vyas, and R. Sapolsky, *Predator cat odors activate sexual arousal pathways in brains of Toxoplasma gondii infected rats.* PLoS One, 2011. **6**(8): p. e23277.

59. Vyas, A., et al., *Behavioral changes induced by Toxoplasma infection of rodents are highly specific to aversion of cat odors.* Proc Natl Acad Sci U S A, 2007. **104**(15): p. 6442-7.

60. Webster, J.P., *Rats, cats, people and parasites: the impact of latent toxoplasmosis on behaviour.* Microbes Infect, 2001. **3**(12): p. 1037-45.

61. Dass, S.A., et al., *Protozoan parasite Toxoplasma gondii manipulates mate choice in rats by enhancing attractiveness of males.* PLoS One, 2011. **6**(11): p. e27229.

62. Bullen, H.E., H. Bisio, and D. Soldati-Favre, *The triumvirate of signaling molecules controlling Toxoplasma microneme exocytosis: Cyclic GMP, calcium, and phosphatidic acid.* PLoS Pathog, 2019. **15**(5): p. e1007670.

63. Dubois, D.J. and D. Soldati-Favre, *Biogenesis and secretion of micronemes in Toxoplasma gondii.* Cell Microbiol, 2019. **21**(5): p. e13018.

64. Carruthers, V.B. and L.D. Sibley, *Mobilization of intracellular calcium stimulates microneme discharge in Toxoplasma gondii.* Molecular Microbiology 1999. **31**(2): p. 421-428.

65. Barclay, J.W., A. Morgan, and R.D. Burgoyne, *Calcium-dependent regulation of exocytosis.* Cell Calcium, 2005. **38**(3-4): p. 343-53.

66. Bargieri, D., et al., *Host cell invasion by apicomplexan parasites: the junction conundrum.* PLoS Pathog, 2014. **10**(9): p. e1004273.

67. Kessler, H., et al., *Microneme protein 8--a new essential invasion factor in Toxoplasma gondii.* J Cell Sci, 2008. **121**(Pt 7): p. 947-56.

68. Brossier, F., et al., *A spatially localized rhomboid protease cleaves cell surface adhesins essential for invasion by Toxoplasma.* Proc Natl Acad Sci U S A, 2005. **102**(11): p. 4146-51.

69. Dowse, T.J., et al., *Apicomplexan rhomboids have a potential role in microneme protein cleavage during host cell invasion.* Int J Parasitol, 2005. **35**(7): p. 747-56.

70. Dubey, J.P., D.S. Lindsay, and C.A. Speer, *Structures of Toxoplasma gondii Tachyzoites, Bradyzoites, and Sporozoites and Biology and Development of Tissue Cysts.* CLINICAL MICROBIOLOGY REVIEW, 1998. **11**(2): p. 267-299.

71. Boothroyd, J.C. and J.F. Dubremetz, *Kiss and spit: the dual roles of Toxoplasma rhoptries.* Nat Rev Microbiol, 2008. **6**(1): p. 79-88.

72. Dubremetz, J.F., *Rhoptries are major players in Toxoplasma gondii invasion and host cell interaction.* Cell Microbiol, 2007. **9**(4): p. 841-8.

73. Bradley, P.J., et al., *Proteomic analysis of rhoptry organelles reveals many novel constituents for host-parasite interactions in Toxoplasma gondii.* J Biol Chem, 2005. **280**(40): p. 34245-58.

74. Besteiro, S., J.F. Dubremetz, and M. Lebrun, *The moving junction of apicomplexan parasites: a key structure for invasion.* Cell Microbiol, 2011. **13**(6): p. 797-805.

75. Lamarque, M., et al., *The RON2-AMA1 interaction is a critical step in moving junction-dependent invasion by apicomplexan parasites.* PLoS Pathog, 2011. **7**(2): p. e1001276.

76. Beck, J.R., et al., *RON5 is critical for organization and function of the Toxoplasma moving junction complex.* PLoS Pathog, 2014. **10**(3): p. e1004025.

77. Alexander, D.L., et al., *Identification of the moving junction complex of Toxoplasma gondii: a collaboration between distinct secretory organelles.* PLoS Pathog, 2005. **1**(2): p. e17.

78. Lebrun, M., et al., *The rhoptry neck protein RON4 re-localizes at the moving junction during Toxoplasma gondii invasion.* Cell Microbiol, 2005. **7**(12): p. 1823-33.

79. Håkansson, S., A. J.Charron, and L.D. Sibley, *Toxoplasma evacuoles- a two-step process of secretion and fusion forms the parasitophorous vacuole.* The EMBO Journal 2001. **20**(12): p. 3132-3144.

80. Mital, J., et al., *Conditional expression of Toxoplasma gondii apical membrane antigen-1 (TgAMA1) demonstrates that TgAMA1 plays a critical role in host cell invasion.* Molecular Biology of the Cell, 2005. **16**: p. 4341–4349.

81. Egarter, S., et al., *The toxoplasma Acto-MyoA motor complex is important but not essential for gliding motility and host cell invasion.* PLoS One, 2014. **9**(3): p. e91819.

82. Gold, D.A., et al., *The Toxoplasma Dense Granule Proteins GRA17 and GRA23 Mediate the Movement of Small Molecules between the Host and the Parasitophorous Vacuole.* Cell Host Microbe, 2015. **17**(5): p. 642-52.

83. Mordue, D.G., et al., *Invasion by Toxoplasma gondii establishes a moving junction that selectively excludes host cell plasma membrane proteins on the basis of their membrane anchoring.* J Exp Med, 1999. **190**(12): p. 1783-92.

84. Nadipuram, S.M., et al., *In Vivo Biotinylation of the Toxoplasma Parasitophorous Vacuole Reveals Novel Dense Granule Proteins Important for Parasite Growth and Pathogenesis.* MBio, 2016. **7**(4).

85. Fleckenstein, M.C., et al., *A Toxoplasma gondii pseudokinase inhibits host IRG resistance proteins.* PLoS Biol, 2012. **10**(7): p. e1001358.

86. Hakimi, M.A., P. Olias, and L.D. Sibley, *Toxoplasma Effectors Targeting Host Signaling and Transcription.* Clin Microbiol Rev, 2017. **30**(3): p. 615-645.

87. Alaganan, A., et al., *Toxoplasma GRA7 effector increases turnover of immunity-related GTPases and contributes to acute virulence in the mouse.* Proc Natl Acad Sci U S A, 2014. **111**(3): p. 1126-31.

88. Etheridge, R.D., et al., *The Toxoplasma pseudokinase ROP5 forms complexes with ROP18 and ROP17 kinases that synergize to control acute virulence in mice.* Cell Host Microbe, 2014. **15**(5): p. 537-50.

89. Niedelman, W., et al., *The rhoptry proteins ROP18 and ROP5 mediate Toxoplasma gondii evasion of the murine, but not the human, interferon-gamma response.* PLoS Pathog, 2012. **8**(6): p. e1002784.

90. Gilbert, L.A., et al., *Toxoplasma gondii targets a protein phosphatase 2C to the nuclei of infected host cells.* Eukaryot Cell, 2007. **6**(1): p. 73-83.

91. Saeij, J.P., et al., *Toxoplasma co-opts host gene expression by injection of a polymorphic kinase homologue.* Nature, 2007. **445**(7125): p. 324-7.

92. Dubremetz, J.F. and D.J.P. Ferguson, *Toxoplasma: Molecular and Cellular Biology.* Molecular and Cellular Biology, Ajioka JW & Soldati D (eds), 2007: p. 17-33. Taylor & Francis.

93. Nam, H.W., *GRA proteins of Toxoplasma gondii: maintenance of host-parasite interactions across the parasitophorous vacuolar membrane.* Korean J Parasitol, 2009. **47 Suppl**: p. S29-37.

94. Labruyere, E., et al., *Differential membrane targeting of the secretory proteins GRA4 and GRA6 within the parasitophorous vacuole formed by Toxoplasma gondii.* Molecular and Biochemical Parasitology 1999. **102**: p. 311-324

95. Ferguson, D.J.P., et al., *The expression and distribution of dense granule proteins in the enteric (Coccidian) forms of Toxoplasma gondii in the small intestine of the cat.* Experimental Parasitology, 1999. **91**: p. 203-211.

96. Sibley, L.D., et al., *Regulated secretion of multi-lamellar vesicles leads to formation of a tubulo-vesicular network in host-cell vacuoles occupied by Toxoplasma gondii.* Journal of Cell Science, 1995. **108**: p. 1669-1677.

97. Lebrun, M., V.B. Carruthers, and M.-F. Cesbron-Delauw, *Toxoplasma Secretory Proteins and Their Roles in Cell Invasion and Intracellular Survival*, in *Toxoplasma Gondii: the model apicomplexan. Perspectives and methods*. 2014. p. 389-453.

98. Striepen, B., et al., *Expression, selection, and organellar targeting of the green fluorescent protein in Toxoplasma gondii.* Mol Biochem Parasitol, 1998. **92**(2): p. 325-38.

99. Striepen, B., et al., *Targeting of soluble proteins to the rhoptries and micronemes in Toxoplasma gondii.* Mol Biochem Parasitol, 2001. **113**(1): p. 45-53.

100. Coppens, I., et al., *Intracellular trafficking of dense granule proteins in Toxoplasma gondii and experimental evidences for a regulated exocytosis.* European Journal of Cell Biology, 1999. **78**(7): p. 463-472.

101. Hoppe, H.C., et al., *Targeting to rhoptry organelles of Toxoplasma gondii involves evolutionarily conserved mechanisms.* Nature Cell Biology, 2000. **2**(7): p. 449-456.

102. Christina, M.D.S., R.; Soldati, D.; Bistoni, F.; Crisanti, A., *Two Conserved Amino Acid Motifs Mediate Protein Targeting to the Micronemes of the Apicomplexan ParasiteToxoplasma gondii.* MOLECULAR AND CELLULAR BIOLOGY, 2000. **20**(07/07/2000): p. 7332-7341.

103. Venugopal, K., et al., *Rab11A regulates dense granule transport and secretion during Toxoplasma gondii invasion of host cells and parasite replication.* PLoS Pathog, 2020. **16**(5): p. e1008106.

104. Mercier, C. and M.F. Cesbron-Delauw, *Toxoplasma secretory granules: one population or more?* Trends Parasitol, 2015. **31**(2): p. 60-71.

105. Wang, Y., et al., *Toxoplasma Mechanisms for Delivery of Proteins and Uptake of Nutrients Across the Host-Pathogen Interface.* Annu Rev Microbiol, 2020. **74**: p. 567-586.

106. Tomita, T., et al., *Toxoplasma gondii Matrix Antigen 1 Is a Secreted Immunomodulatory Effector.* mBio, 2021. **12**(3).

107. Rosenberg, A. and L.D. Sibley, *Toxoplasma gondii secreted effectors co-opt host repressor complexes to inhibit necroptosis.* Cell Host Microbe, 2021. **29**(7): p. 1186-1198.e8.

108. Panas, M.W., et al., *Toxoplasma Controls Host Cyclin E Expression through the Use of a Novel MYR1-Dependent Effector Protein, HCE1.* mBio, 2019. **10**(2).

109. Olias, P., et al., *Toxoplasma Effector Recruits the Mi-2/NuRD Complex to Repress STAT1 Transcription and Block IFN-gamma-Dependent Gene Expression.* Cell Host Microbe, 2016. **20**(1): p. 72-82.

110. Mercier, C., et al., *Dense granules: are they key organelles to help understand the parasitophorous vacuole of all apicomplexa parasites?* Int J Parasitol, 2005. **35**(8): p. 829-49.

111. He, H., et al., *Characterization of a Toxoplasma effector uncovers an alternative GSK3/β-catenin-regulatory pathway of inflammation.* Elife, 2018. **7**.

112. Braun, L., et al., *A Toxoplasma dense granule protein, GRA24, modulates the early immune response to infection by promoting a direct and sustained host p38 MAPK activation.* J Exp Med, 2013. **210**(10): p. 2071-86.

113. Braun, L., et al., *The Toxoplasma effector TEEGR promotes parasite persistence by modulating NF-kappaB signalling via EZH2.* Nat Microbiol, 2019. **4**(7): p. 1208-1220.

114. Bougdour, A., et al., *Host cell subversion by Toxoplasma GRA16, an exported dense granule protein that targets the host cell nucleus and alters gene expression.* Cell Host Microbe, 2013. **13**(4): p. 489-500.

115. Gov, L., et al., *Human innate immunity to Toxoplasma gondii is mediated by host caspase-1 and ASC and parasite GRA15.* mBio, 2013. **4**(4).

116. Rosowski, E.E., et al., *Strain-specific activation of the NF-kappaB pathway by GRA15, a novel Toxoplasma gondii dense granule protein.* J Exp Med, 2011. **208**(1): p. 195-212.

117. Ma, J.S., et al., *Selective and strain-specific NFAT4 activation by the Toxoplasma gondii polymorphic dense granule protein GRA6.* J Exp Med, 2014. **211**(10): p. 2013-32.

118. Shastri, A.J., et al., *GRA25 is a novel virulence factor of Toxoplasma gondii and influences the host immune response.* Infect Immun, 2014. **82**(6): p. 2595-605.

119. Rudzki, E.N., et al., *Toxoplasma gondii GRA28 Is Required for Placenta-Specific Induction of the Regulatory Chemokine CCL22 in Human and Mouse.* mBio, 2021. **12**(6): p. e0159121.

120. Coppens, I., et al., *Toxoplasma gondii sequesters lysosomes from mammalian hosts in the vacuolar space.* Cell, 2006. **125**(2): p. 261-74.

121. Wang, Y., et al., *Three Toxoplasma gondii Dense Granule Proteins Are Required for Induction of Lewis Rat Macrophage Pyroptosis.* mBio, 2019. **10**(1).

122. Franco, M., et al., *A Novel Secreted Protein, MYR1, Is Central to Toxoplasma's Manipulation of Host Cells.* mBio, 2016. **7**(1): p. e02231-15.

123. Panas, M.W., et al., *Translocation of Dense Granule Effectors across the Parasitophorous Vacuole Membrane in Toxoplasma-Infected Cells Requires the Activity of ROP17, a Rhoptry Protein Kinase.* mSphere, 2019. **4**(4).

124. Coffey, M.J., et al., *Aspartyl protease 5 matures dense granule proteins that reside at the host-parasite interface in Toxoplasma gondii.* mBio 9:e01796-18, 2018.

125. Hammoudi, P.M., et al., *Fundamental Roles of the Golgi-Associated Toxoplasma Aspartyl Protease, ASP5, at the Host-Parasite Interface.* PLoS Pathog, 2015. **11**(10): p. e1005211.

126. Cygan, A.M., et al., *Coimmunoprecipitation with MYR1 Identifies Three Additional Proteins within the Toxoplasma gondii Parasitophorous Vacuole Required for Translocation of Dense Granule Effectors into Host Cells.* mSphere, 2020. **5**(1).

127. Rosenberg, A. and L.D. Sibley, *Toxoplasma gondii secreted effectors co-opt host repressor complexes to inhibit necroptosis.* Cell Host Microbe, 2021. **29**(7): p. 1186-1198 e8.

128. Lavine, M.D. and G. Arrizabalaga, *Induction of mitotic S-phase of host and neighboring cells by Toxoplasma gondii enhances parasite invasion.* Mol Biochem Parasitol, 2009. **164**(1): p. 95-9.

129. Molestina, R.E., N. El-Guendy, and A.P. Sinai, *Infection with Toxoplasma gondii results in dysregulation of the host cell cycle.* Cell Microbiol, 2008. **10**(5): p. 1153-65.

130. Brunet, J., et al., *Toxoplasma gondii exploits UHRF1 and induces host cell cycle arrest at G2 to enable its proliferation.* Cell Microbiol, 2008. **10**(4): p. 908-20.

131. Pelletier, L., et al., *Golgi biogenesis in Toxoplasma gondii.* Nature, 2002. **418**(6897): p. 548-552.

132. Peng, R. and D. Gallwitz, *Sly1 protein bound to Golgi syntaxin Sed5p allows assembly and contributes to specificity of SNARE fusion complexes.* J Cell Biol, 2002. **157**(4): p. 645-55.

133. Balderhaar, H.J. and C. Ungermann, *CORVET and HOPS tethering complexes - coordinators of endosome and lysosome fusion.* J Cell Sci, 2013. **126**(Pt 6): p. 1307-16.

134. Venugopal, K. and S. Marion, *Secretory organelle trafficking in Toxoplasma gondii: A long story for a short travel.* Int J Med Microbiol, 2018. **308**(7): p. 751-760.

135. Pieperhoff, M.S., et al., *The role of clathrin in post-Golgi trafficking in Toxoplasma gondii.* PLoS One, 2013. **8**(10): p. e77620.

136. Sakura, T., et al., *A Critical Role for Toxoplasma gondii Vacuolar Protein Sorting VPS9 in Secretory Organelle Biogenesis and Host Infection.* Sci Rep, 2016. **6**: p. 38842.

137. Sloves, P.J., et al., *Toxoplasma sortilin-like receptor regulates protein transport and is essential for apical secretory organelle biogenesis and host infection.* Cell Host Microbe, 2012. **11**(5): p. 515-27.

138. Morlon-Guyot, J., et al., *Toxoplasma gondii Vps11, a subunit of HOPS and CORVET tethering complexes, is essential for the biogenesis of secretory organelles.* Cell Microbiol, 2015. **17**(8): p. 1157-78.

139. Rink, J., et al., *Rab conversion as a mechanism of progression from early to late endosomes.* Cell, 2005. **122**(5): p. 735-49.

140. Parussini, F., et al., *Cathepsin L occupies a vacuolar compartment and is a protein maturase within the endo/exocytic system of Toxoplasma gondii.* Mol Microbiol, 2010. **76**(6): p. 1340-57.

141. Miranda, K., et al., *Characterization of a novel organelle in Toxoplasma gondii with similar composition and function to the plant vacuole.* Mol Microbiol, 2010. **76**(6): p. 1358-75.

142. Chasen, N.M., et al., *A Glycosylphosphatidylinositol-Anchored Carbonic Anhydrase-Related Protein of Toxoplasma gondii Is Important for Rhoptry Biogenesis and Virulence.* mSphere, 2017. **2**(3).

143. Bisio, H., et al., *The ZIP Code of Vesicle Trafficking in Apicomplexa: SEC1/Munc18 and SNARE Proteins.* mBio, 2020. **11**(5).

144. Pelletier, L., et al., *Golgi biogenesis in Toxoplasma gondii.* Nature, 2002. **418**(6897): p. 548-52.

145. Nishi, M., et al., *Organellar dynamics during the cell cycle of Toxoplasma gondii.* J Cell Sci, 2008. **121**(Pt 9): p. 1559-68.

146. Kim, K. and S.K.G. Gadila, *Cargo trafficking from the trans-Golgi network towards the endosome.* Biol Cell, 2016. **108**(8): p. 205-18.

147. Stedman, T.T., A.R. Sussmann, and K.A. Joiner, *Toxoplasma gondii Rab6 mediates a retrograde pathway for sorting of constitutively secreted proteins to the Golgi complex.* J Biol Chem, 2003. **278**(7): p. 5433-43.

1.7. FIGURES

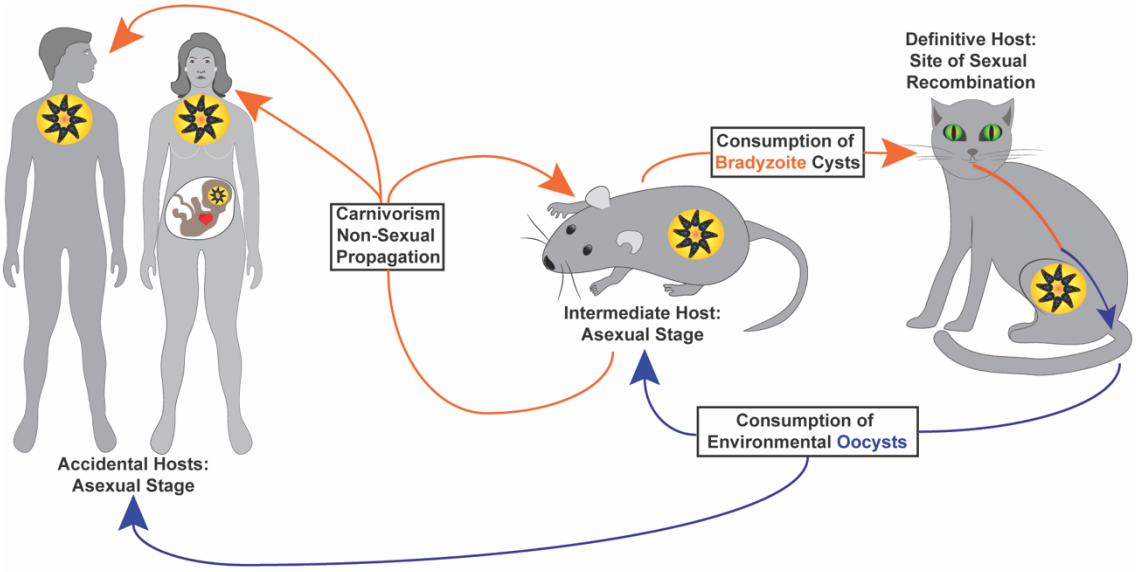

Figure 1.1: The life cycle of *Toxoplasma gondii*.

In its intermediate host (e.g. rodents), *T. gondii* undergoes asexual propagation and eventually converts to its semi-dormant bradyzoite tissue cyst form as part of the chronic stage of infection. Consumption of the latent tissue cysts by its definitive host (felids) results in parasite conversion to the sexual stages that localize in neural and muscle tissue and mating followed by excretion of environmentally stable oocysts that can be transmitted to new intermediate hosts, including humans.

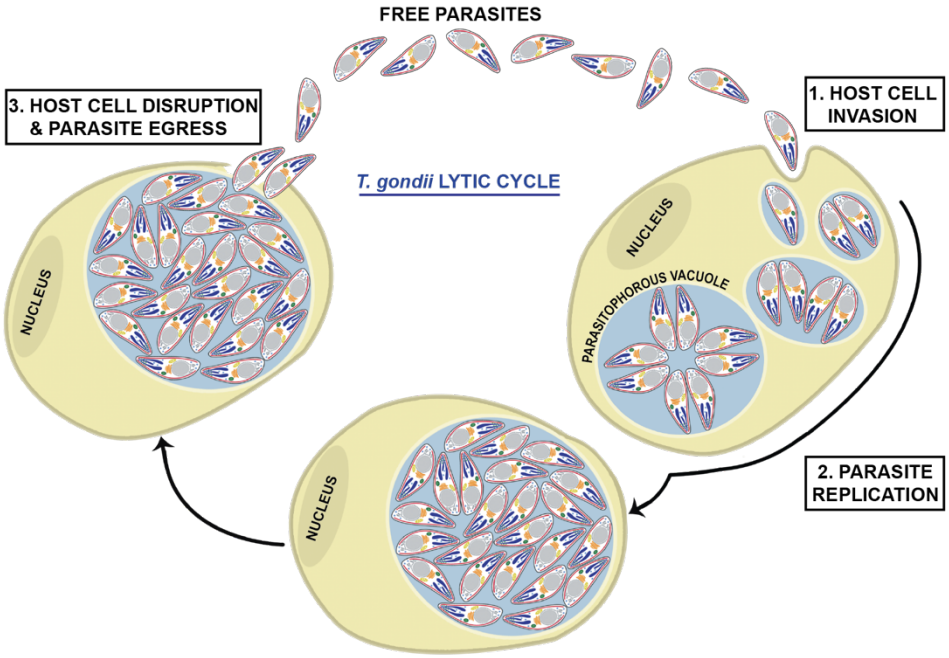

Figure 1.2: The lytic cycle of *Toxoplasma gondii*.

The lytic cycle of *T. gondii* consist of parasite motility, attachment/invasion, replication (endodyogeny) and egress.

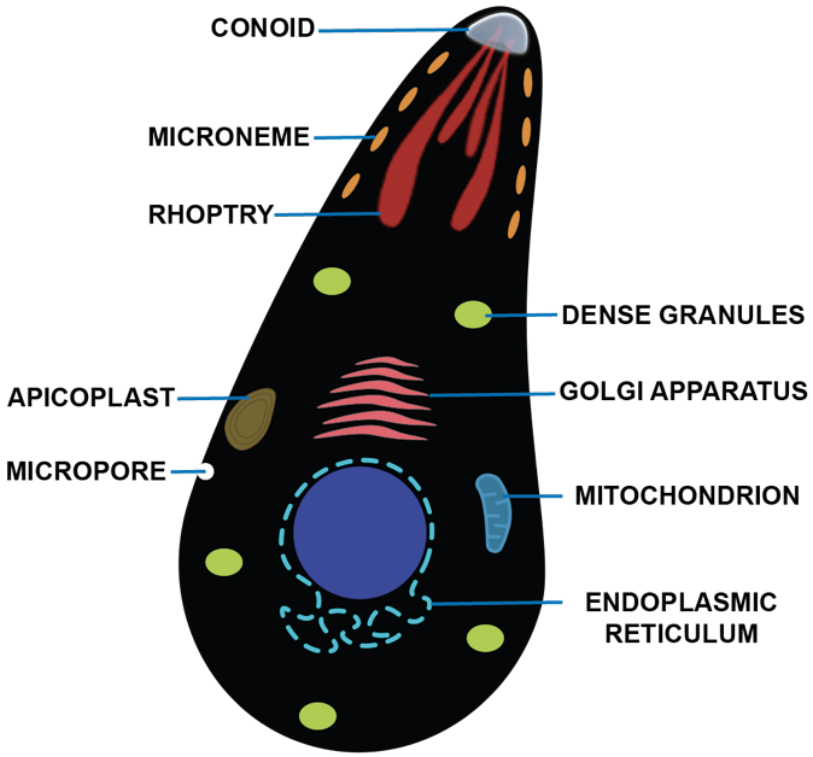

Figure 1.3: Schematic of *Toxoplasma gondii* endomembranes. The scheme displays the different organelles of *T. gondii*: Conoid, Micronemes, Rhoptries, Apicoplast, Micropore, Dense Granules, Golgi Apparatus, Mitochondrion and Endoplasmic Reticulum.

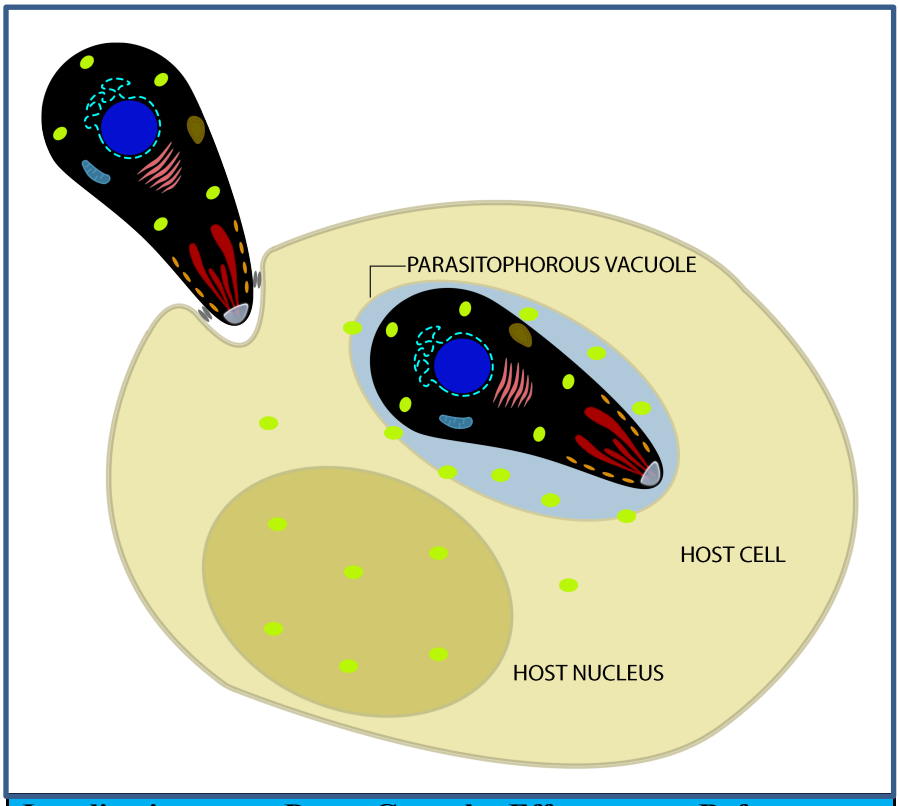

Localization	Dense Granules Effector	Reference
Host Cytosol	MAG1 and GRA18	[106, 111]
Host Nucleus	GRA16, GRA24, GRA28, IST, HCE1/TEEGR, and TgNSM	[86, 107-109, 112-114, 119]
Parasitophorous Vacuole Membrane (PVM)	GRA3, GRA5, GRA7, GRA8, GRA10, GRA14, GRA15, GRA17, GRA19, GRA20, GRA21, GRA22, GRA23, GRA25, GRA35, GRA44 and GRA45	Reviewed in [104, 105, 110]

Vacuolar Space	GRA1, GRA2, GRA4, GRA6, GRA9 and GRA12	Reviewed in [104, 105]

Figure 1.4: Schematic of *Toxoplasma gondii* secreted dense granules effectors localization.

This scheme displays the dense granule effectors and their localization: host cytosol, host nucleus, parasitophorous vacuole membrane and vacuolar space.

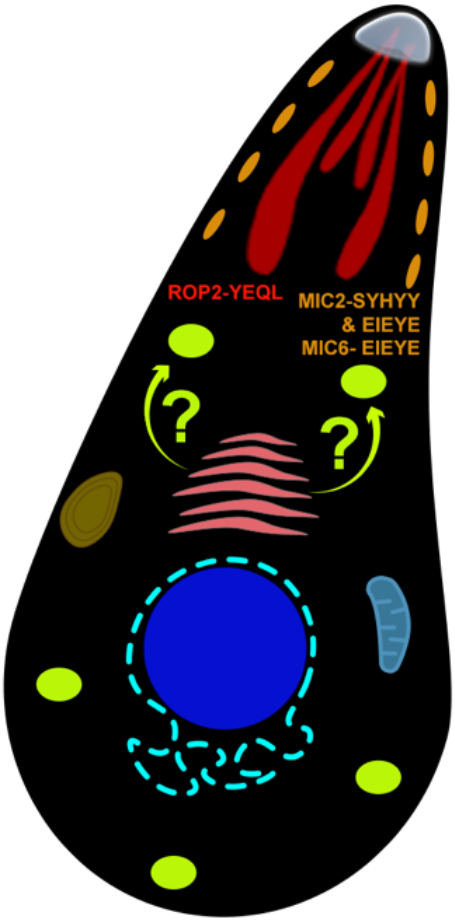

Figure 1.5: Schematic of sorting motif of the secretory vesicles of *Toxoplasma gondii.*

T. gondii schematic showing MIC and ROP proteins ([97]MIC2/MIC6 and [96]ROP2 respectively) containing motifs necessary to determine their trafficking to the rhoptries or micronemes organelles. Dense granules sorting motifs remain an enigma.

CHAPTER 2

DISRUPTION OF *TOXOPLASMA GONDII* INDUCED HOST CELL DNA REPLICATION IS DEPENDENT ON CONTACT INHIBITION AND HOST CELL TYPE

Edwin Pierre-Louis, Menna G. Etheridge, Rodrigo Baptista, Asis Khan, Nathan Chasen, Ronald D. Etheridge. To be submitted to mSphere.

2.1. ABSTRACT

The protozoan *Toxoplasma gondii* is a highly successful obligate intracellular parasite that, upon invasion of its host cell, releases an array of host modulating protein effectors in order to counter host defenses and further its own replication and dissemination. Early studies investigating the impact of *T. gondii* infection on host cell function revealed that this parasite can force normally quiescent cells to activate their cell cycle program. Recent reports by two independent groups identified the dense granule protein effector HCE1/TEEGR as being solely responsible for driving host cell transcriptional changes through its direct interaction with the Cyclin E regulatory complex DP1 and associated transcription factors. Our group independently identified HCE1/TEEGR through the presence of distinct repeated regions also found in a number of host nuclear targeted parasite effectors and verified its central role in initiating host cell cycle changes. Additionally, we report here the time-resolved kinetics of host cell cycle transition in response to HCE1/TEEGR, using the fluorescence ubiquitination cell cycle indicator reporter line (FUCCI), and reveal the existence of a block in S-phase progression and host DNA synthesis in several cell lines commonly used in the study of *T. gondii*. Importantly, we have observed that this S-phase block is not due to additional dense granule effectors, but rather is dependent on the host cell line background and contact inhibition status of the host monolayer *in vitro*. This work highlights intriguing differences in the host response to reprogramming by the parasite and raises interesting questions regarding how parasite effectors may differentially manipulate its host cell depending on the *in vitro* or *in vivo* context.

Keywords: *Toxoplasma gondii*, cell cycle, Cyclin E, FUCCI, S-phase, HCE1/TEEGR, host-parasite interaction, parasite effectors.

2.2. INTRODUCTION

The protozoan *Toxoplasma gondii* is an obligate intracellular pathogen that chronically infects approximately one-third of the human population [1]. This widespread prevalence can be attributed, at least in part, to the successful manipulation of host defense mechanisms [2-4]. Infection is typically initiated either through oral ingestion of tissue cysts from undercooked meat or oocysts that have been shed into the environment by infected felids, the definitive hosts of *T. gondii* [5]. During the acute stage of infection, the rapidly dividing tachyzoite form of the parasite disseminates into multiple organs including the immune-privileged regions of the body such as the central nervous system. Despite a robust mobilization of the adaptive immune response that resolves acute parasitemia, what remains behind, often undetected, are long-lived slow-growing tissue cysts [6, 7]. As a result, in the U.S. more than 60 million people remain chronically infected by *T. gondii*, with disease typically manifesting in those whose immune systems become weakened or compromised [8, 9]. Currently, the few drugs that effectively target this parasite are unable to cure chronic infection and thus allow for multiple rounds of reactivation in susceptible individuals [10].

T. gondii and other related members of the Apicomplexan phylum are defined by the presence of an apical complex structure that serves as a conduit to release, in a temporally regulated manner, the contents of three distinct apical targeted secretory organelles known as micronemes, rhoptries and dense granules, which play a central role in parasite movement, invasion, and modulation of host cells [11-13]. Over the last decade, researchers have shown that as a result of *T. gondii* infection, there is an active global reprogramming of host gene expression with distinct changes manifesting in pathways related to metabolism, transcriptional regulation, cell signaling, inflammation and the cell cycle ([14-16] and reviewed in [4, 17, 18]). The parasite achieves this

remarkable degree of cellular and organismal manipulation, in part, via an arsenal of secreted molecular effectors that it deploys against distinct host targets. Although considerable research efforts have highlighted the important role that the rhoptry secretory organelles play in parasite defense against the host, the dense granules (DG) have risen to a place of prominence as the source of numerous effectors that are critical for host manipulation by the parasite [19-25].

Of the many host transcriptional changes resulting from *T. gondii* infection, one of the most profound and consistent shifts is centered on the host cell cycle program itself [26-28]. The extensively characterized eukaryotic cell cycle consists of four consecutive stages abbreviated as G1, S-phase, G2 and M. The G1/G2 gap (or growth) phases separate the DNA synthesis phase (S-phase) and M or mitotic phase where the replicated genomes are divided into the new daughter cells prior to cytokinesis. The programmed advance of cells from one stage of the cell cycle to the next is tightly controlled by the phosphorylating activities of Cyclins and their associated Cyclin-dependent kinases (Cdk) which are, in turn, regulated by an extensive array of internal and external stimuli ([29]and reviewed in [30]). Initial reports demonstrated that *T. gondii* infection induces a sustained increase in expression of mRNA transcripts association with the G1/S-phase transition [26], while ultimately arresting infected cells at the G2/M transition boundary [27]. The parasite effector responsible for these observed changes has since been identified and shown to be a host nuclear targeted dense granule protein, identified simultaneously by two groups, and referred to both as HCE1 for inducer of host Cyclin E [31] and TEEGR for *Toxoplasma* E2F4-associated EZH2-inducing gene regulator [32]. The HCE1/TEEGR effector was shown to bind and activate the heterodimeric E2F/DP1 transcription factor complex leading to the production of the cell cycle regulator Cyclin E [31] while also activating the epigenetic silencer EZH2 in order to counteract the nuclear factor κB (NF-κB) pro-inflammatory response to parasite infection [32]. In this study

we independently identified HCE1/TEEGR via the presence of distinct internal repeat regions in this protein that are commonly found in many previously identified nuclear targeted effectors of *T. gondii* [33-38]. Although we observed no overt changes in parasite growth *in vitro* or virulence in mice as a result of loss of HCE1/TEEGR, we clearly observed distinct transcriptional signatures belonging to both the activation of the cell cycle program and suppression of NF-κB target genes. Due to the numerous prior reports highlighting the effect of *T. gondii* infection on the cell cycle and the magnitude of activation of the cell cycle program, our study focused primarily on this dimension of HCE1/TEEGR function. To interrogate the actions of this parasite effector on the cell cycle more closely, we implemented the Fluorescence Ubiquitination Cell Cycle Indicator reporter line known as FUCCI and determined the distinct kinetics of S-phase transition which is dependent on both HCE1/TEEGR and the ability of *T. gondii* parasites to effectively traffic DG proteins across the parasitophorous vacuole (PV) membrane [39, 40]. We observed that although infected human foreskin fibroblasts (HFF) and FUCCI (NIH-3T3) cells produced considerable levels of Cyclin E and transitioned into S-phase, they were unable to progress through S-phase and synthesize new genomic DNA (gDNA) independent of the cell culture growth conditions. Recently derived primary mouse fibroblasts (MF), on the other hand, were able to progress through S-phase in an HCE1/TEEGR and contact inhibition dependent manner. This data suggests that the ability of HCE1/TEEGR to drive infected host cells to transit through and complete S-phase is both dependent on the cell line background as well as the status of contact inhibition.

2.3. RESULT

HCE1 (TGGT1_239010) is a host nuclear targeted dense granule protein requiring MYR1 for export.

To date, numerous reports have characterized, in detail, an array of secreted dense granule (DG) proteins of *T. gondii* that are targeted to the infected cell nucleus and directly modulate a variety of host transcriptional pathways. Of the host nuclear targeted DG effectors such as GRA16, GRA24, GRA28, TgIST and TgNSM, it was noted in each published report the presence of internally repeated regions within these proteins that ranged from ~40 to 80 amino acids in length [33-38]. Despite their seemingly ubiquitous presence in host nuclear targeted effectors, there has been no clear universal functional role ascribed to these repeats. The prevalence of this repeat pattern, however, suggested this may be a common feature of nuclear targeted parasite proteins that could be used to identify novel DG effectors. To assess this possibility, we analyzed all *T. gondii* protein sequences containing predicted signal peptides (toxodb.org) using the online genome data-mining tool XSTREAM (https://amnewmanlab.stanford.edu/xstream/). This algorithm allowed for the broad identification of repeated regions in proteins ranging from a perfect match to highly degenerate. Using the XSTREAM program, we identified a hypothetical protein (TGGT1_239010) which contained a duplication of approximately 85 amino acids and a predicted nuclear localization signal (blue) (Figures 2.1A and 2.1B). A phylogenetic analysis demonstrated the presence of this gene in the reference strains of *T. gondii* as well as the closely related *H. hammondi* (Supplementary Figure 2.1A). Of note, is the altered structure of the repeated regions which potentially underwent several rounds of duplication with *H. hammondi* lacking these repeats, Type I and III *T. gondii* strains containing a single duplication and Type II strains having three copies of this repeated region

(Figure 2.1B and Supplementary Figure 2.1B). Although the functional significance of the repeats remains unknown, this duplication suggests the presence of selective pressure to expand these regions. In prior reports this protein effector has been referred to as both HCE1 for inducer of host Cyclin E [31] or TEEGR for *Toxoplasma* E2F4-associated EZH2-inducing gene regulator [32] and so for simplicity, we often to refer to this effector primarily as HCE1 due to the similarity in focus on the host cell cycle phenotype analogous to that reported in the 2019 Panas *et al.,* study. Cellular localization studies were carried out using the parental Type I RH *Δku80Δhxgprt* strain [41] of *T. gondii* combined with CRISPR/Cas9 based introduction of a C-terminal Ty-tag epitope onto the endogenous *hce1* gene [42, 43]. The resulting HCE1-Ty tagged line, referred to here as the Wild Type (WT) strain, was used to infect human foreskin fibroblasts (HFF) for 20 hours (hr) followed by an immunofluorescence microscopy assay (IFA). This assay confirmed that HCE1-Ty is a host nuclear targeted DG protein through colocalization with the dense granule marker GRA7 [44-46] and accumulation of this protein in the infected host cell nucleus (Figure 2.1C top). Because all secreted DG effectors previously observed to traffic to the host cell nucleus appear to require the action of the MYR translocon, we also tagged HCE1 with a Ty-epitope in the *Δmyr1* background and found that the protein was no longer able to be transported across the PV into the host cell and thus failed to accumulate in the host nucleus (Figure 2.1C bottom panel) [31, 47]. The epitope tagging of HCE1 was also verified via Western blotting (Figure 2.1D) and through diagnostic PCR (Supplemental Figure 2.1C) using the methods outlined in Supplemental Figure 2.1D.

HCE1 promotes transcriptional changes to the host cell cycle program.

In order to assess the role of HCE1 in parasite growth and virulence, we generated gene deletion mutants in our epitope tagged cell line (Wild Type) using CRISPR/Cas9 induced breaks in the *hce1* coding region followed by homology repair with the dihydrofolate reductase (DHFR)

drug marker to generate an *Δhce1* Knockout line (Supplemental Figures 2.1C and 2.1D schematic) [42]. The deletion mutant no longer contained the *hce1* gene as verified using diagnostic PCR (Supplemental Figure 2.1C) resulting in loss of expression as depicted in the Western blotting and IFA of infected cells (Figures 2.2C and 2.2D). HCE1 deletion resulted in no significant defect in parasite growth in vitro as demonstrated in our plaquing assays (Figure 2.2A) or virulence in CD1 mice (Supplemental Figure 2.2A), suggesting that HCE1 does not play an essential role in viability in vitro or infection in the mammalian host in the highly virulent Type I strain. In the absence of an overt phenotype, we conducted a whole transcriptome sequencing experiment (RNA-Seq) of HFFs comparing host cells infected with parasites expressing HCE1-Ty (WT) to those in which the *hce1* gene had been deleted (Knockout). HFFs were infected for 16 hrs at a multiplicity of infection (MOI) of 5:1 followed by total RNA isolation and Illumina based sequencing. The resulting data (Figures 2.2B, 2.2C and 2.2D) demonstrated that HCE1 was responsible for the upregulation of pathways associated with the host cell cycle. In this analysis we also observed a downregulation of genes associated with the nuclear factor κB (NF-κB) pro-inflammatory response (Supplemental Figure 2.2B) which supports previously reported data on the effects of HCE1 [31] and TEEGR [32] on infected host cell transcription. As shown in Figure 2.2B, the majority of genes that were significantly differentially expressed (red dots) were downregulated (left quadrant) in the *Δhce1* infected host cells with the red triangles representing specific genes with known involvement in controlling the host cell cycle (reviewed in [30]). Using the DAVID6.8 and KEGG pathway analysis, we examined the top 94 genes with the highest differential expression that were affiliated with known cellular pathways (Figure 2.2C) and observed an enrichment in pathways associate with the “Cell cycle” and “DNA replication”. In examining the top 16 genes that were significantly downregulated across the three replicates (Figure 2.2D) we

observed a concentration of genes involved in cell cycle progression. Although we observed genes that were also being downregulated by HCE1 (Supplemental Figure 2.2B), we have focused on those that were no longer being induced in the Knockout infected host cell for the remainder of the study. Of note, was the upregulation of Cyclin E (CCNE2) and its associated cyclin dependent kinase (CDK2) as well as the machinery involved in origin licensing (e.g. CDT1, CDC6 and MCM2/6) all of which suggested a role for HCE1 in promoting a cellular transition into S-phase [48-50]. This enrichment in genes associated with the host cell cycle was particularly intriguing as numerous prior reports had described the unique effect of *T. gondii* infection inducing a "proliferation response" and arresting cells in G2/M [26-28]. A mechanistic understanding of how HCE1 drives host cell cycle gene expression can now be attributed to the fact that HCE1 interacts with and activates the E2F/DP1 heterodimer leading to induction of cell cycle gene expression [31] while also activating the epigenetic silencer EZH2 which modulates the NF-κB pro-inflammatory response to *T. gondii* infection [32].

HCE1 induces infected host cells into S-phase.

One of the major checkpoints in the transition of mammalian cells into S-phase is the firing of origin replication complexes (ORC) which initiates the process of gDNA synthesis and genome duplication [51, 52]. This event results from the buildup, during G1, of active Cyclin E/CDK2 complexes and the loading of replication machinery at the origins by Cdt1 [50]. The subsequent firing of ORCs is then followed by rapid destruction of Cdt1 (G1 marker) and the buildup of the Cdt1 inhibitor protein Geminin (S-phase marker) in order to prevent the reinitiation of replication [53]. The cyclical buildup and destruction of Cdt1 and Geminin has been shown to be mediated via their interaction with distinct F-box proteins and associated ubiquitin ligases that control the abundance of these S-phase regulators by inducing proteasomal degradation (reviewed in [54]).

Using this information, several groups have fused the F-box targeting domain of Cdt1 and Geminin to fluorescent proteins in order to observe transit through the cell cycle in live cells [55]. Commonly referred to as FUCCI for Fluorescence Ubiquitination Cell Cycle Indicator, these reporters have been integrated in a variety of cell lines and whole animal models to examine factors (e.g. cell type, genes, growth factors and chemical agents) that influence the progression of cells through the cell cycle [39, 40]. To observe the effects of *T. gondii* infection on the host cell cycle directly, we used a FUCCI cell cycle reporter line generated via the transfection of immortalized mouse embryonic fibroblast (NIH-3T3) cells with a FUCCI expressing lentivirus (a generous gift from Dr. Jonathan Eggenschwiler). In this FUCCI cell line the red fluorescent reporter represents Cdt1 levels (G1 phase) while green fluorescence serves as a stand-in for Geminin (S-phase). We infected confluent monolayers of FUCCI reporter cells arrested in G0/G1 with Wild Type (HCE1-Ty tagged), Knockout (*Δhce1*-Ty) and Complemented (*Δhce1*-Ty::HCE1-HA) parasites at a multiplicity of infection (MOI) of 5:1 and observed the host monolayer fluorescence at 20 hrs post-infection. Through examining the fluorescence of infected host nuclei, we observed a clear transition of the majority of FUCCI cells in the monolayer from the G0/G1 (red) into S-phase (green) in both the Wild Type and Complemented line infections (Figure 2.3A left and right). Importantly, we failed to observe any significant fluorescence transition in FUCCI cells infected with the *Δhce1* Knockout line (Figure 2.3A middle). To examine the dependence of S-phase transition on HCE1 at the single cell level, we stained infected FUCCI cells with antibodies to the parasite protein GAP45 to highlight intracellular *T. gondii* and observed that the induction of the green fluorescent S-phase nuclear reporter occurred only in cells infected with Wild Type parasites (Figure 2.3B top) and not in the Knockout infection (Figure 2.3B bottom) [56]. The exact kinetics of this transition to S-phase and the dose-dependence of HCE1 on this transition, however, were

still unclear since our original observations relied only on a single time-point (20 hrs) and MOI (5:1). We next infected FUCCI cells with a range of MOIs (1:1, 5:1, 10:1 and 20:1) and assessed, in real-time, the rate of transition into S-phase following infection. Using automated time course live-cell microscopy, we assessed the kinetics of S-phase transition in host cells infected with increasing MOIs of Wild Type *T. gondii* parasites. Over a period of 20 hrs, we acquired images of infected FUCCI cells at 10-minute intervals and counted the total number of host cell nuclei expressing green fluorescent protein as a readout of S-phase transition (Figure 2.3C). We observed that although the total number of FUCCI cells that transitioned into S-phase was MOI dependent, and likely a function of infection rate, the timing of transition into S-phase was independent of MOI and occurred at approximately 8 hrs post-infection (Figure 2.3C arrow). Therefore, because of the consistency in the kinetics of S-phase induction, we reason that the quantity of secreted HCE1 from an individual Wild Type parasite is sufficient to promote S-phase transition at the maximum rate. To validate the dependence on S-phase transition kinetics on HCE1, we infected FUCCI cells with Wild Type, Knockout and Complemented lines as well as *Δmyr1* and *Δasp5* knockout lines which are known to be defective in DG protein translocation and processing respectively [47, 57]. When *Δhce1* parasites were allowed to infect FUCCI cells, no S-phase transition was observed by immunofluorescence and this phenotype was restored in the Complemented line with kinetics similar to the Wild Type parental strain (Figure 2.3D). Additionally, the loss of MYR1 or ASP5 phenocopied the loss of HCE1, further confirming their role in the localization and maturation of this DG protein. A quantitative analysis and comparison of the number of host cells in S-phase at three time points (0, 12 and 20 hours post-infection) using these different parasite strains demonstrated a clear dependence on secreted HCE1 for the capacity of *T. gondii* infection to drive FUCCI cells into S-phase (Figure 2.3E). These observations are

consistent with prior studies of parasites either lacking HCE1 or lacking the ability to effectively secrete dense granule proteins being unable to promote cell cycle transition in infected cells [31].

HCE1 promotes S-phase progression via Cyclin E production.

As observed in both our RNA-Seq analysis and prior reports on HCE1 effects on the host cell cycle [31], the transcription of Cyclin E (CCNE2) is highly upregulated during *T. gondii* infection. This cyclin plays a well-studied and critical role in the G1 to S-phase transition in replicating cells through its association and activation of the cyclin dependent kinase CDK2 (reviewed in [58, 59]). To examine Cyclin E production at the protein level, we examined human foreskin fibroblasts (HFF) infected with either Wild Type, Knockout, HCE1 Complemented or *Δmyr1* Knockout strains and assessed the relative change in Cyclin E production after 24 hrs of infection. We observed a clear dependence of HCE1 export for *T. gondii* parasites (red) to be able to induce the production of nuclear targeted Cyclin E (green) in infected HFFs (Figure 2.4A). Parasite strains lacking HCE1 (Knockout) or unable to export HCE1 into the host cell (MYR1 Knockout) were not able to induce Cyclin E expression while the Complemented line demonstrated robust nuclear expression of this critical cell cycle regulator. The HCE1 dependent induction of Cyclin E production was also confirmed using Western blotting (Figure 2.4B). At 24 hrs post-infection, we compared Wild Type, Knockout and HCE1 Complemented lines and observed a significant increase in Cyclin E. A time dependent increase in Cyclin E was also demonstrated in a time course analysis of cyclin production at 8, 16 and 24 hrs post-infection (Figure 2.4C). The use of antibodies to GAP45 highlighted the expanding number of replicating parasites across the time course while antibodies to the host actin protein (hActin) was used to ensure equal loading of uninfected (UI) and infected host cell material. The increase in parasite GAP45 levels also supported our prior observations that a lack of HCE1 does not appear to

significantly impact parasite growth in vitro (Figure 2.2A plaque assay). We finally wanted to determine if additional effectors from the parasite or aspects of the infection process itself were playing a cooperative role with HCE1 in the induction of Cyclin E expression. To achieve this, we conducted a heterologous expression experiment where we transfected HFF cells with an overexpression vector containing HCE1-Ty with GFP fused to its N-terminus as a test of sufficiency. We noted the localization of this protein fusion product in the nucleus of transfected cells, observing green fluorescence from the GFP N-terminal fusion and also labeling of the Ty-epitope which is fused to the C-terminus of HCE1 (Figure 2.4D top). We next assessed whether or not the expression of the HCE1-Ty fusion protein in HFFs also activated Cyclin E production and observed that all HFF cells expressing HCE1 (green) also showed increased expression of Cyclin E (red) at 24 hrs post-transfection (Figure 2.4D bottom). This work confirmed prior observations that HCE1 alone is sufficient to drive the production of Cyclin E and thus an activation of the cell cycle transition into S-phase [31].

Infected HFF and FUCCI cells fail to progress through S-phase.

Prior reports on the ability of *T. gondii* infection to promote host cells to enter into the cell cycle have, with few exceptions, concluded that infection leads to progression through S-phase with arrest in G2/M and with infected cells failing to undergo mitosis and cytokinesis [26, 47, 60]. To address this aspect of the cell cycle progression, we examined the ability of infected cells to replicate their genome via the incorporation of the alkyne containing thymidine analogue 5-ethynyl-2′-deoxyuridine (EdU) and its subsequent detection by a fluorescent azide reporter through a copper catalyzed click-chemistry reaction [61]. Using actively dividing HFFs (i.e. sub-confluent monolayer growing in 20% serum) as a positive control, we saw clear incorporation of EdU (green), highlighting the ability of these cells to synthesize new gDNA as part of their normal

replication program (Figure 2.5A top). Interestingly, we found that when confluent HFFs were infected with Wild Type *T. gondii*, we observed no evidence of cells being able to transit through S-phase and incorporate EdU in spite of an abundance of S-phase cyclins being produced in response to infection (Figure 2.5A bottom). Using HFFs, we could not rule out the possibility that although they were producing high levels of Cyclin E as seen throughout Figure 2.4 they, unlike the FUCCI cells, were unable to fire their origins of replication and actually enter in S-phase. To examine this further, we decided to use flow cytometry to observe gDNA replication directly in FUCCI cells that had been infected with Wild Type parasites. We compared uninfected confluent G0/G1 arrested FUCCI cells (UI 1% Serum) to both actively growing uninfected FUCCI cells (UI 20% Serum) and FUCCI cells infected with Wild Type parasites (Figure 2.5B left). As expected, a significant proportion of actively growing uninfected and parasite infected FUCCI cells transitioned into S-phase as demonstrated by the accumulation of green fluorescence signal in these cells. We next gated solely on those FUCCI cells that had transitioned into S-phase (green) and examined the level of EdU incorporation present in these S-phase cells. Curiously, we observed that only the uninfected, actively growing, FUCCI cells (UI 20% Serum) appeared to be synthesizing new gDNA (Figure 2.5B right panel gray population). Thus, much like our observations in HFF cells (Figure 2.5A), there was no detectable gDNA replication in the infected FUCCI cells despite a clear transition into S-phase. This suggested that although the infected cells fired their origins of replication and increased their S-phase Geminin levels (green), they were blocked in their ability to effectively progress through this stage.

As has been described in multiple cell cycle studies, there are secondary control systems in place to block the ability of mammalian cells to progress through S-phase despite an abundance of necessary cyclin-cdk complexes and growth stimuli. These negative regulation mechanisms are

varied and can be activated by DNA damage, stress or contact inhibition [62-64]. Although there are reports that *T. gondii* infection can induce DNA damage in infected host cells, we initially suspected that contact inhibition may be responsible for blocking S-phase progression [65]. To examine the effect of contact inhibition on this block more closely, we employed techniques pioneered by groups studying fibroblast wound healing to assess the effect of release from contact inhibition on S-phase progression [66, 67]. As depicted in Figure 2.5C, we used a four chamber 35 mm cell culture dish containing a removable four quadrant insert for our assay. When removed, the resulting scar breaks contact inhibition on the monolayer and stimulates the entrance of cells into the barren region between quadrants in order to reestablish confluency. The use of these four chambered culture dishes allowed us to also ensure intraexperimental consistency as the host monolayer in each dish was subjected to the same media and growth conditions. For simplicity, we have color-coded the experimental conditions applied to each of the four regions; beginning in the top left quadrant and moving clockwise, we have the uninfected host cell control (UI) (blue), followed by the Wild Type (WT) (green), the *Δhce1* Knockout (KO) (red) and the HCE1 Complemented (Comp) infections (orange). We first sought to examine the potential effect of release of contact inhibition on S-phase progression and EdU incorporation using both our HFF and FUCCI cell lines in this four-quadrant wound healing assay format. Using HFF cells, we observed that irrespective of the infection status and whether the insert was present (Figure 2.5D top (+ contact inhibition)) or removed (Figure 2.5D bottom (- contact inhibition)), these cells could not effectively progress through S-phase and incorporate EdU. Using this same experimental setup applied to FUCCI cells (Figure 2.5E) we again found no effect of contact inhibition on S-phase progression at 20 hrs post-infection. Similar to wounding the monolayer, studies have demonstrated that ‘splitting and replating’ the cells at lower density supplemented with fresh serum

can quickly reinstate proliferation in contacted-inhibited cells [64]. However, when we employed this technique on infected HFF cells that were trypsinized, removed from the dish and replated in 20% serum they, unlike uninfected HFF cells, failed to actively synthesize gDNA (Supplemental Figures 2.5A and 2.5B). This suggested the presence of either a parasite driven mechanism blocking S-phase progression or an as yet unknown cell-intrinsic mechanism. We repeated the replating experiment using *Δmyr1* parasites and again observed no return to S-phase progression with EdU incorporation rates remaining unchanged making it unlikely that a dense granule effector was blocking gDNA synthesis (Supplemental Figure 2.5C) [47, 68].

Contact inhibition is required to block S-phase progression in primary mouse fibroblasts.

The cell lines we examined thus far were either high passage primary lines (HFF) or immortalized (FUCCI NIH-3T3), and so we decided to examine the ability of parasites to induce progression through S-phase in recently isolated mouse fibroblasts (MF). We first isolated primary MFs from C57BL/6 mouse tissue, grew cells to confluency in each quadrant of the four-chamber dish and subjected each quadrant to conditions analogous to those previously described (see Figures 2.5C, 2.5D and 2.5E). Infection was allowed to progress for 20 hrs in the presence of EdU in 1% serum before analysis. In the initial control experiment, the chamber insert was retained in order to preserve contact inhibition and we observed that regardless of the parasite strain or conditions used during infection, no increase in incorporation of EdU was seen (Figure 2.6A top). Focusing at a higher magnification on the center of the four-quadrant junction (Figure 2.6A bottom), we are able to assess the level of *T. gondii* infection using the parasite specific GAP45 antibody (red) and the presence of DAPI stained host cell nuclei (blue) [56]. A quantitative analysis demonstrated no significant change in EdU incorporation irrespective of the infection condition or

parasite strain used (Figure 2.6B). To assess the role of contact inhibition, we again infected each chamber of confluent cells with their respective strains as before, however, directly following infection we removed the chamber insert (- contact inhibition) and allowed the infection to proceed overnight in the presence of EdU and 1% serum. At 20 hrs post-infection we fixed, stained cells and examined the level of EdU incorporation (Figure 2.6C top) with a focus on the central junction. Under these conditions, we observed a striking increase in EdU positive cells (green) in both the WT and Comp infected quadrants when contact inhibition was removed and failed to see comparable changes in either the uninfected (UI) or *Δhce1* Knockout (KO) infected monolayers (Figure 2.6C top). This difference is also clearly illustrated when we focus on the central junction of the plate to highlight each quadrant (Figure 2.6C bottom). Quantitative analysis of three independent replicates demonstrated a significant increase in the percentage of cells synthesizing new gDNA in the WT and Comp infected MFs with no significant change in the uninfected (UI) or *Δhce1* (KO) infected quadrants (Figure 2.6D). To visually highlight the dramatic differences observed, we also examined central regions of each quadrant in both the presence (Figure 2.6E) and absence (Figure 2.6F) of contact inhibition with each quadrant color-coded to match the starting quadrant. From this work, it appears that a lack of gDNA replication observed in *T. gondii* infected cells could result from either a cell line specific block as seen in HFFs and NIH-3T3 cells or to contact inhibition as seen with MF infections.

2.4. DISCUSSION

The work presented here not only supports many of the prior published observations concerning the action of the HCE1/TEEGR effector, but also furthers our understanding of how *T. gondii* manipulates the host cell cycle in distinct ways. In our transcriptome analysis, we

confirmed the ability of this nuclear targeted dense granule effector to drive both the transcriptional activation of the cell cycle program as well as downregulation of NF-κB pro-inflammatory genes [31, 32]. Due to the prominence of the cell cycle pathways activated by HCE1, and because multiple prior studies had described this phenomenon, we focused our work primarily on dissecting this dimension of HCE1's function in more detail. In our initial studies, we did not observe overt changes to parasite growth in vitro or virulence in mice when HCE1 was absent, which we suspect is likely due to distinct growth conditions and the use of the highly virulent RH Type I strain of *T. gondii* for these experiments. It seems that many of the secreted DG proteins studied to date, similarly do not individually contribute in a significant way to parasite growth in vitro and their contribution to virulence is often masked in the Type I strain due to the plethora of effectors it deploys to effectively defend against innate cellular defenses ([33, 34, 36, 37, 47, 68] and reviewed in [4]). It should be noted that in many of the preceding reports on secreted parasite effectors, the use of the intermediate virulent ME49 (Type II) strain was, which allowed for the detection of more subtle differences in growth and virulence. Our initial interest in the manipulation of the host cell cycle by HCE1 prompted us to use the FUCCI cell cycle reporter line to investigate the kinetics of S-phase transition after infection. We were led to this option after repeated attempts to assess the host cell cycle status using standard DNA staining and flow cytometry failed to produce clear distinctions between the major stages (G1, S-phase, G2). We suspect that the DNA content contributed by growing parasites within infected cells may have been confounding our ability to accurately assess changes in host DNA content. Our examination of the infected host cell cycle using FUCCI cells, therefore, allowed us to directly measure the timing of transition into S-phase that could be looked at across an infection time course. From these experiments, we were able to pinpoint the approximate timing of S-phase transition after the

beginning of infection (approximately 8 hours) and realized that this timing could not be accelerated by increasing the multiplicity of infection of individual host cells. This suggested that the amount of HCE1 secreted by a single invaded tachyzoite is sufficient to induce host cell transition into S-phase at the maximal rate. The RNAseq and Western blotting experiments confirmed prior observations showing that HCE1 induced a dramatic increase in the host transcript and protein levels of Cyclin E (CCNE2) over time [31]. We validated that heterologous expression of HCE1 in HFF cells was also sufficient to induce Cyclin E production. In our continued analysis, however, we noted that despite the assumption that infected cells are blocked in G2/M, we never observed host nuclei that appeared enlarged or even in an intermediate stage of mitosis. We assumed that if S-phase initiated at 8 hours post-infection, we should be seeing cells at some stage of mitosis 20 hrs post-infection even if cytokinesis was being hindered by parasite replication and potential steric hindrance. To look at this more closely, we used the click-chemistry amenable thymidine analogue (EdU) in order to visualize this process [69]. Curiously, we found that infected HFF cells failed to incorporate EdU at levels we could measure either using microscopy or flow cytometry and thus appeared blocked in their ability to progress through S-phase. We were unsure, however, if infected HFFs were in fact transitioning fully into S-phase. Conveniently, the FUCCI cells allowed us to resolve this issue since we had already observed that, when infected, these cells transition into S-phase as evidenced by the destruction of their reporter of Cdt1 (red) and the accumulation of the Geminin reporter (green). These fluorescent reporters gave us a window into the process of pre-replication complex destruction that occurs following the initiation of DNA replication [55]. Unexpectedly, even when pushed into S-phase the FUCCI line (mouse NIH-3T3) failed to synthesize new DNA, mirroring the observations from infected HFF cells. Our first concern was that this may be due, in part, to the negative feedback signals on cell cycle progression

such as contact inhibition [29]. As a result, we conducted a hybrid infection/wound healing assay in order to produce a controlled release from contact inhibition in infected cells. We surmised that following such release, this inhibitory signal would be removed and, therefore, should allow DNA replication to proceed [66, 70]. Instead, we found that breaking contact inhibition did not rescue DNA replication even when infected cells were replated at a sub-confluent concentration under conditions normally supporting active growth. Due to the fact that prior work examining other DG proteins such as GRA16 and GRA24 had demonstrated that these effectors manipulate both the tumor suppressor protein p53 and the mitogen activated kinase signaling pathway p38 respectively, it seemed plausible that additional DG effectors could be contributing to the block in DNA synthesis [33, 34]. We suspected that *T. gondii* may be both inducing entrance into S-phase with HCE1, while also blocking progression through S-phase via an additional unidentified effector. However, we observed that even when HFF cells were infected with the *Δmyr1* stain of *T. gondii*, they were unable to initiate DNA replication even when replated under active growing conditions [47]. This suggested that the DNA replication block we observed was likely not due to the presence of an additional secreted DG protein effector and the fact that all of the cancer lines we have tested are able to progress through S-phase and replicate their genomes argued against a possible rhoptry effector being responsible. Other possible reasons for the block in S-phase progression were the presence of cell cycle inhibitors being activated due to host DNA damage or some other infection associated stress. The first potential cell cycle regulator we sought to investigate was the DNA damage responsive cyclin-cdk inhibitor p21 (Cip) and the contact inhibitor p27 (Kip) [71-74]. Due to the commercial availability of homozygous $p21^{-/-}$ knockout mice, we isolated primary fibroblasts (MF) from both wild type and $p21^{-/-}$ C57BL/6 mice in order to examine the role of p21 on the observed block in DNA replication in *T. gondii* infected cells and noticed there was no

difference between the infected cell lines (data not shown) [75]. This suggests that p21 does not play a role in suppressing DNA replication in *T. gondii*-infected cells. We further evaluate the MF cells to establish the assay methodology and confirm that wild type MFs would be unable to replicate their DNA following infection as seen in HFFs and FUCCI cells. When confluent monolayers of wild type MFs were infected, we observed, as expected, an inability of these cells to incorporate EdU and progress through S-phase. To our surprise, however, when we removed contact inhibition from infected wild type MFs, we observed, for the first time, the restoration of DNA replication that was also completely dependent on the presence of HCE1. This observation demonstrated that contact inhibition was indeed playing a role in suppressing DNA replication in infected confluent monolayers. However, this also highlighted that there was an additional cell intrinsic block in S-phase progression that seemed to be operating in our HFF and FUCCI cells. This result raises the question as to what cell intrinsic differences are responsible for this block in HFFs and FUCCI NIH-3T3 cells [76]? Although still unclear, if we compare our two primary fibroblast cell lines (HFFs and MFs), it is worth noting that our in-house derived MFs were freshly isolated and at a low passage number (~1-3) while our HFFs were often used after 20+ passages. The effects of high passage number and continuous culture may have, unexpectedly, selected for primary fibroblasts that have significantly modified their cell cycle programs and thus are altered in their sensitivity to culture conditions or even infection. This observation does raise the possibility that even primary cell lines can respond differently to infection based on their origin or passage history.

It still remains to be determined exactly how *T. gondii* benefits from driving its infected host cell into the cell cycle since, at least for the tachyzoite form of the parasite, the lytic cycle is extremely rapid. At the moment we cannot rule out the possibility that the main function of HCE1

is, in fact, to manipulate the NF-κB response to infection with the concomitant influence on the host cell cycle being simply a secondary effect. Regardless, the overlap in these pathways is intriguing as a number of studies have observed significant levels of crosstalk between the NF-κB signaling pathway and progression through the cell cycle [77]. In considering this parasites desire to influence its host cell cycle, it has been shown that *T. gondii* appears to have an innate preference for host cells that are in the G1 or S-phases of the cell cycle, while seeming to avoid infecting cells that are in G2/M [78]. Additionally, *T. gondii* exhibits a diminished rate of growth and tendency to convert into cyst-forming bradyzoites in host cells that overexpress autoantigen-1, a negative regulator of the cell cycle [79]. These phenomena suggest that the parasite may benefit in some way by choosing to infect host cells with the capacity to enter into S-phase during the lytic cycle. Although our studies have yet to determine the mechanistic basis for the block in DNA synthesis in HFF or FUCCI cells, it is likely that these phenomena are anomalous as recently derived, and arguably more physiologically relevant, host cell fibroblasts can be driven to replicate their genomes through the actions of HCE1. Further studies will be necessary to determine if the duplication of the host genome occurs in other low passage mammalian cell types and if this provides any benefit for parasite expansion or long-term persistence during in vivo animal infections.

2.5. ACKNOWLEDGMENTS

We would like to sincerely thank Jonathan Eggenschwiler, Beejan Asady and the Silvia Moreno lab at the University of Georgia for help and reagent support. We also thank Peter Bradley for helpful discussions and reagents, John Boothroyd and Mohamed-ali Hakimi for kindly supplying important cell lines. Our work would not have been possible without the support of the

members of the Center for Tropical and Emerging Global Diseases (CTEGD), Julie Nelson and the CTEGD Cytometry Shared Resource Laboratory, the T32 Training in Tropical and Emerging Global Diseases grant (T32AI060546) and funding from the NIH/NIAID (R21AI142431).

2.6. MATERIALS AND METHODS

Parasite and Cell Culture

T. gondii tachyzoites were maintained by serial passage in both human telomerase reverse transcriptase (hTERT) and human foreskin fibroblast (HFF) monolayers grown in complete Dulbecco's modified Eagle's medium (DMEM) containing 4.5 g/L glucose, 4 mM L-glutamine, 1X penicillin-streptomycin solution (Corning) with 10% cosmic calf serum (CCS) at 37°C in 5% CO_2. Parasite strains used in this study are listed in Table S2.1. Primer sets and plasmids are respectively listed in Table S2.2 and S2.3. Stable transgenic parasites were selected in 25 μg/mL mycophenolic acid (MPA) and 25 μg/mL xanthine (Xa), 3mM pyrimethamine (Pyr), or fluorodeoxyribose resistance (FUDR) (Sigma).

The CRISPR-Cas9 system was used to generate endogenous tagged, gene disrupted and complemented strains [43, 80]. For this study, all the CRISPR/Cas9 vectors (pSAG1::Cas9-U6::sgRNA (variable region)) were generated in a similar fashion done by Shen et al., 2014 to change the UPRT targeting gRNA to other specific guide sgRNA listed in Table S2.2. To generate the endogenous TgRH *Δku80, Δhxgprt*, *hce1*-Ty-tagged line, the TgRH *Δku80, Δhxgprt* was used. About 1 kb of *hce1* gene was amplified from the parental genomic DNA via PCR (Table S2.2). The resulting fragment, placed in frame with the Ty epitope tag followed by a stop codon, was subsequently inserted via Gibson assembly into the pLIC vector harboring the *hxgprt* gene that can be used as a selection cassette. The targeting vector along with the (pSAG1::Cas9-U6::sgHCE1) construct were used for co-transfection hTERTs cells with parental parasites and

selected with the appropriate drugs (Table S2.1). This CRISPR/Cas9 vector (pSAG1::Cas9-U6::sgHCE1) was generated with *hce1* targeting sgRNA via PCR mutagenesis in the original CRISPR/Cas9 plasmid (pSAG1::Cas9-U6::sgUPRT). The Q5 site-directed mutagenesis kit (New England BioLabs) was used to perform the PCR mutagenesis with pSAG1::Cas9-U6::sgUPRT plasmid as template. Parasites were single-cloned into 96-well plates by limiting dilution, screened for endogenous integration at the correct locus via IFA (immunofluorescence imaging) and PCR (Table S2.2, Figure 2.1C and Supplemental Figure 2.1C).

To generate the HCE1 knockout line TgRH *Δku80, Δhxgprt, hce1*-Ty-HXGPRT, *Δhce1*-Ty::Pyr, the endogenous tagged line TgRH *Δku80, Δhxgprt, hce1*-Ty-HXGPRT was used. Firstly, the "pSAG1::Cas9-U6::sgUPRT" vector was altered to sgRNA targeting the *hce1* gene to generate the CRISPR cutting vector "pSAG1::Cas9-U6::sg*hce1* cutting" using Q5 site-directed mutagenesis kit (New England BioLabs). Secondly, the DHFR drug marker amplicon with 40bp homology flanking region to *hce1* was amplified. The resulting CRISPR cutting vector "pSAG1::Cas9-U6::sg*hce1* cutting" was used along with the DHFR amplicon to subsequently transfect the endogenous HCE1-Ty tagged parasites TgRH *Δku80, Δhxgprt, hce1*-Ty-*HXGPRT*. The parasites were then selected with Pyrimethamine (Table S1) and were screened via IFA and PCR for gene disruption of the *hce1* gene (Table S2.2, Figure 2.1C and Supplemental Figure 2.1C).

The complemented strain TgRH *Δku80, Δhxgprt, hce1*-Ty-HXGPRT*, Δhce1*-Ty::Pyr, *Δuprt*::*hce1*-HA-Fudr was generated using the "pUPRT-*vha1* cDNA-3xHA" shuttle vector (81), a gift from Moreno Silvia, University of Georgia Athens, which contains the 5' and 3' UTR's of the *uprt* gene [82, 83] and the corresponding CRISPR vector. A generated "pUPRT-*hce1*-HA" vector was first assembled via Gibson Assembly (NEB) using amplicon from the pUPRT-*vha1* cDNA-

3xHA vector and the amplicon from genomic DNA wild type RH *Δku80, Δhxgprt* for *hce1*. The CRISPR plasmid was then generated as previously described above with the corresponding sgRNA for the *uprt* gene locus to construct "pSAG1::Cas9-U6::sgUPRT". Both plasmids were subsequently used to co-transfect knockout parasites TgRH *Δku80, Δhxgprt, hce1*-Ty-HXGPRT, *Δhce1*-Ty::Pyr, then selected for FUDR resistance in order to successfully generate the complemented strain TgRH *Δku80, Δhxgprt, hce1*-Ty-HXGPRT, Δ*hce1*-Ty::Pyr, Δ*uprt*::*hce1*-HA-Fudr via limiting dilution. Complementation was further assessed by visualizing the effector translocation via IFA and PCR for gene insertion and crossover was checked for the *hce1* and *uprt* (Table S2.2, Figure 2.1C and Supplemental Figure 2.1C). Additional primers were used to check each strain lysate for positive ROP18 *Toxoplasma gondii* and construct the pUltra/eGFP-HCE1-Ty mammalian expression vector.

Immunofluorescence Assays

HFF cells were grown on 12mm glass coverslips to confluency and then infected. Samples were fixed with 4% formaldehyde in PBS for 10 minutes, then permeabilized with 0.5% Triton X-100 in PBS for 10 minutes and blocked in 5% cosmic calf serum (CCS) in PBS for 30 minutes. Cells were incubated with primary antibodies for 30 to 60 minutes and then washed three times in PBS (see Table S2.4 for primary antibodies used). Secondary antibodies, goat anti-mouse IgG Alexa fluor 488 and goat anti-rabbit IgG Alexa fluor 594 (Life Technologies) as well as DAPI were added for 30 to 60 minutes followed by a PBS wash. Coverslips were mounted with Fluoro-Gel (Electron Microscopy Sciences) and samples were examined using the Lionheart™ FX Automated Microscope (BioTek Instruments, Inc.).

Plaque Assay

Confluent monolayers of HFF cells grown in 6 well plates were infected with 100 tachyzoites/well. Plates were incubated at 37˚C with 5% CO_2 for 7 days without disruption. On day 7, the wells were washed once with PBS, incubated in 100% ethanol for 5 minutes followed by staining with crystal violet (CV). Plates were washed with deionized (DI) water, air-dried and were visualized using the ChemiDocTM MP Imaging System (Biorad).

RNA-seq Mapping and Differential Expression Analysis

Six Paired-end samples, corresponding to three biological replicates WT and KO were individually aligned to the human reference genome (GRCh38/hg38) using the software HISAT2 (PMID: 31375807) under default parameters. For the differential expression analysis, we used HTseq (PMID: 25260700) and Bioconductor/DESEq2 (PMID: 25516281). HTseq-count tool was used to transform genetic depth information into a count of readings by gene overlapping into the gtf annotation of GRCh38 genome. Count output files were obtained for each replicate for each condition (WTs and KOs). The DESeq2 Bioconductor package version 1.26.0 was used to determine differentially expressed genes, data normalization was performed using the median of ratios method, and the default parameters were followed, the transcripts showing a log2 fold change > 1.5 and that they presented a statistically significant differential expression (padj = <0.05) were selected. The genes differentially expressed by DESeq2 were classified between down-regulated and up-regulated. Visualization of heatmaps and volcano plots were made by using gplots/heatmap3 and Bioconductor EnhancedVolcano R packages.

EdU Assay

For flow cytometry, infected and control monolayers were cultured in DMEM complete media containing 2 μm EdU (5-ethynyl-2'-deoxyuridine) for 24 hours. Immunofluorescence

assays were performed on HFF cells using the Click-iT® EdU Alexa Fluor® 488 kit (Invitrogen) and imaged with the Lionheart™ FX Automated Microscope (BioTek Instruments, Inc.). FUCCI (Fluorescent Ubiquitination-based Cell-Cycle Indicator) cells were stained using the Click-iT® EdU Alexa Fluor® 405 kit (Invitrogen) and analyzed with the CytoFLEX flow cytometer (Beckman Coulter) and FlowJo software (Tree Star).

To assess DNA replication in monolayers, confluent and quiescent HFF cells were infected with wild type or mutants parasites for about 4 to 6 hours and positive control monolayers were cultured in DMEM complete media. All monolayers were washed with HBSS, trypsinized, resuspended with either 1 or 20% CCS DMEM depending on the condition of the experiment; the cells were subsequently seeded to new coverslips ranging 60 to 80% confluency per well. Analysis of the percentage of cells in S-phase was determined by dividing the number of EdU incorporation in actively growing cells (Alexa Fluor 488) by the total number of cells labeled with DAPI nuclei. GAP45 antibody was used to stain parasites membrane.

Wound Healing Assay in mouse fibroblast (MF) cells.

Mice ears were obtained from C57BL/6 mice wild type for tissue biopsy following the Jaenisch Lab protocol by Kathy Hoover of the Jones Lab with few modifications done by Tarleton lab at University of Georgia Athens (UGA) and our group. The ears were gifts from Kim Klonowsky lab at UGA and the mice were purchased from Charles River Laboratories (Wilmington, MA). These cells were harvested and when reached confluency they were passed or frozen for future experiments. They were then cultured in DMEM complete media containing 10% CCS or FBS. All monolayers were washed with HBSS (Hanks' Balanced Salt Solution), trypsinized, resuspended with either 10% CCS or FBS then the cells were subsequently seeded to culture-insert 4 well Ibidi u-Dish^{35mm} ranging 60 to 80% confluency per well in 5% CO_2 high-

humidity incubator at 37°C. The cells were infected with the appropriate parasites lines for about 4 hours resulting to a complete monolayer invasion, then the monolayer was gently washed with 1% CCS to be subsequently cultured with 2μM EdU (5-ethynyl-2'-deoxyuridine) for about 18 to 20 hours for the MF cells and 24 hours for the HFF and FUCCI cells before the wound get completely saturated with cells if any. An immunofluorescence and a Click-iT® EdU assays were subsequently performed on the MF (or HFF and FUCCI cells) to analyze cells in S-phase as previously described above.

Western Blotting

HFF cells were collected at 8, 16, and 24 hours post infection. Monolayers were lysed in 100μl of 1X laemmli buffer, resolved by SDS-PAGE, and transferred onto nitrocellulose membranes. Immunoblots were probed with primary antibodies in 3% milk in PBS for 1 hour (see Table S2.4 for antibodies used), washed in 0.5% PBS-Tween, and then incubated for 1 hour with secondary antibodies conjugated to IRDye 680CW (goat anti-rabbit or goat anti-mouse) or IRDye 800CW (goat anti-rabbit or goat anti-mouse) (LI-COR Biosciences) and signals detected using the ChemiDocTM MP Imaging System (Biorad).

FUCCI Cell Cycle Analysis

Fluorescence Ubiquitination-based Cell Cycle Indicator (FUCCI) cells were seeded in 24 well plates and grown to confluency. Cells were synchronized to G1 phase (red) by serum depletion 24 hours prior to infection. Parasites were collected and washed once in hanks balanced salt solution (HBSS). Monolayers were infected with an MOI of 20. Using the Lionheart™ FX Automated Microscope (BioTek Instruments, Inc.) the plate was incubated at 37˚C with 5% CO_2 and time course images were collected every 10 minutes for 20 hours. Red and green FUCCI cells were counted for each time point using the Gen5 3.0 software (BioTek Instruments, Inc.).

Phylogenetic Analysis

Orthologs of TGGT1_239010 from reference strains of 12 different haplogroups of *T. gondii* and an out group of *Hammondia hammondi* were retrieved from ToxoDB (www.toxodb.org) and aligned using Clustal (84) with a gap opening penalty of 30 and extension penalty of 0.75. The evolutionary history was inferred by using the Maximum Likelihood method and JTT matrix-based model (85) in MEGA X (86) based on 1000 bootstrap replicates [87]. Initial tree(s) for the heuristic search were obtained automatically by applying the Maximum Parsimony method.

2.7. AUTHOR CONTRIBUTION

EPL, MGE and RDE designed and performed the experiments, analyzed the data and generated the figures. RB analyzed the RNA-Seq data and generated the resulting figures. AK and NC contributed the phylogenetic analyses and associated trees. RDE and EPL wrote the manuscript with author input.

2.8. DECLARATION OF INTERESTS

The authors declare no conflict of interest.

2.9. REFERENCES

1. Pappas G, Roussos N, Falagas ME. Toxoplasmosis snapshots: global status of Toxoplasma gondii seroprevalence and implications for pregnancy and congenital toxoplasmosis. Int J Parasitol. 2009;39(12):1385-94. Epub 2009/05/13. doi: 10.1016/j.ijpara.2009.04.003. PubMed PMID: 19433092.

2. Dubey JP, Beattie CP. Toxoplasmosis of animals and man. Boca Raton: CRC Press; 1988. 220 p.

3. Chitnis CE, Blackman MJ. Host cell invasion by malaria parasites. Parasitol Today. 2000;16(10):411-5. PubMed PMID: 11006471.

4. Hakimi MA, Olias P, Sibley LD. Toxoplasma Effectors Targeting Host Signaling and Transcription. Clin Microbiol Rev. 2017;30(3):615-45. Epub 2017/04/14. doi: 10.1128/CMR.00005-17. PubMed PMID: 28404792; PMCID: PMC5475222.

5. Dubey JP. The history and life cycle of Toxoplasma gondii. In: Weiss LM, Kim K, editors. Toxoplasma gondii the model Apicomplexan: perspectives and methods. New York: Academic Press, Elsevier; 2007. p. 1-17.

6. Barragan A, Sibley LD. Migration of Toxoplasma gondii across biological barriers. Trends Microbiol. 2003;11.

7. Ferguson DJ, Hutchison WM, Pettersen E. Tissue cyst rupture in mice chronically infected with Toxoplasma gondii. An immunocytochemical and ultrastructural study. Parasitol Res. 1989;75(8):599-603. Epub 1989/01/01. doi: 10.1007/BF00930955. PubMed PMID: 2771928.

8. Luft BJ, Remington JS. Toxoplasmic encephalitis in AIDS. Clin Infect Dis. 1992;15(2):211-22. PubMed PMID: 1520757.

9. Israelski DM, Remington JS. Toxoplasmosis in the non-AIDS immunocompromised host. Curr Clin Top Infect Dis. 1993;13:322-56. PubMed PMID: 8397917.

10. Rajapakse S, Chrishan Shivanthan M, Samaranayake N, Rodrigo C, Deepika Fernando S. Antibiotics for human toxoplasmosis: a systematic review of randomized trials. Pathog Glob Health. 2013;107(4):162-9. doi: 10.1179/2047773213Y.0000000094. PubMed PMID: 23816507; PMCID: PMC4001466.

11. Morrissette NS, Sibley LD. Cytoskeleton of apicomplexan parasites. Microbiol Mol Biol Rev. 2002;66:21-38.

12. Dubremetz JF, Achbarou A, Bermudes D, Joiner KA. Kinetics and pattern of organelle exocytosis during Toxoplasma gondii/ host-cell interaction. Parasitol Res. 1993;79:402-8.

13. Carruthers VB, Sibley LD. Sequential protein secretion from three distinct organelles of Toxoplasma gondii accompanies invasion of human fibroblasts. Eur J Cell Biol. 1997;73:114-23.

14. Molestina RE, Sinai AP. Host and parasite-derived IKK activities direct distinct temporal phases of NF-kappaB activation and target gene expression following Toxoplasma gondii infection. J Cell Sci. 2005;118(Pt 24):5785-96. Epub 2005/12/13. doi: 10.1242/jcs.02709. PubMed PMID: 16339966.

15. Blader IJ, Manger ID, Boothroyd JC. Microarray analysis reveals previously unknown changes in Toxoplasma gondii-infected human cells. J Biol Chem. 2001;276(26):24223-31. Epub 2001/04/11. doi: 10.1074/jbc.M100951200. PubMed PMID: 11294868.

16. Rastogi S, Xue Y, Quake SR, Boothroyd JC. Differential Impacts on Host Transcription by ROP and GRA Effectors from the Intracellular Parasite Toxoplasma gondii. mBio. 2020;11(3). Epub 2020/06/11. doi: 10.1128/mBio.00182-20. PubMed PMID: 32518180; PMCID: PMC7373195.

17. Hakimi MA, Bougdour A. Toxoplasma's ways of manipulating the host transcriptome via secreted effectors. Curr Opin Microbiol. 2015;26:24-31. doi: 10.1016/j.mib.2015.04.003. PubMed PMID: 25912924.

18. Bougdour A, Tardieux I, Hakimi MA. Toxoplasma exports dense granule proteins beyond the vacuole to the host cell nucleus and rewires the host genome expression. Cell Microbiol. 2014;16(3):334-43. Epub 2014/01/01. doi: 10.1111/cmi.12255. PubMed PMID: 24373221.

19. Taylor S, Barragan A, Su C, Fux B, Fentress SJ, Tang K, Beatty WL, Hajj HE, Jerome M, Behnke MS, White M, Wootton JC, Sibley LD. A secreted serine-threonine kinase determines virulence in the eukaryotic pathogen Toxoplasma gondii. Science. 2006;314(5806):1776-80. Epub 2006/12/16. doi: 10.1126/science.1133643. PubMed PMID: 17170305.

20. Boothroyd JC, Dubremetz JF. Kiss and spit: the dual roles of Toxoplasma rhoptries. Nat Rev Microbiol. 2008;6(1):79-88. Epub 2007/12/07. doi: 10.1038/nrmicro1800. PubMed PMID: 18059289.

21. Saeij JP, Boyle JP, Coller S, Taylor S, Sibley LD, Brooke-Powell ET, Ajioka JW, Boothroyd JC. Polymorphic secreted kinases are key virulence factors in toxoplasmosis. Science. 2006;314(5806):1780-3. Epub 2006/12/16. doi: 10.1126/science.1133690. PubMed PMID: 17170306; PMCID: PMC2646183.

22. Olias P, Etheridge RD, Zhang Y, Holtzman MJ, Sibley LD. Toxoplasma Effector Recruits the Mi-2/NuRD Complex to Repress STAT1 Transcription and Block IFN-gamma-Dependent Gene Expression. Cell Host Microbe. 2016;20(1):72-82. Epub 2016/07/16. doi: 10.1016/j.chom.2016.06.006. PubMed PMID: 27414498; PMCID: PMC4947229.

23. Gay G, Braun L, Brenier-Pinchart MP, Vollaire J, Josserand V, Bertini RL, Varesano A, Touquet B, De Bock PJ, Coute Y, Tardieux I, Bougdour A, Hakimi MA. Toxoplasma gondii

TgIST co-opts host chromatin repressors dampening STAT1-dependent gene regulation and IFN-gamma-mediated host defenses. J Exp Med. 2016;213(9):1779-98. Epub 2016/08/10. doi: 10.1084/jem.20160340. PubMed PMID: 27503074; PMCID: PMC4995087.

24. Bougdour A, Durandau E, Brenier-Pinchart MP, Ortet P, Barakat M, Kieffer S, Curt-Varesano A, Curt-Bertini RL, Bastien O, Coute Y, Pelloux H, Hakimi MA. Host cell subversion by Toxoplasma GRA16, an exported dense granule protein that targets the host cell nucleus and alters gene expression. Cell Host Microbe. 2013;13(4):489-500. Epub 2013/04/23. doi: 10.1016/j.chom.2013.03.002. PubMed PMID: 23601110.

25. Braun L, Brenier-Pinchart MP, Yogavel M, Curt-Varesano A, Curt-Bertini RL, Hussain T, Kieffer-Jaquinod S, Coute Y, Pelloux H, Tardieux I, Sharma A, Belrhali H, Bougdour A, Hakimi MA. A Toxoplasma dense granule protein, GRA24, modulates the early immune response to infection by promoting a direct and sustained host p38 MAPK activation. J Exp Med. 2013;210(10):2071-86. Epub 2013/09/18. doi: 10.1084/jem.20130103. PubMed PMID: 24043761; PMCID: PMC3782045.

26. Molestina RE, El-Guendy N, Sinai AP. Infection with Toxoplasma gondii results in dysregulation of the host cell cycle. Cell Microbiol. 2008;10(5):1153-65. Epub 2008/01/10. doi: 10.1111/j.1462-5822.2008.01117.x. PubMed PMID: 18182087; PMCID: PMC2647804.

27. Brunet J, Pfaff AW, Abidi A, Unoki M, Nakamura Y, Guinard M, Klein JP, Candolfi E, Mousli M. Toxoplasma gondii exploits UHRF1 and induces host cell cycle arrest at G2 to enable its proliferation. Cell Microbiol. 2008;10(4):908-20. Epub 2007/11/17. doi: 10.1111/j.1462-5822.2007.01093.x. PubMed PMID: 18005238.

28. Lavine MD, Arrizabalaga G. Induction of mitotic S-phase of host and neighboring cells by Toxoplasma gondii enhances parasite invasion. Mol Biochem Parasitol. 2009;164(1):95-9. Epub

2008/12/30. doi: 10.1016/j.molbiopara.2008.11.014. PubMed PMID: 19111577; PMCID: PMC2654716.

29. Bendris N, Lemmers B, Blanchard JM. Cell cycle, cytoskeleton dynamics and beyond: the many functions of cyclins and CDK inhibitors. Cell Cycle. 2015;14(12):1786-98. Epub 2015/03/20. doi: 10.1080/15384101.2014.998085. PubMed PMID: 25789852; PMCID: PMC4614797.

30. Malumbres M, Barbacid M. Cell cycle, CDKs and cancer: a changing paradigm. Nat Rev Cancer. 2009;9(3):153-66. Epub 2009/02/25. doi: 10.1038/nrc2602. PubMed PMID: 19238148.

31. Panas MW, Naor A, Cygan AM, Boothroyd JC. Toxoplasma Controls Host Cyclin E Expression through the Use of a Novel MYR1-Dependent Effector Protein, HCE1. mBio. 2019;10(2). Epub 2019/05/02. doi: 10.1128/mBio.00674-19. PubMed PMID: 31040242; PMCID: PMC6495377.

32. Braun L, Brenier-Pinchart MP, Hammoudi PM, Cannella D, Kieffer-Jaquinod S, Vollaire J, Josserand V, Touquet B, Coute Y, Tardieux I, Bougdour A, Hakimi MA. The Toxoplasma effector TEEGR promotes parasite persistence by modulating NF-kappaB signalling via EZH2. Nat Microbiol. 2019;4(7):1208-20. Epub 2019/05/01. doi: 10.1038/s41564-019-0431-8. PubMed PMID: 31036909; PMCID: PMC6591128.

33. Bougdour A, Durandau E, Brenier-Pinchart M-P, Ortet P, Barakat M, Kieffer S, Curt-Varesano A, Curt-Bertini R-L, Bastien O, Coute Y. Host cell subversion by Toxoplasma GRA16, an exported dense granule protein that targets the host cell nucleus and alters gene expression. Cell host & microbe. 2013;13(4):489-500.

34. Braun L, Brenier-Pinchart M-P, Yogavel M, Curt-Varesano A, Curt-Bertini R-L, Hussain T, Kieffer-Jaquinod S, Coute Y, Pelloux H, Tardieux I. A Toxoplasma dense granule protein,

GRA24, modulates the early immune response to infection by promoting a direct and sustained host p38 MAPK activation. Journal of Experimental Medicine. 2013:jem. 20130103.

35. Gay G, Braun L, Brenier-Pinchart M-P, Vollaire J, Josserand V, Bertini R-L, Varesano A, Touquet B, De Bock P-J, Coute Y. Toxoplasma gondii TgIST co-opts host chromatin repressors dampening STAT1-dependent gene regulation and IFN-γ–mediated host defenses. Journal of Experimental Medicine. 2016:jem. 20160340.

36. Olias P, Etheridge RD, Zhang Y, Holtzman MJ, Sibley LD. Toxoplasma effector recruits the Mi-2/NuRD complex to repress STAT1 transcription and block IFN-γ-dependent gene expression. Cell host & microbe. 2016;20(1):72-82.

37. Rosenberg A, Sibley LD. Toxoplasma gondii secreted effectors co-opt host repressor complexes to inhibit necroptosis. Cell Host Microbe. 2021;29(7):1186-98 e8. Epub 2021/05/28. doi: 10.1016/j.chom.2021.04.016. PubMed PMID: 34043960.

38. Nadipuram SM, Kim EW, Vashisht AA, Lin AH, Bell HN, Coppens I, Wohlschlegel JA, Bradley PJ. In Vivo Biotinylation of the Toxoplasma Parasitophorous Vacuole Reveals Novel Dense Granule Proteins Important for Parasite Growth and Pathogenesis. MBio. 2016;7(4). doi: 10.1128/mBio.00808-16. PubMed PMID: 27486190; PMCID: PMC4981711.

39. Zambon AC, Hsu T, Kim SE, Klinck M, Stowe J, Henderson LM, Singer D, Patam L, Lim C, McCulloch AD, Hu B, Hickerson AI. Methods and sensors for functional genomic studies of cell-cycle transitions in single cells. Physiol Genomics. 2020;52(10):468-77. Epub 2020/09/01. doi: 10.1152/physiolgenomics.00065.2020. PubMed PMID: 32866086.

40. Sakaue-Sawano A, Kurokawa H, Morimura T, Hanyu A, Hama H, Osawa H, Kashiwagi S, Fukami K, Miyata T, Miyoshi H, Imamura T, Ogawa M, Masai H, Miyawaki A. Visualizing

spatiotemporal dynamics of multicellular cell-cycle progression. Cell. 2008;132(3):487-98. Epub 2008/02/13. doi: 10.1016/j.cell.2007.12.033. PubMed PMID: 18267078.

41. Huynh MH, Carruthers VB. Tagging of endogenous genes in a Toxoplasma gondii strain lacking Ku80. Eukaryot Cell. 2009;8(4):530-9. Epub 2009/02/17. doi: 10.1128/EC.00358-08. PubMed PMID: 19218426; PMCID: PMC2669203.

42. Sidik SM, Hackett CG, Tran F, Westwood NJ, Lourido S. Efficient Genome Engineering of Toxoplasma gondii Using CRISPR/Cas9. Plos One. 2014;9(6). doi: ARTN e100450 10.1371/journal.pone.0100450. PubMed PMID: WOS:000338512200032.

43. Shen B, Brown KM, Lee TD, Sibley LD. Efficient Gene Disruption in Diverse Strains of Toxoplasma gondii Using CRISPR/CAS9. Mbio. 2014;5(3). doi: ARTN e01114-14 10.1128/mBio.01114-14. PubMed PMID: WOS:000338875900061.

44. Fischer HG, Stachelhaus S, Sahm M, Meyer HE, Reichmann G. GRA7, an excretory 29 kDa Toxoplasma gondii dense granule antigen released by infected host cells. Mol Biochem Parasitol. 1998;91(2):251-62. Epub 1998/05/05. doi: 10.1016/s0166-6851(97)00227-2. PubMed PMID: 9566518.

45. Jacobs D, Dubremetz JF, Loyens A, Bosman F, Saman E. Identification and heterologous expression of a new dense granule protein (GRA7) from Toxoplasma gondii. Mol Biochem Parasitol. 1998;91(2):237-49. Epub 1998/05/05. doi: 10.1016/s0166-6851(97)00204-1. PubMed PMID: 9566517.

46. Alaganan A, Fentress SJ, Tang K, Wang Q, Sibley LD. Toxoplasma GRA7 effector increases turnover of immunity-related GTPases and contributes to acute virulence in the mouse. Proceedings of the National Academy of Sciences. 2014;111(3):1126-31.

47. Franco M, Panas MW, Marino ND, Lee MC, Buchholz KR, Kelly FD, Bednarski JJ, Sleckman BP, Pourmand N, Boothroyd JC. A Novel Secreted Protein, MYR1, Is Central to Toxoplasma's Manipulation of Host Cells. mBio. 2016;7(1):e02231-15. Epub 2016/02/04. doi: 10.1128/mBio.02231-15. PubMed PMID: 26838724; PMCID: PMC4742717.

48. Maiorano D, Rul W, Mechali M. Cell cycle regulation of the licensing activity of Cdt1 in Xenopus laevis. Exp Cell Res. 2004;295(1):138-49. Epub 2004/03/31. doi: 10.1016/j.yexcr.2003.11.018. PubMed PMID: 15051497.

49. Lee PH, Osley MA. Who gets a license: DNA synthesis in quiescent cells re-entering the cell cycle. Curr Genet. 2021;67(4):539-43. Epub 2021/03/09. doi: 10.1007/s00294-021-01170-7. PubMed PMID: 33682029; PMCID: PMC8254781.

50. Zhang H. Regulation of DNA Replication Licensing and Re-Replication by Cdt1. Int J Mol Sci. 2021;22(10). Epub 2021/06/03. doi: 10.3390/ijms22105195. PubMed PMID: 34068957; PMCID: PMC8155957.

51. Kumar C, Remus D. Eukaryotic replication origins: Strength in flexibility. Nucleus. 2016;7(3):292-300. Epub 2016/07/16. doi: 10.1080/19491034.2016.1187353. PubMed PMID: 27416360; PMCID: PMC4991242.

52. Tognetti S, Riera A, Speck C. Switch on the engine: how the eukaryotic replicative helicase MCM2-7 becomes activated. Chromosoma. 2015;124(1):13-26. Epub 2014/10/14. doi: 10.1007/s00412-014-0489-2. PubMed PMID: 25308420.

53. Arias EE, Walter JC. Replication-dependent destruction of Cdt1 limits DNA replication to a single round per cell cycle in Xenopus egg extracts. Genes Dev. 2005;19(1):114-26. Epub 2004/12/16. doi: 10.1101/gad.1255805. PubMed PMID: 15598982; PMCID: PMC540230.

54. Caillat C, Perrakis A. Cdt1 and geminin in DNA replication initiation. Subcell Biochem. 2012;62:71-87. Epub 2012/08/25. doi: 10.1007/978-94-007-4572-8_5. PubMed PMID: 22918581.

55. Zielke N, Edgar BA. FUCCI sensors: powerful new tools for analysis of cell proliferation. Wiley Interdiscip Rev Dev Biol. 2015;4(5):469-87. Epub 2015/04/02. doi: 10.1002/wdev.189. PubMed PMID: 25827130; PMCID: PMC6681141.

56. Gaskins E, Gilk S, DeVore N, Mann T, Ward G, Beckers C. Identification of the membrane receptor of a class XIV myosin in Toxoplasma gondii. J Cell Biol. 2004;165(3):383-93. Epub 2004/05/05. doi: 10.1083/jcb.200311137. PubMed PMID: 15123738; PMCID: PMC2172186.

57. Coffey MJ, Sleebs BE, Uboldi AD, Garnham A, Franco M, Marino ND, Panas MW, Ferguson DJ, Enciso M, O'Neill MT, Lopaticki S, Stewart RJ, Dewson G, Smyth GK, Smith BJ, Masters SL, Boothroyd JC, Boddey JA, Tonkin CJ. An aspartyl protease defines a novel pathway for export of Toxoplasma proteins into the host cell. Elife. 2015;4. Epub 2015/11/19. doi: 10.7554/eLife.10809. PubMed PMID: 26576949; PMCID: PMC4764566.

58. Hwang HC, Clurman BE. Cyclin E in normal and neoplastic cell cycles. Oncogene. 2005;24(17):2776-86. doi: 10.1038/sj.onc.1208613. PubMed PMID: WOS:000228465800004.

59. Chu C, Geng Y, Zhou Y, Sicinski P. Cyclin E in normal physiology and disease states. Trends Cell Biol. 2021;31(9):732-46. Epub 2021/05/31. doi: 10.1016/j.tcb.2021.05.001. PubMed PMID: 34052101; PMCID: PMC8364501.

60. Velasquez ZD, Conejeros I, Larrazabal C, Kerner K, Hermosilla C, Taubert A. Toxoplasma gondii-induced host cellular cell cycle dysregulation is linked to chromosome missegregation and cytokinesis failure in primary endothelial host cells. Sci Rep. 2019;9(1):12496. Epub 2019/08/31. doi: 10.1038/s41598-019-48961-0. PubMed PMID: 31467333; PMCID: PMC6715697.

61. Salic A, Mitchison TJ. A chemical method for fast and sensitive detection of DNA synthesis in vivo. Proc Natl Acad Sci U S A. 2008;105(7):2415-20. Epub 2008/02/15. doi: 10.1073/pnas.0712168105. PubMed PMID: 18272492; PMCID: PMC2268151.

62. Besson A, Dowdy SF, Roberts JM. CDK inhibitors: cell cycle regulators and beyond. Dev Cell. 2008;14(2):159-69. Epub 2008/02/13. doi: 10.1016/j.devcel.2008.01.013. PubMed PMID: 18267085.

63. Li A, Blow JJ. The origin of CDK regulation. Nat Cell Biol. 2001;3(8):E182-4. Epub 2001/08/03. doi: 10.1038/35087119. PubMed PMID: 11483974; PMCID: PMC3604809.

64. Fornace AJJ, Daniel W. Nebert DW, Hollander MC, Luethy JD, Papathasiou M, Fargnoli J, J. HN. Mammalian Genes Coordinately Regulated by Growth Arrest Signals and DNA-Damaging Agents. MOLECULAR AND CELLULAR BIOLOGY. 1989;9. No. 10:4196-203.

65. Zhuang H, Yao C, Zhao X, Chen X, Yang Y, Huang S, Pan L, Du A, Yang Y. DNA double-strand breaks in the Toxoplasma gondii-infected cells by the action of reactive oxygen species. Parasit Vectors. 2020;13(1):490. Epub 2020/09/30. doi: 10.1186/s13071-020-04324-7. PubMed PMID: 32988387; PMCID: PMC7523337.

66. Liarte S, Bernabe-Garcia A, Armero-Barranco D, Nicolas FJ. Microscopy Based Methods for the Assessment of Epithelial Cell Migration During In Vitro Wound Healing. J Vis Exp. 2018(131). Epub 2018/01/25. doi: 10.3791/56799. PubMed PMID: 29364245; PMCID: PMC5908412.

67. Jonkman JE, Cathcart JA, Xu F, Bartolini ME, Amon JE, Stevens KM, Colarusso P. An introduction to the wound healing assay using live-cell microscopy. Cell Adh Migr. 2014;8(5):440-51. Epub 2014/12/09. doi: 10.4161/cam.36224. PubMed PMID: 25482647; PMCID: PMC5154238.

68. Naor A, Panas MW, Marino N, Coffey MJ, Tonkin CJ, Boothroyd JC. MYR1-Dependent Effectors Are the Major Drivers of a Host Cell's Early Response to Toxoplasma, Including Counteracting MYR1-Independent Effects. mBio. 2018;9(2). Epub 2018/04/05. doi: 10.1128/mBio.02401-17. PubMed PMID: 29615509; PMCID: PMC5885026.

69. Cavanagh BL, Walker T, Norazit A, Meedeniya AC. Thymidine analogues for tracking DNA synthesis. Molecules. 2011;16(9):7980-93. Epub 2011/09/17. doi: 10.3390/molecules16097980. PubMed PMID: 21921870; PMCID: PMC6264245.

70. Liang CC, Park AY, Guan JL. In vitro scratch assay: a convenient and inexpensive method for analysis of cell migration in vitro. Nat Protoc. 2007;2(2):329-33. Epub 2007/04/05. doi: 10.1038/nprot.2007.30. PubMed PMID: 17406593.

71. Coats S, Flanagan WM, Nourse J, Roberts JM. Requirement of p27Kip1 for restriction point control of the fibroblast cell cycle. Science. 1996;272(5263):877-80. Epub 1996/05/10. doi: 10.1126/science.272.5263.877. PubMed PMID: 8629023.

72. Cassimere EK, Mauvais C, Denicourt C. p27Kip1 Is Required to Mediate a G1 Cell Cycle Arrest Downstream of ATM following Genotoxic Stress. PLoS One. 2016;11(9):e0162806. Epub 2016/09/10. doi: 10.1371/journal.pone.0162806. PubMed PMID: 27611996; PMCID: PMC5017644.

73. Al Bitar S, Gali-Muhtasib H. The Role of the Cyclin Dependent Kinase Inhibitor p21(cip1/waf1) in Targeting Cancer: Molecular Mechanisms and Novel Therapeutics. Cancers (Basel). 2019;11(10). Epub 2019/10/03. doi: 10.3390/cancers11101475. PubMed PMID: 31575057; PMCID: PMC6826572.

74. Karimian A, Ahmadi Y, Yousefi B. Multiple functions of p21 in cell cycle, apoptosis and transcriptional regulation after DNA damage. DNA Repair (Amst). 2016;42:63-71. Epub 2016/05/09. doi: 10.1016/j.dnarep.2016.04.008. PubMed PMID: 27156098.

75. Cerqueira A, Martin A, Symonds CE, Odajima J, Dubus P, Barbacid M, Santamaria D. Genetic characterization of the role of the Cip/Kip family of proteins as cyclin-dependent kinase inhibitors and assembly factors. Mol Cell Biol. 2014;34(8):1452-9. Epub 2014/02/12. doi: 10.1128/MCB.01163-13. PubMed PMID: 24515438; PMCID: PMC3993583.

76. Todaro GJ, Green H. Quantitative studies of the growth of mouse embryo cells in culture and their development into established lines. J Cell Biol. 1963;17:299-313. Epub 1963/05/01. doi: 10.1083/jcb.17.2.299. PubMed PMID: 13985244; PMCID: PMC2106200.

77. Chen F, Castranova V, Shi XL. New insights into the role of nuclear factor-kappa B in cell growth regulation. American Journal of Pathology. 2001;159(2):387-97. doi: Doi 10.1016/S0002-9440(10)61708-7. PubMed PMID: WOS:000170356500001.

78. Youn JH, Nam HW, Kim DJ, Park YM, Kim WK, Kim WS, Choi WY. Cell cycle-dependent entry of Toxoplasma gondii into synchronized HL-60 cells. Kisaengchunghak Chapchi. 1991;29(2):121-8. Epub 1991/06/01. doi: 10.3347/kjp.1991.29.2.121. PubMed PMID: 1954195.

79. Radke JR, Donald RG, Eibs A, Jerome ME, Behnke MS, Liberator P, White MW. Changes in the expression of human cell division autoantigen-1 influence Toxoplasma gondii growth and development. PLoS Pathog. 2006;2(10):e105. Epub 2006/10/31. doi: 10.1371/journal.ppat.0020105. PubMed PMID: 17069459; PMCID: PMC1626100.

80. Shen B, Brown K, Long S, Sibley LD. Development of CRISPR/Cas9 for Efficient Genome Editing in Toxoplasma gondii. Methods Mol Biol. 2017;1498:79-103. Epub 2016/10/07. doi: 10.1007/978-1-4939-6472-7_6. PubMed PMID: 27709570.

81. Stasic AJ, Chasen NM, Dykes EJ, Vella SA, Asady B, Starai VJ, Moreno SNJ. The Toxoplasma Vacuolar H(+)-ATPase Regulates Intracellular pH and Impacts the Maturation of Essential Secretory Proteins. Cell Rep. 2019;27(7):2132-46 e7. Epub 2019/05/16. doi: 10.1016/j.celrep.2019.04.038. PubMed PMID: 31091451; PMCID: PMC6760873.

82. Donald RG, Carter D, Ullman B, Roos DS. Insertional tagging, cloning, and expression of the Toxoplasma gondii hypoxanthine-xanthine-guanine phosphoribosyltransferase gene. Use as a selectable marker for stable transformation. J Biol Chem. 1996;271(24):14010-9. Epub 1996/06/14. doi: 10.1074/jbc.271.24.14010. PubMed PMID: 8662859.

83. Donald RG, Roos DS. Insertional mutagenesis and marker rescue in a protozoan parasite: cloning of the uracil phosphoribosyltransferase locus from Toxoplasma gondii. Proc Natl Acad Sci U S A. 1995;92(12):5749-53. Epub 1995/06/06. doi: 10.1073/pnas.92.12.5749. PubMed PMID: 7777580; PMCID: PMC41774.

84. Higgins DG, Thompson JD, Gibson TJ. Using CLUSTAL for multiple sequence alignments. Method Enzymol. 1996;266:383-402. PubMed PMID: WOS:A1996BF77C00022.

85. Jones DT, Taylor WR, Thornton JM. The rapid generation of mutation data matrices from protein sequences. Comput Appl Biosci. 1992;8(3):275-82. Epub 1992/06/01. doi: 10.1093/bioinformatics/8.3.275. PubMed PMID: 1633570.

86. Kumar S, Stecher G, Li M, Knyaz C, Tamura K. MEGA X: Molecular Evolutionary Genetics Analysis across Computing Platforms. Mol Biol Evol. 2018;35(6):1547-9. Epub 2018/05/04. doi: 10.1093/molbev/msy096. PubMed PMID: 29722887; PMCID: PMC5967553.

87. Felsenstein J. Confidence-Limits on Phylogenies - an Approach Using the Bootstrap. Evolution. 1985;39(4):783-91. doi: Doi 10.2307/2408678. PubMed PMID: WOS:A1985APJ8100007.

FIGURES

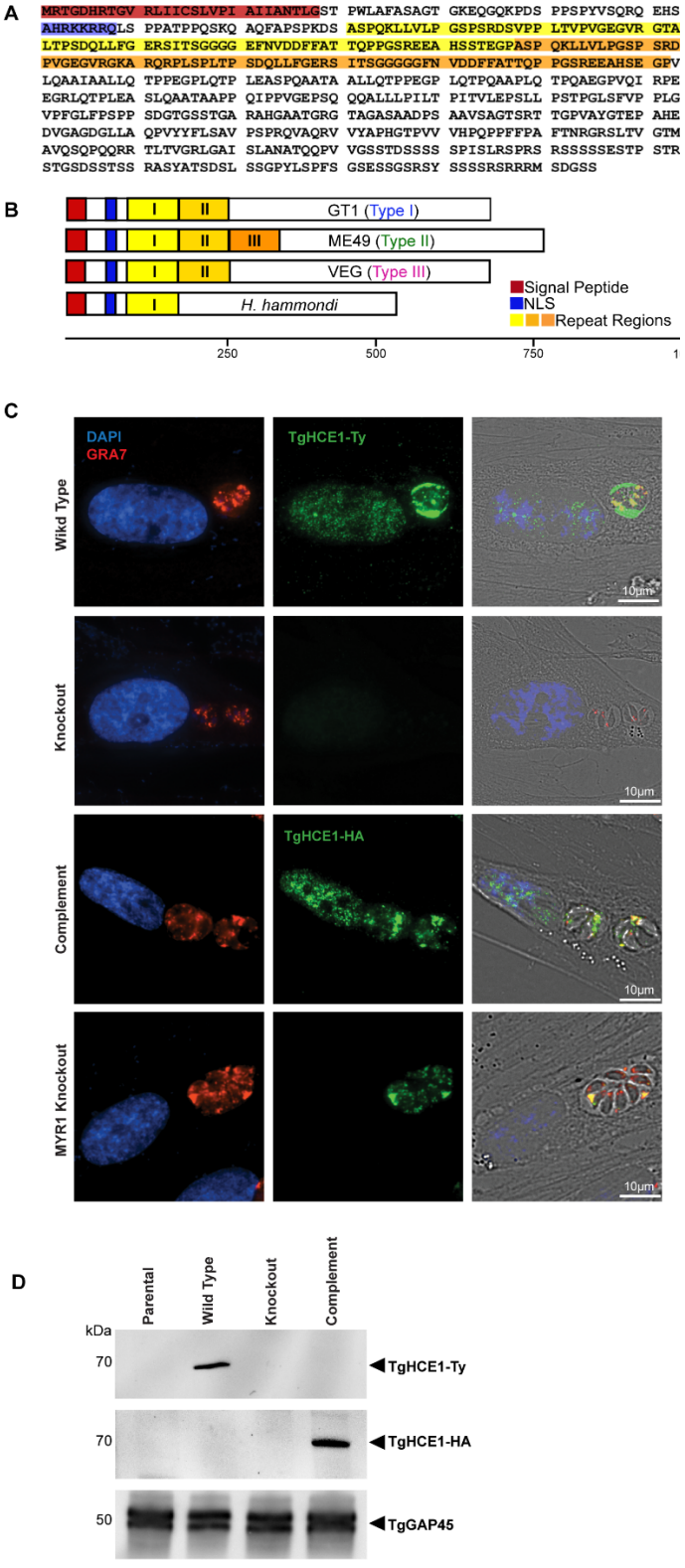
A
MRTGDHRTGV RLIICSLVPI AIIANTLGST PWLAFASAGT GKEQGQKPDS PPSPYVSQRQ EHS
AHRKKRRQLS PPATPPQSKQ AQFAPSPKDS ASPQKLLVLP GSPSRDSVPP LTVPVGEGVR GTA
LTPSDQLLFG ERSITSGGGG EFNVDDFFAT TQPPGSREEA HSSTEGPASP QKLLVLPGSP SRD
PVGEGVRGKA RQRPLSPLTP SDQLLFGERS ITSGGGGGFN VDDFFATTQP PGSREEAHSE GPV
LQAAIAALLQ TPPEGPLQTP LEASPQAATA ALLQTPPEGP LQTPQAAPLQ TPQAEGPVQI RPE
EGRLQTPLEA SLQAATAAPP QIPPVGEPSQ QQALLLPILT PITVLEPSLL PSTPGLSFVP PLG
VPFGLFPSPP SDGTGSSTGA RAHGAATGRG TAGASAADPS AAVSAGTSRT TGPVAYGTEP AHE
DVGAGDGLLA QPVYYFLSAV PSPRQVAQRV VYAPHGTPVV VHPQPPFFPA FTNRGRSLTV GTM
AVQSQPQQRR TLTVGRLGAI SLANATQQPV VGSSTDSSSS SPISLRSPRS RSSSSSESTP STR
STGSDSSTSS RASYATSDSL SSGPYLSPFS GSESSGSRSY SSSSRSRRRM SDGSS
B
GT1 (Type I)
ME49 (Type II)
VEG (Type III)
H. hammondi
Signal Peptide
NLS
Repeat Regions
250
500
750
1
C
DAPI
GRA7
TgHCE1-Ty
TgHCE1-HA
Wikd Type
Knockout
Complement
MYR1 Knockout
10µm
D
Parental
Wild Type
Knockout
Complement
kDa
70
TgHCE1-Ty
70
TgHCE1-HA
50
TgGAP45

Figure 2.1. TgHCE1 is a host nuclear targeted dense granule protein.

(**A)** Amino acid sequence of TgHCE1 in the GT1 Type I strain displaying a predicted signal peptide in red, a nuclear localization signal (NLS) in blue and two internal repeats sequences in yellow/orange. (**B**) Schematic representation of TgHCE1 comparing Type I, Type II, Type III strains and the closely related species *H. hammondi*. The signal peptide (red), the nuclear localization signal (blue), and the differing numbers of repeated domains (light and dark orange) are highlighted. (**C**) HFF cells infected (20 hrs) with Wild Type (TgHCE1-Ty), Knockout (Tg*Δhce1-Ty*), Complement (Tg*Δhce1-Ty*::HCE1-HA), and MYR1 Knockout (Tg*Δmyr1*::HCE1-Ty) expressing *T. gondii*. HCE1 (green), dense granule marker GRA7 (red) and DAPI nuclei (blue) are highlighted. Scale 10 μm. Right = merge with bright field. (**D**) Western blot analysis of total infected host lysates confirming Ty-epitope tagging of TgHCE1 and Tg*Δhce1-Ty*, and HA-epitope tagging of TgHCE1 in the Complement.

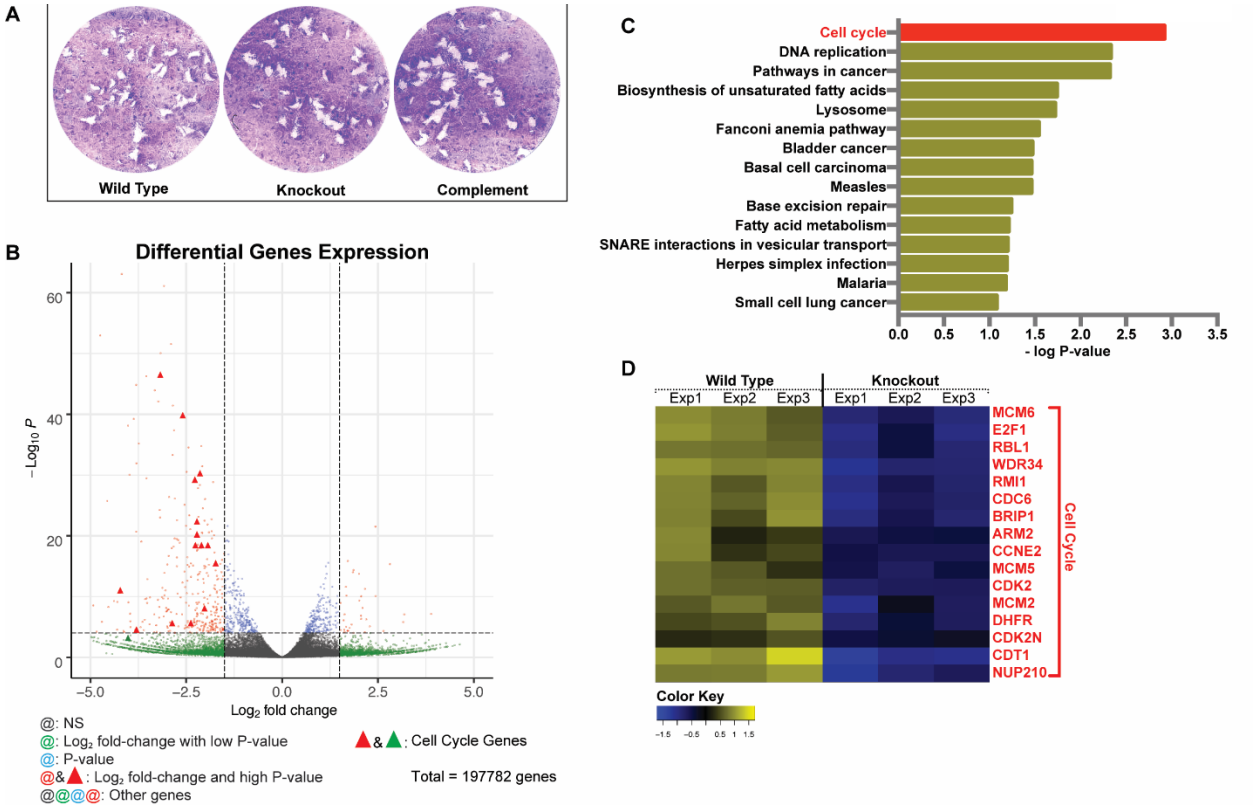
A
Wild Type
Knockout
Complement
B
Differential Genes Expression
−Log10 P
Log2 fold change
@: NS
@: Log2 fold-change with low P-value
@: P-value
@&▲: Log2 fold-change and high P-value
@@@@: Other genes
▲&▲: Cell Cycle Genes
Total = 197782 genes
C
Cell cycle
DNA replication
Pathways in cancer
Biosynthesis of unsaturated fatty acids
Lysosome
Fanconi anemia pathway
Bladder cancer
Basal cell carcinoma
Measles
Base excision repair
Fatty acid metabolism
SNARE interactions in vesicular transport
Herpes simplex infection
Malaria
Small cell lung cancer
- log P-value
D
Wild Type
Knockout
Exp1 Exp2 Exp3 Exp1 Exp2 Exp3
MCM6
E2F1
RBL1
WDR34
RMI1
CDC6
BRIP1
ARM2
CCNE2
MCM5
CDK2
MCM2
DHFR
CDK2N
CDT1
NUP210
Cell Cycle
Color Key

Figure 2.2 TgHCE1 promotes activation of the host cell cycle program.

(**A**) Plaque assays of Wild Type (TgHCE1-Ty), Knockout (Tg*Δhce1-Ty)* and Complement (Tg*Δhce1-Ty*::HCE1-HA) tachyzoites on HFF monolayers. Each well was infected with 100 parasites and the monolayers were fixed seven days post infection and stained with crystal violet. (**B**) Volcano plot illustration of RNAseq data depicting fold change of genes that are statistically significant in Tg*Δhce1-Ty* infected HFFs showing upregulated genes (right quadrant/red dots) and downregulated genes (left quadrant/red dots and triangles). Red dots represent genes that have the highest P-value with more than 1.5 log2 fold change. Red triangles are genes that are downregulated in Tg*Δhce1-Ty* (Knockout) that are involved in the cell cycle. (**C**) Representation of top 94 differentially expressed genes that were identified with known pathway affiliations. Following the same parameters with transcripts showing a log2 fold change > 1.5 and representing a statistically significant differential expression (adjusted P-value = <0.05) they were selected and classified into 15 pathways of the most upregulated and downregulated genes in TgHCE1-Ty and Tg*Δhce1-Ty* infected HFFs respectively using DAVID6.8 and KEGG pathway analyses. (**D**) Differential expression of the top 16 genes that are upregulated by Wild Type (TgHCE1-Ty) in infected HFF (yellow) for 24 hrs and downregulated in Knockout (Tg*Δhce1-Ty*) infected HFF (blue).

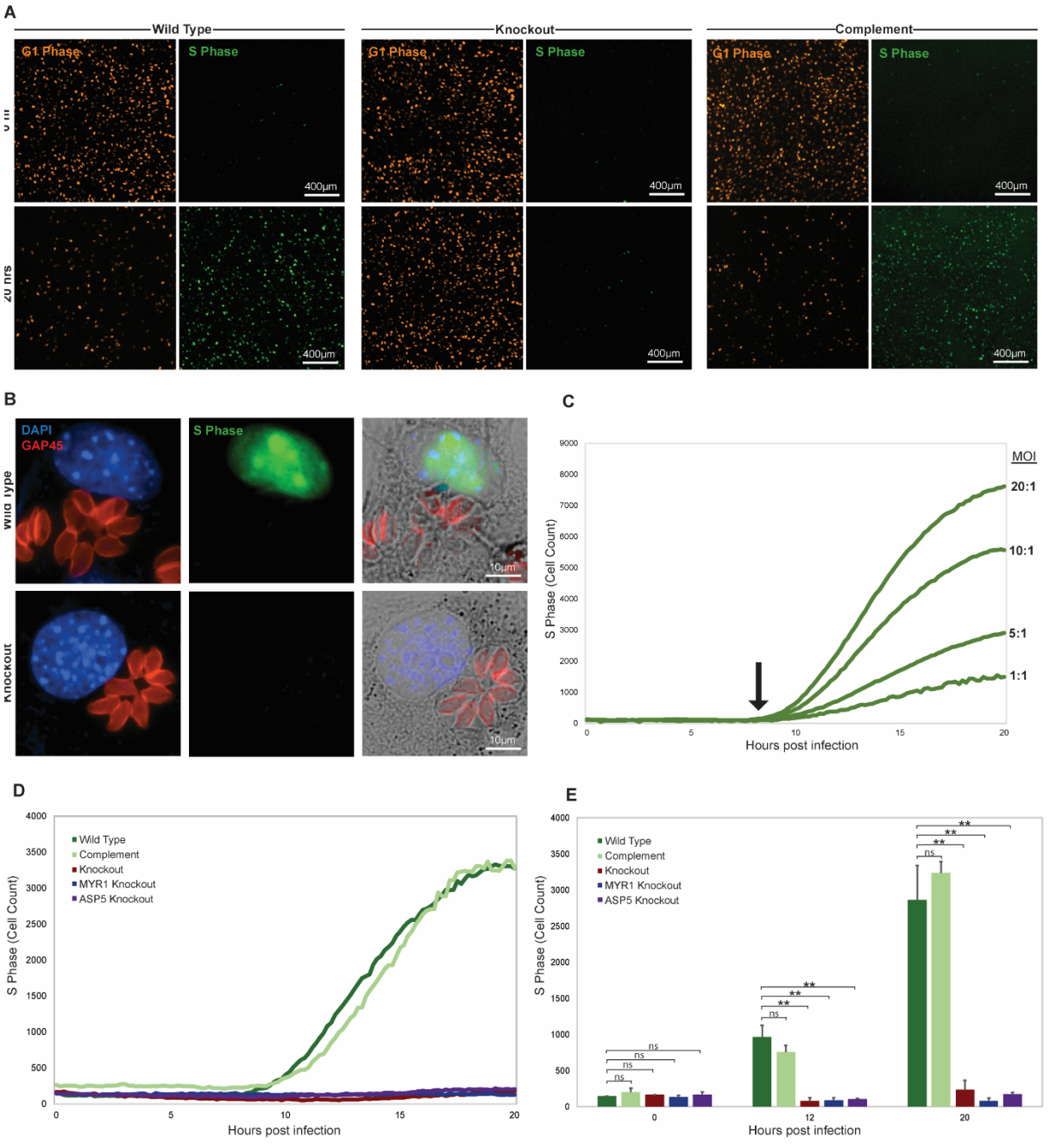
A
Wild Type
Knockout
Complement
G1 Phase
S Phase
400µm
B
DAPI
GAP45
S Phase
10µm
C
MOI
20:1
10:1
5:1
1:1
S Phase (Cell Count)
Hours post infection
D
Wild Type
Complement
Knockout
MYR1 Knockout
ASP5 Knockout
S Phase (Cell Count)
Hours post infection
E
ns
**
S Phase (Cell Count)
Hours post infection

Figure 2.3 TgHCE1 drives infected host cells into S-phase.

(**A**) FUCCI cells infected with Wild Type (TgHCE1-Ty), Knockout (Tg*Δhce1-Ty*), and Complement (Tg*Δhce1-Ty*::HCE1-HA) at 0 (top rows) and 20 (bottom rows) hrs post infection. G1 phase (left column) and S-phase (right column) of the same field of FUCCI cells. Scale 400µm. (**B**) FUCCI Cells infected (20 hrs) with TgHCE1-Ty (top row) and Tg*Δhce1-Ty* (bottom row) expressing *T. gondii*. GAP45 parasite marker (red) and DAPI nuclei (blue), S-phase FUCCI (green). Scale 10 µm. Right = merge with bright field. (**C**) Multiplicity of infection (MOI) ratios for TgHCE1-Ty infected FUCCI cells over 20 hrs. Ratios shown are 20:1, 10:1, 5:1, and 1:1 (*T. gondii* to FUCCI cell). (**D and E**) G1 to S-phase conversion of FUCCI cells infected with Wild Type (TgHCE1-Ty) in dark green, Knockout (Tg*Δhce1-Ty*) in red, and Complement (Tg*Δhce1-Ty*::HCE1-HA) in light green, MYR1 Knockout (Tg*Δmyr1)* in blue and ASP5 Knockout (Tg*Δasp5)* in purple. Representative of three experimental replicates quantified in (E). Cell count represents total green nuclei in host cells. Statistical analysis was done using a Student's t-test, where *$p<0.05$, **$p<0.01$, ns: not significant.

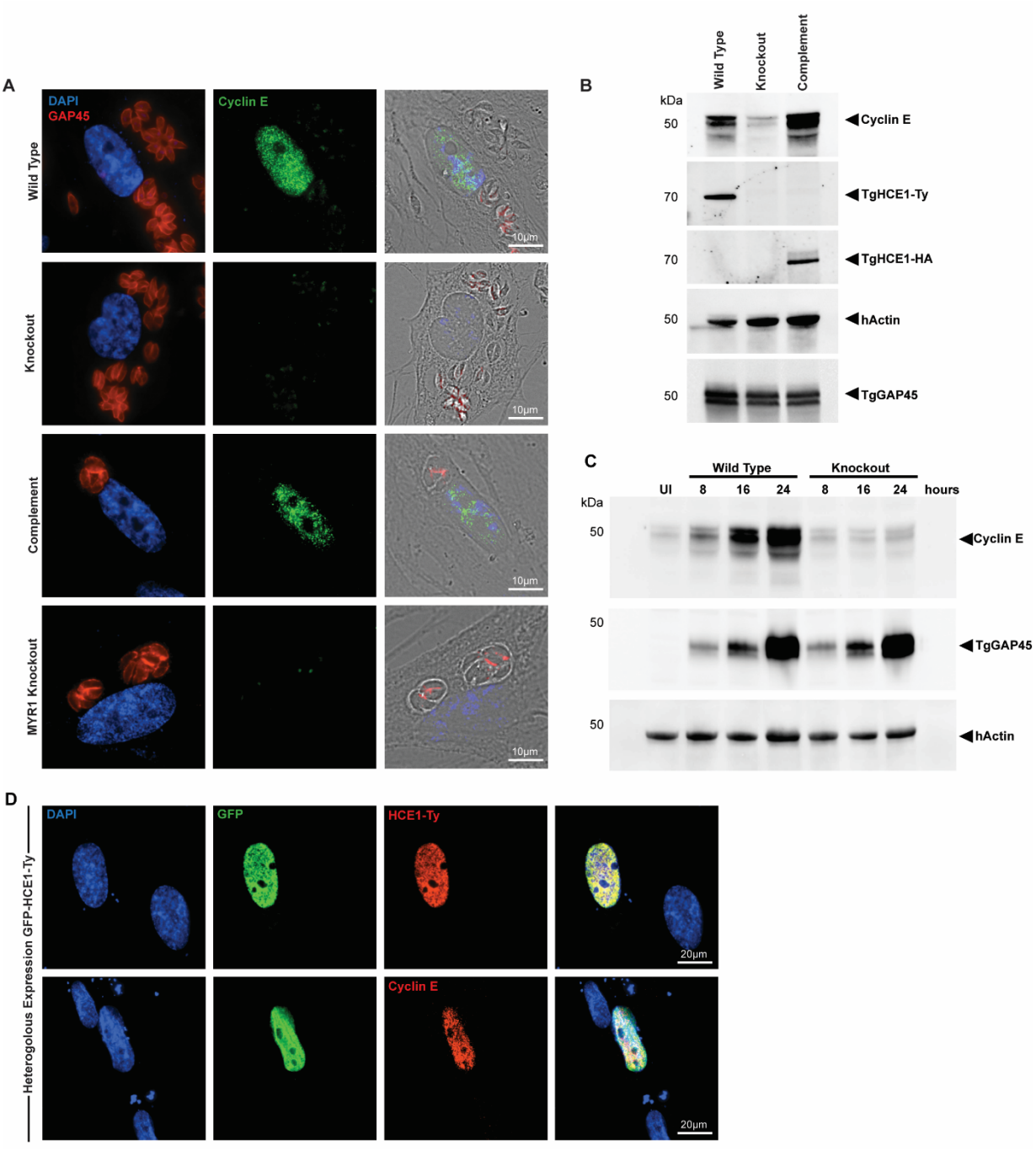
A
DAPI
GAP45
Cyclin E
Wild Type
Knockout
Complement
MYR1 Knockout
10µm
B
Wild Type
Knockout
Complement
kDa
50
Cyclin E
70
TgHCE1-Ty
70
TgHCE1-HA
50
hActin
50
TgGAP45
C
Wild Type
Knockout
UI
8
16
24
8
16
24
hours
kDa
50
Cyclin E
50
TgGAP45
50
hActin
D
Heterogolous Expression GFP-HCE1-Ty
DAPI
GFP
HCE1-Ty
Cyclin E
20µm

Figure 2.4. TgHCE1 induces production of host Cyclin E.

(**A**) HFF cells infected (24 hrs) with Wild Type (TgHCE1-Ty), Knockout (Tg*Δhce1-Ty*), and Complement (Tg*Δhce1-Ty*::HCE1-HA) and MYR1 Knockout expressing HCE1-Ty (Tg*Δmyr1*::HCE1-T) *T. gondii*. Cyclin E (green), GAP45 parasite (red) and DAPI nuclei (blue). Scale 10 μm. Right = merge with bright field. (**B**) Western Blot analysis of Cyclin E expression from Wild Type (TgHCE1-Ty), Knockout (Tg*Δhce1-Ty*), and Complement (Tg*Δhce1-Ty*::HCE1-HA) infected HFF cells after 24 hrs. (**C**) Western Blot analysis of Cyclin E expression from uninfected (UI) as well as Wild Type (TgHCE1-Ty) and Knockout (Tg*Δhce1-Ty*) infected HFF cells. Nuclear lysates were collected at 8, 16, and 24 hrs post infection. (**D**) HFF cells transfected with pGFP-HCE1-Ty (24 hrs). DAPI nuclei (blue), GFP (green), Cyclin E (red-top panel) or Ty-epitope (red-bottom panel). Scale 20 μm. Right = merge.

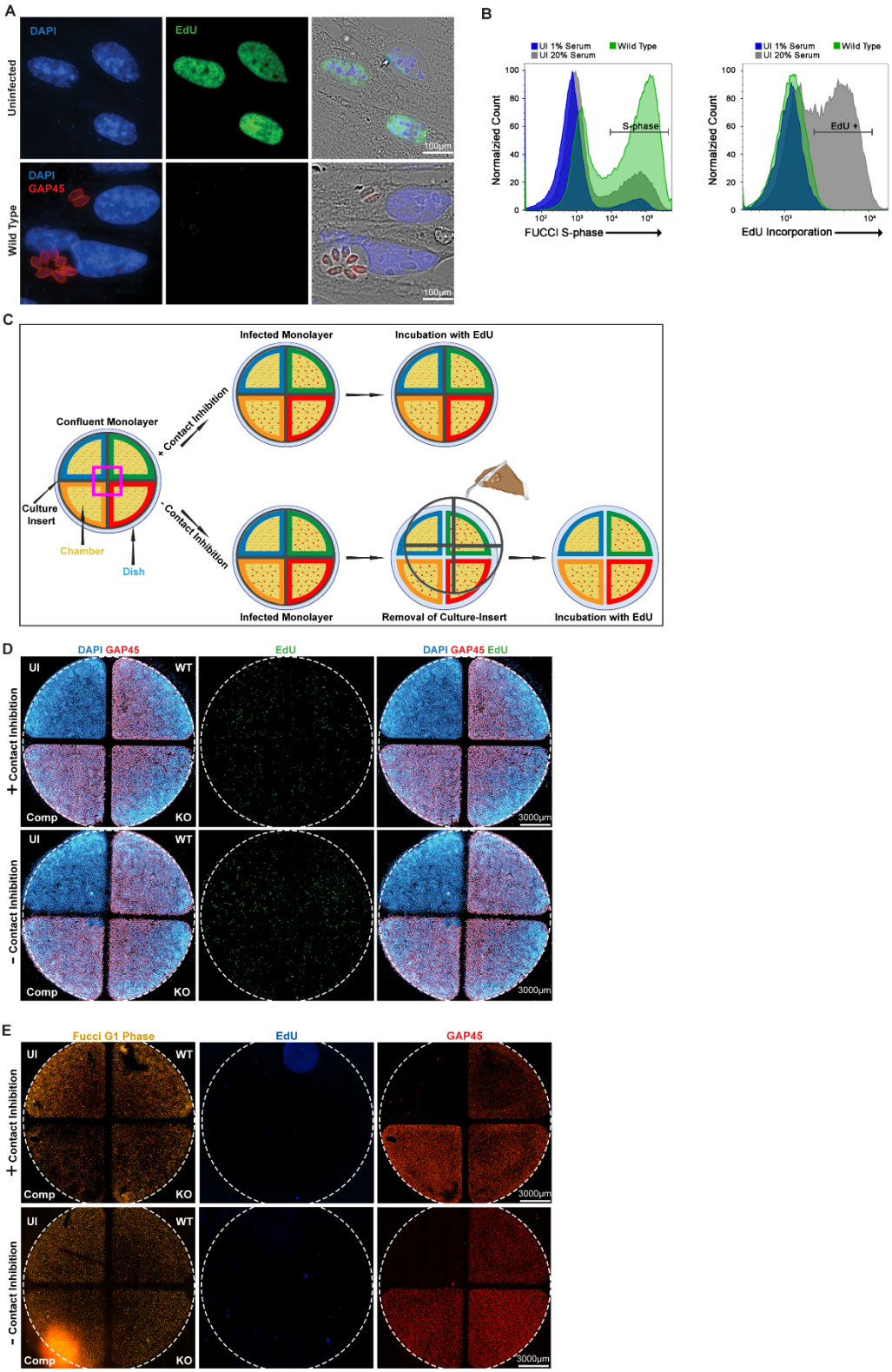
A
DAPI
EdU
Uninfected
DAPI
GAP45
Wild Type
100µm
B
UI 1% Serum
UI 20% Serum
Wild Type
Normalized Count
S-phase
FUCCI S-phase
EdU +
EdU Incorporation
C
Infected Monolayer
Incubation with EdU
Confluent Monolayer
+ Contact Inhibition
Culture Insert
Chamber
Dish
- Contact Inhibition
Infected Monolayer
Removal of Culture-Insert
Incubation with EdU
D
DAPI GAP45
EdU
DAPI GAP45 EdU
+ Contact Inhibition
- Contact Inhibition
UI
WT
Comp
KO
3000µm
E
Fucci G1 Phase
EdU
GAP45
+ Contact Inhibition
- Contact Inhibition
UI
WT
Comp
KO
3000µm

Figure 2.5. Infected HFF and FUCCI cells in S-phase are unable to synthesize new DNA.

(**A**) HFF cells were incubated with EdU and either left uninfected or infected with Wild Type (TgHCE1-Ty). Monolayers were fixed after 24 hrs and stained for EdU incorporation using Alexa Fluor 488 (green), parasites using α-GAP45 (red), and nuclei using DAPI (blue). Scale 100 μm. (**B**) Histogram of FUCCI cells analyzed by flow cytometry. Cells were incubated with EdU and either uninfected grown in 1% or 20% serum or infected with Wild Type (TgHCE1-Ty) *T. gondii*. Cells were fixed at 24 hrs and labeled with EdU and Alexa Fluor 405. (**C**) Schematic displaying the procedure for the "Wound Healing Assay" to assess contact inhibition. Pink box represents area of zoom. (**D and E**) Wound healing assay either in the presence (+ Contact Inhibition) or absence (- Contact Inhibition) of contact inhibition using HFF (D) or FUCCI (E) cells. Cells were either left uninfected (UI) or infected with Wild Type (TgHCE1-Ty), Knockout (Tg*Δhce1-Ty*) or Complement (Tg*Δhce1-Ty*::HCE1-HA) lines. Monolayers were then incubated for 24 hrs with EdU in media containing 1% serum. Scale 3000 μm.

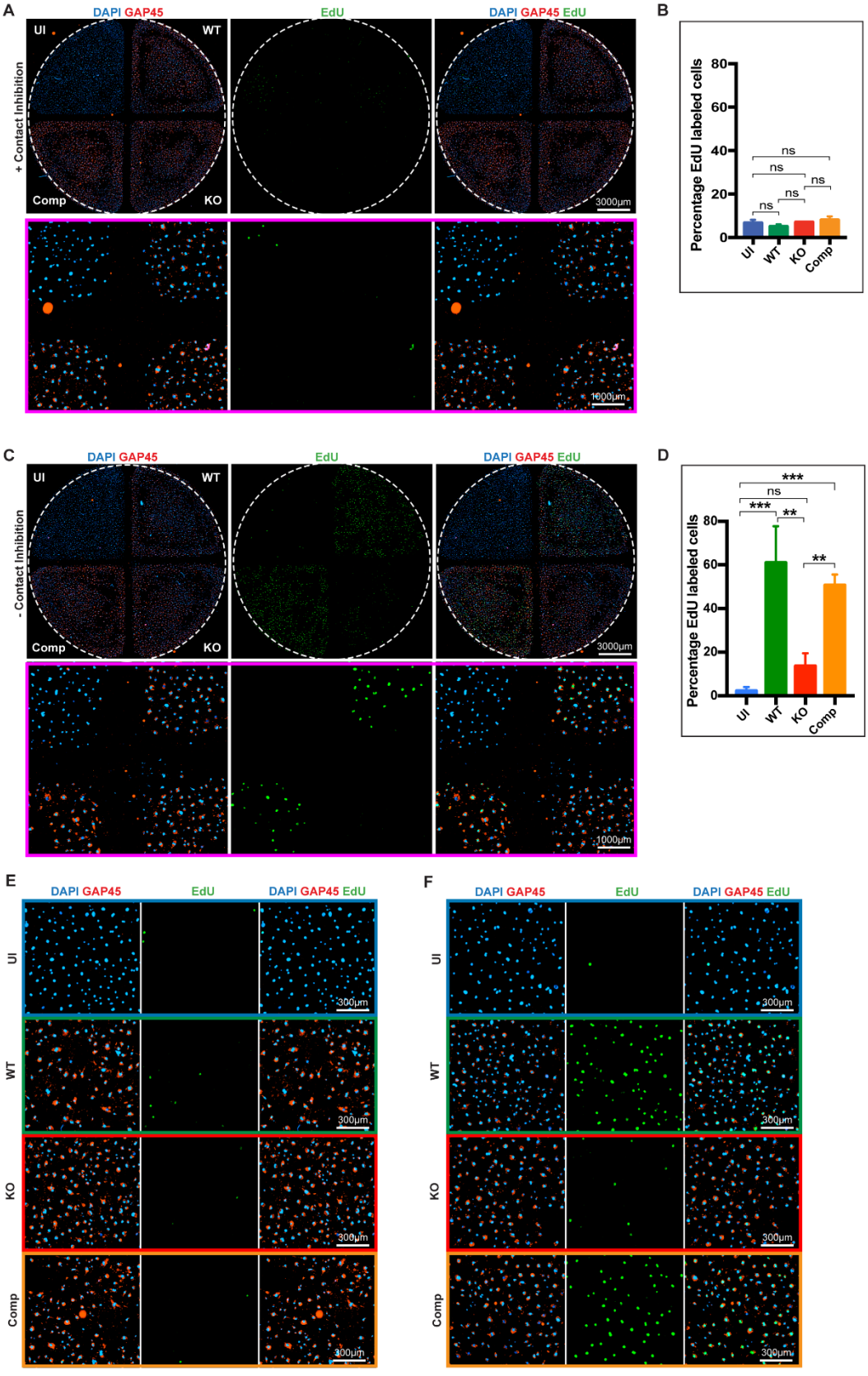
A
DAPI GAP45
EdU
DAPI GAP45 EdU
UI
WT
+ Contact Inhibition
Comp
KO
3000μm
1000μm
B
Percentage EdU labeled cells
80
60
40
20
0
ns
ns
ns
ns
ns
UI
WT
KO
Comp
C
DAPI GAP45
EdU
DAPI GAP45 EdU
UI
WT
- Contact Inhibition
Comp
KO
3000μm
1000μm
D
Percentage EdU labeled cells
80
60
40
20
0
***
ns
***
**
**
UI
WT
KO
Comp
E
DAPI GAP45
EdU
DAPI GAP45 EdU
UI
WT
KO
Comp
300μm
F
DAPI GAP45
EdU
DAPI GAP45 EdU
UI
WT
KO
Comp
300μm

Figure 2.6. TgHCE1 induces S-phase DNA replication in primary mouse fibroblasts upon removal of contact inhibition.

(**A**) Wound healing assay using mouse fibroblasts (MF) in the presence of contact inhibition. Host cell DNA stained with DAPI (blue), parasites stained with GAP45 (red) and EdU (green). Top: view of all 4 quadrants with uninfected (UI), infected WT (TgHCE1-Ty), KO (Tg*Δhce1-Ty*) or Comp (Tg*Δhce1-Ty*::HCE1-HA) parasite lines (scale 3000 μm). Bottom: zoom of central junction of 4 quadrant dish (scale 1000 μm). (**B**) Quantitation of 3 biological replicates of (A). (**C**) Wound healing assay as in (A) with contact inhibition removed. Top: all quadrants (scale 3000 μm). Bottom: zoom of central junction of 4 quadrant dish (scale 1000 μm). (**D**) Quantitation of 3 biological replicates of (C). (**E**) Zoom of central portion of each quadrant (A: + contact inhibition) (scale 300 μm). (**F**) Zoom of central portion of each quadrant (C: - contact inhibition) (scale 300 μm). Confluent monolayers were then incubated for 20 hours with EdU in media containing 1% serum. Graphs represent three biological replicates comparing the different conditions in the presence or absence of Contact Inhibition. Statistical analysis was done using one-way Anova test, where *$p<0.05$, **$p<0.01$,***$p<0.001$ ns: not significant.

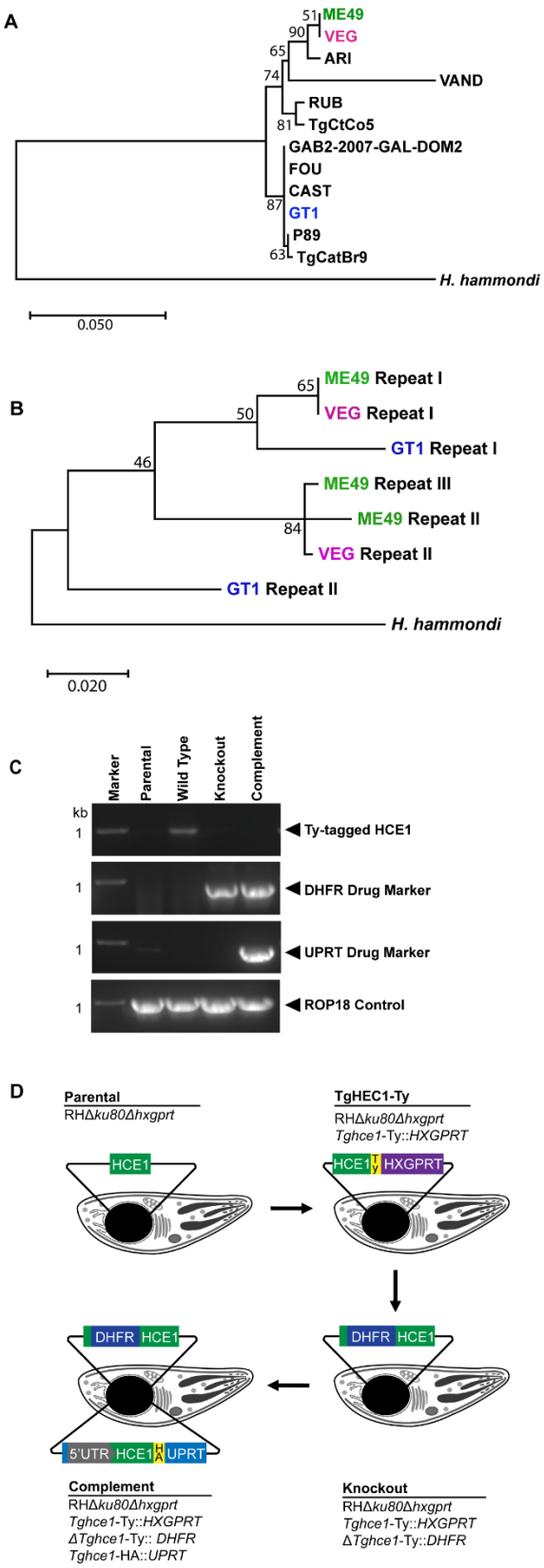
A
51
ME49
90
VEG
65
ARI
74
VAND
RUB
81
TgCtCo5
GAB2-2007-GAL-DOM2
FOU
CAST
87
GT1
P89
63
TgCatBr9
H. hammondi
0.050
B
65
ME49 Repeat I
50
VEG Repeat I
GT1 Repeat I
46
ME49 Repeat III
ME49 Repeat II
84
VEG Repeat II
GT1 Repeat II
H. hammondi
0.020
C
Marker
Parental
Wild Type
Knockout
Complement
kb
1
Ty-tagged HCE1
1
DHFR Drug Marker
1
UPRT Drug Marker
1
ROP18 Control
D
Parental
RHΔku80Δhxgprt
HCE1
TgHEC1-Ty
RHΔku80Δhxgprt
Tghce1-Ty::HXGPRT
HCE1 Ty HXGPRT
DHFR HCE1
DHFR HCE1
5'UTR HCE1 HA UPRT
Complement
RHΔku80Δhxgprt
Tghce1-Ty::HXGPRT
ΔTghce1-Ty:: DHFR
Tghce1-HA::UPRT
Knockout
RHΔku80Δhxgprt
Tghce1-Ty::HXGPRT
ΔTghce1-Ty::DHFR

Supplemental Figure 2.1.

(**A**) Phylogenetic analysis of HCE1 in major T. gondii strains including *H. hammondi* (**B**) Phylogenetic analysis of the first repeat of the *T. gondii* strains suggesting that the first repeat was the original domain prior to duplication. Specific alignment of the repeats from the Type I domain likely occurred after the strain divergence. Tree analysis of repeats from Type I (blue) and Type II (green) reveals that Repeat 1 has fewer substitutions per site between strains (0.03) is more similar between strains than Repeat 1 and Repeat 2 within strains (0.06 and 0.05). (**C**) PCR verification of genetic manipulations used for generating the Wild Type, Knockout and Complemented strains. Primers for PCR are listed in Table S2. (**D**) Schematic describing the generation of Wild Type, Knockout and Complement lines in the RH*Δku80Δhxgprt* background.

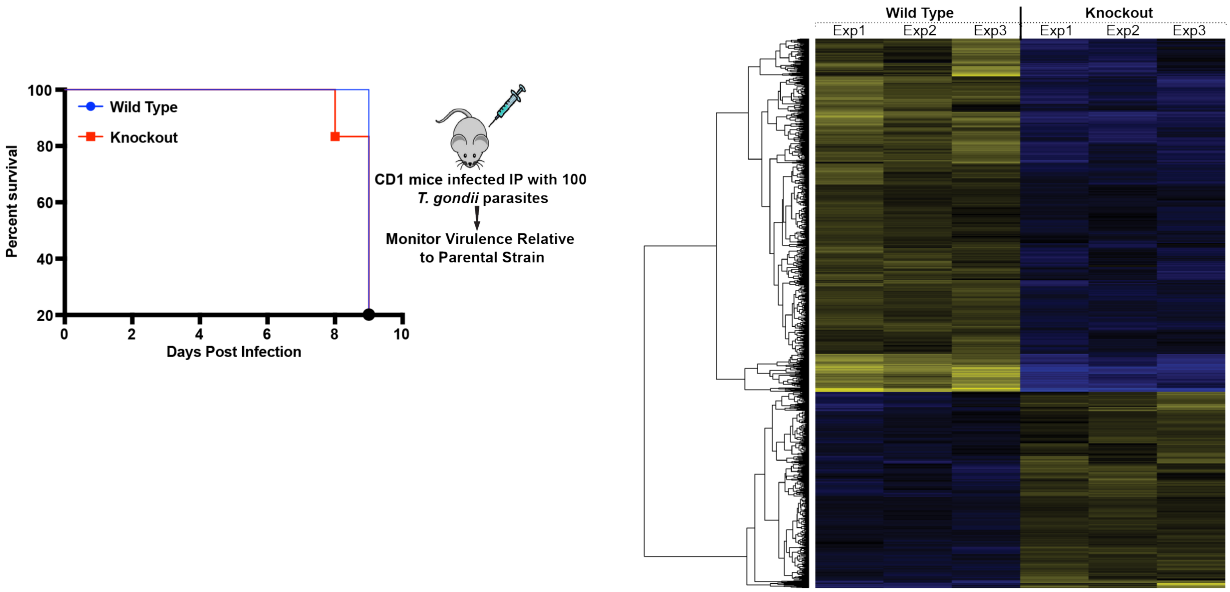

Supplemental Figure 2.2.

(**A**) Virulence in the mouse model of infection. Mice were injected intraperitoneal (IP) with 100 T. gondii and monitored for survival. Survival curve for CD1 mice infected with Wild Type and Knockout parasites over 9 days. (**B**) Global impact analysis of differentially expressed genes comparing both significance and fold change of upregulated and downregulated genes during Wild Type and Knockout infections. Three biological replicates are shown.

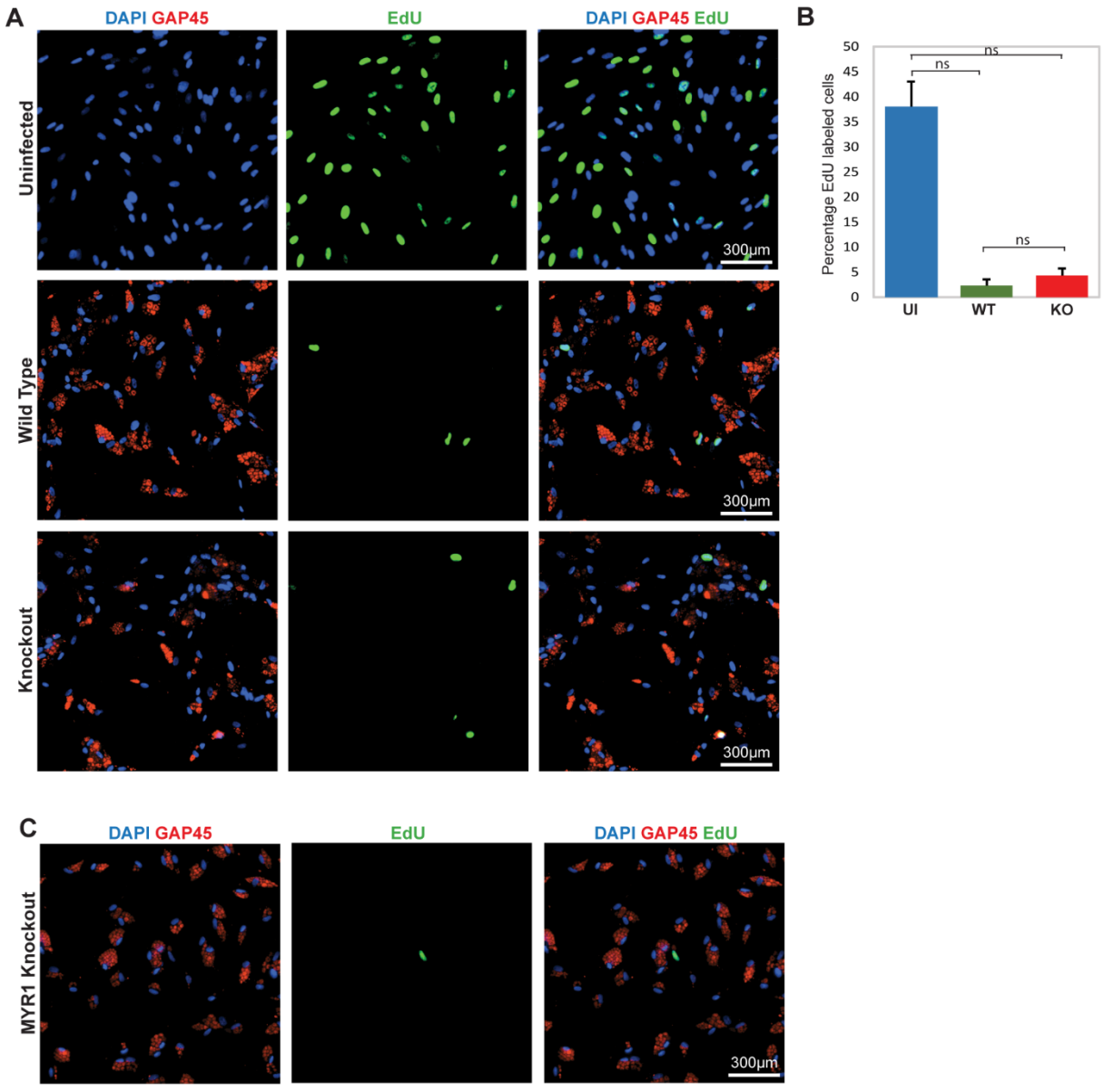
A
DAPI GAP45
EdU
DAPI GAP45 EdU
Uninfected
Wild Type
Knockout
300µm
B
Percentage EdU labeled cells
50
45
40
35
30
25
20
15
10
5
0
ns
ns
ns
UI
WT
KO
C
DAPI GAP45
EdU
DAPI GAP45 EdU
MYR1 Knockout
300µm

Supplemental Figure 2.5.

(**A, B**) HFF cells were either uninfected or infected with Wild Type or KO *T. gondii* for 2 hours. Monolayers were then replated and seeded subconfluent and incubated with EdU in media containing 20% serum. Top panel represents uninfected cells that were replated as positive control. Parasites stained with GAP45 (red), host nuclei with DAPI (blue) and replicating DNA with EdU (green). Quantitation composed of three biological replicates. Statistical analysis was done using a Student's t-test, where *p<0.05, **p<0.01,***p<0.01 ns: not significant. Scale 300 μm. (**C**) HFF cells were infected with Tg*Δmyr1*::HCE1-Ty for 2 hours. Monolayers were then replated, seeded subconfluent and incubated with EdU in media containing 20% serum. Scale 300 μm.

	Percentage EdU labeled cells (% of EdU/DAPI)			
Cells Name	**1%CCS/DMEM**	**20%CCS/DMEM**	**Wild Type**	**Knockout**
Hela	46	45	50	54
MDA-MB-231	56	51	49	34
Asp-1 (Pancr	71	76	62	71
SW480 (Colon)	54	51	45	48
SW620 (Colon)	57	71	74	75
HT-29 (Colon)	51	70	85	79
NEURO-2	83	87	81	82
PANC-1	44	35	57	47
hTERT	37	41	48	46

A

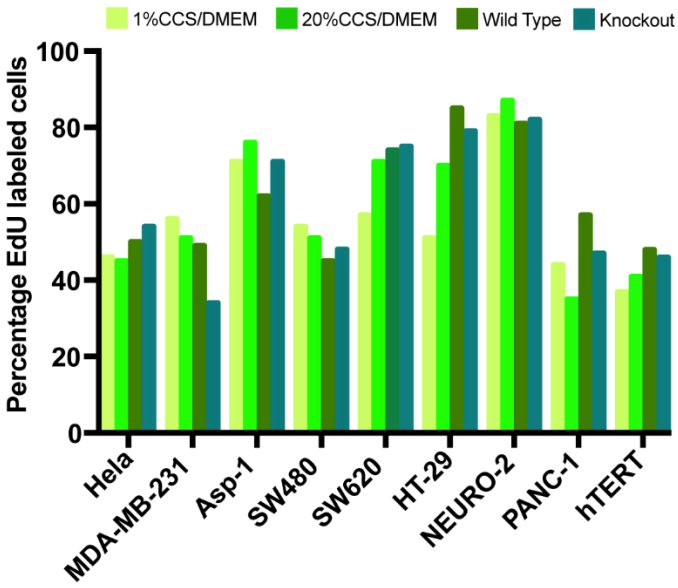

Supplemental Figure 2.6.

(A) Cells from various immortalized/cancerous cell lines were either uninfected (in presence of low or high serum) or infected with Wild Type or HCE1 Knockout *T. gondii* parasites for 20 hrs in the presence of EdU. Monolayers were fixed after 20 hrs and stained for EdU incorporation using Alexa Fluor 488 (green). The percentage of EdU positive nuclei are shown. (**B**) Graphical representation from the data in (A).

TABLES

Table S2.1. *Toxoplasma gondii* parasite strains used in this study.

Common Name	Genotype	Drug Selection	Description
RH *Δku80 Δhxgprt* (Parental)	TgRH *Δku80, Δhxgprt*	N/A	Parental type I RH *T. gondii* used as background strain to make mutant lines.
RH *Δku80 Δhxgprt* TgHCE1-Ty (TgHCE1-Ty)	TgRH *Δku80, Δhxgprt, hce1*-Ty-HXGPRT	MPA/Xan	Tg*hce1* endogenously-tagged line with insertion of HXGPRT drug selection marker in Tg*hce1* coding region.
RH *Δku80 Δhxgprt* TgΔHCE1-Ty *(*Knockout or TgΔHCE1-Ty)	TgRH *Δku80, Δhxgprt, hce1*-Ty-HXGPRT, Δ*hce1*-Ty::Pyr,	Pyr	Tg*hce1* disruptant mutant line with insertion of DHFR drug selection marker in Tg*hce1* coding region and integrants were selected for pyrimethamine resistance.
RH *Δku80 Δhxgprt* TgHCE1-HA (Complement)	TgRH *Δku80, Δhxgprt, hce1*-Ty-HXGPRT, *Δhce1*-Ty::Pyr,	FUDR	The RH Tg*hce1* Knockout line is used where HA-tagged Tg*hce1* was inserted into the UPRT locus and integrants

	Δuprt::*hce1*-HA-Fudr		were selected for FUDR resistance.

Table S2.2. Primers used for cloning of *Toxoplasma gondii* strains, vectors and PCR validation.

Number & Name	**#**	**Sequence (5' to 3')**	**Polarity**
Fw for *hce1* gene ~999kb fragment I05	1	AACCTCAGCCTTTCGCTGTACGCCTAC AGACTCCGCTAGA	sense
Rev for *hce1* gene ~999kb fragment I04	2	GAATGTCGGACGGATCTTCCGAGGTC CACACGAACCAGGA	anti-sense
Fw for pLIC *hce1*-Ty tagging I03	3	GAATGTCGGACGGATCTTCCGAGGTC CACACGAACCAGGA	sense
Rv for pLIC *hce1*-Ty tagging I06	4	AACCTCAGCCTTTCGCTGTACGCCTAC AGACTCCGCTAGA	anti-sense
Fw with sgRNA for HCE1Ty Tagging H99	5	CGGATCTTCCTGACATCAGTGTTTTAG AGCTAGAAATAGC	sense
Rev for CRISPR HCE1Ty tagging F4	6	GTAAATGGGGATGTCAAGTT	anti-sense
A33 PCR Diagnostic Fw	7	TGCCACAGCGGCTCCCCCACAGATT	sense
A34 PCR Diagnostic Rev	8	GTCCAGGGGGTCCTGGTTGGTGTGCA CCTC	anti-sense
K80 PCR Diagnostic Fw	9	CAGTCAAAGCAAGCGCAATTTGCACC AAGCCC	sense

K81 PCR Diagnostic Rev	10	GCGGTATCGGCTCTCCCAGTGGTGGC ACAAATG	anti-sense
Fw sgRNA/hr (for *hce1* cutting (KO))	11	GTTCCTTTACAGACTCCCCGTTTTAGA GCTAGAAATAGC	sense
DHFR fw with 40bd HR	12	AACCTCAGCCTTTCGCTGTAATGAGG ACCGGCGATCACCGCACAGGGGTGCG ACTCATCA	sense
DHFR Rev with 40bd HR	13	TTCGAGCCGATCCCGAAGAAGAATGT CGGACGGATCTTCCTAGAATTCATGG TGAGCAAG	anti-sense
PCR Diagnostic Fw 5'UTR + I12	14	GCATTCATGTGAAGAGCTGGCGGTGT G	sense
PCR Diagnostic Rev 5'UTR +A65	15	GTCGAACAAAGCACGGAGGAGAGAC GGAAAG	Anti-sense
A64 (fw 3'UPRT)	16	ACGACGTCCCGGACTACGCTTAAGCT AGCGTCTCTAGTTTTTTTGACAGACCG CTGACGG	sense
A15 (Rev UPRT)	17	GACGGTTCACTCACTTCACGTTTAGAA GCCCTGTGGACAGGTCCGACGAA	anti-sense
A18 (fw *hce1* gene)	18	GGCTTCTAAACGTGAAGTGAGTGAAC CGTCGGTTCTTGAGAAAACAGGCA	sense

A63 (rev *hce1* gene+HA end)	19	CGAAGAAGAATGTCGGACGGATCTTC CGGTACCTACCCGTACGACGTCCCGG ACTACGCT	Anti-sense
sgRNA for UPRT A19	20	TCTAGACTTTCAACTGACGTGTTTTAG AGCTAGAAATAGC	Sense
A35 PCR Diagnostic Fw	21	GACGTGGGAGCAGGTGACGGATTACT CGCC	sense
A36 PCR Diagnostic Rev	22	CGCCTCGTAAACATTCCCGTTACAGGT GTA	Anti-sense
C88 PCR Diagnostic Fw for ROP18	23	GCGACAGAAAGCACTCGAGACGTTTC ATTG	Sense
C89 PCR Diagnostic Rev for ROP18	24	CTTTCAAGAGGAGGAAATTCGCCGGT TTG	Anti-sense
A90 HCE1Ty Fw pultra	25	GCATGGACGAGCTGTACAAGATGACG CCATGGTTGGCTTTTGCAAGCGCC	sense
B10 HCE1Ty Rev pUltra	26	GAGGTGCACACCAACCAGGACCCCCT GGACTGATCAGAATTCGTTCCGGA	Anti-sense
A97 pUltra fw	27	TGATCAGAATTCGTTCCGGAGTCGTC GACTCGACAATCAA	Sense
B6 pUltra rev	28	CCGGGATCACTCTCGGCATGGACGAG CTGTACAAG	Anti-sense

M83 Seq primer	29	GGTGGCTCACTGGTTCATCTACAGGA AGC	sense
T3 for CRISPR Seq +	30	TCCCTTTAGTGAGGGTTAAT	Anti-sense
EGFP_C_Primer	31	CATGGTCCTGCTGGAGTTCGTG	sense

Table S2.3. Plasmids used in this study

Common Name	Description	Source
pSAG1-CAS9-U6gRNA (UPRT)	Vector expression a fused CRISPR/Cas9 to GFP with a gRNA target sequence within the UPRT locus driven by the U6 promoter. It was then used in mutagenesis to create HCE1 and UPRT targeted CRISPR cutting vectors.	This paper
pLIC-YFP-HXGPRT	Vector containing a ligation independent cloning site (LIC) fused in frame to YFP and the HXGPRT *T. gondii* selectable drug marker.	From Vernon B. Carruthers' lab
pUltra/eGFP Mammalian Expression Vector	A human ubiquitin C (hUbC) promoter driven vector used to clone in Tg*hce1*- EGFP for expression in transient transfection in HFF cells.	Gift from Silvia Moreno's Lab

Table S2.4. Antibodies and reagents used in this study.

Category	Target (clone)	Species	Source	Dilution	Product #
Immunofluorescence Assays: Primary	Ty-Tag	mouse	In house	1/1000	
	GAP45	rabbit	In house/Lampire Biologicals	1/1000	
	GRA7	rabbit	David Sibley	1/1000	
	Cyclin E (E-4)	mouse	Santa Cruz	1/1000	sc-377100
	HA-Tag (6E2)	mouse	Cell Signaling	1/1000	2367
	GFP	rabbit	Invitrogen	1/200	A6455
Immunofluorescence Assays: Secondary	Mouse IgG	Goat conjugated to Alexa488	Life Technologies	1/1000	A11029
	Rabbit IgG	Goat conjugated to Alexa594	Life Technologies	1/1000	A11037

Western Blotting: Primary	Ty-Tag	mouse	In house	1/1000	
	GAP45	rabbit	In house	1/1000	
	HA-Tag (6E2)	mouse	Cell Signaling	1/1000	2367
	GFP	rabbit	Invitrogen	1/2000	A6455
	Cyclin E (HE12)	mouse	Santa Cruz	1/1000	sc-247
	hFAB™ Rhodamine Anti-Actin	human	Bio-Rad	1/1000	12004163
Western Blotting: Secondary	Mouse IgG	Goat conjugated to IRDye 680CW	LI-COR Biosciences	1/2000	926-68070 lot#: C80619-05
	Mouse IgG	Goat conjugated to IRDye 800CW	LI-COR Biosciences	1/1000	926-32210 lot#: C60726-02
Betadine Solution			Fisher Scientific		19027132
Liberase TM			Roche		05401020001
Penicillin Streptomycin			Cytiva / Hyclone		SV30010

Hanks' Balanced Salt Solution			Corning		55-022-PB Lot#: 31420016

CHAPTER 3

CHARACTERIZATION OF AN ESSENTIAL GOLGI LOCALIZED SECRETED EFFECTOR BINDING PROTEIN OF *TOXOPLASMA GONDII*

3.1 INTRODUCTION

The obligate intracellular, *Toxoplasma gondii,* has a remarkable ability to invade and replicate in a wide range of eukaryotic host cell types. While the feline family serves as its definitive host, it is reported to infect a wide range of ruminants, avians and mammals as intermediate hosts, including over two billion people worldwide, resulting in life-long chronic infection. The pathogenesis of human infection is due primarily to the parasite's lytic cycle, which causes host cell destruction and tissue damage. Completion of the *Toxoplasma* lytic cycle requires parasite motility, host cell invasion, and egress, which are facilitated by the exocytosis of an array of proteins from specialized secretory organelles, known as micronemes, rhoptries and dense granules (DGs). Proteins from the DG are the last to discharge and participate in the structural modification of a host-derived membrane called the parasitophorous vacuole (PV). The secretion of micronemes and rhoptries appear to be tightly regulated, whereas the secretion from DGs displays both constitutive and regulated characteristics. To selectively release proteins whose functions are both temporally and spatially distinct, the parasite must first accurately sort these proteins into their respective organelles. Here, we show a novel, essential, parasite Golgi-resident protein, Secreted Effector Binding protein 1 (SEB1), co-purifies both with known secreted proteins and newly discovered secreted *T. gondii* proteins. SEB1 contains a signal sequence and a predicted transmembrane domain. Additionally, through co-immunoprecipitation (coIP) and mass

spectrometry analyses, we identify a number of known DG-targeted and secreted effectors that associate with SEB1. Among these proteins we discovered several highly-conserved vesicular trafficking proteins and a number of signal peptide-containing hypothetical proteins. Downregulation of SEB1 protein expression induces a disorganization of multiple parasite endomembranes, possibly explaining a parasite replication defect. Bioinformatic alignment of the SEB1 amino acid sequence from *Toxoplasma gondii* to the closely related coccidians *Hammondia hammondi* and *Neospora caninum* reveals a highly conserved cytoplasmic tail, suggesting a critical functional role for this domain. Thus, these data establish the function of SEB1 for parasite survival and present preliminary work that will help unravelling the mechanism of this protein.

3.2 RESULTS

Identification of a TgIST secreted effector binding protein 1: SEB1

A previous study by Etheridge *et al.,* 2016 demonstrated that *Toxoplasma* inhibitor of STAT1-dependent transcription (TgIST), a secreted nuclear targeted effector, downregulates IFN-γ signaling to block immune functions [1]. As part of the inhibition of IFN-γ, TgIST and *Toxoplasma* NCoR/SMRT modulator (TgNSM) are together responsible for the induction of necroptotic gene expression in bradyzoite infected cells [2]. This protein recruits the Mi-2/NuRD complex that is known to interact with an array of transcription factors during development to STAT1-dependent promoters, resulting in altered chromatin and blocked transcription [1]. This study also showed when TgIST was utilized as bait for immunoprecipitation (IP) followed by mass spectrometry (MS), a number of novel hypothetical proteins were found with interesting sequence features, including a hypothetical protein that we termed Secreted Effector Binding protein 1. (SEB1). The *seb1* gene encodes for a protein of 1373 amino acids with a predicted molecular

weight of 144 kDa and is annotated as a hypothetical protein (TGGT1_221870 on toxodb.org) (Figures 3.1A and 3.1B). Several different analyses of the SEB1 amino acid sequence predicted that it contains a signal sequence, a putative Type I transmembrane domain, and two repeat domains (Figures 3.1A and 3.1B). Additionally, the *seb1* gene product was analyzed using IUPred3 webserver and revealed regions of protein intrinsic disorder displaying its ability to have protein-protein interactions (Figure 3.1C) [3] . The signal sequence and transmembrane domain of SEB1 are indicated by the low disordered regions (Figure 3.1C). SEB1 was found to be conserved among the coccidia group of apicomplexan parasites as revealed by toxodb.org and blast search. An alignment of the amino acid sequence of SEB1 with its orthologous sequences from other apicomplexans and a phylogenic tree analysis show that it is only present in the coccidian group (Figure 3.1D and Supplemental Figure 3.1). A conserved region of the carboxyl end of the SEB1 amino acid sequence illustrates that this part of the protein is only found within the cyst forming coccidian (Figure 3.1E). This suggests that this C-terminal end may have been recently acquired by the coccidians.

SEB1 is a Golgi apparatus resident protein.

To functionally characterize and localize SEB1, the previously established CRISPR-Cas9 protocols previously established by our lab and others in the *Toxoplasma* field were used [4, 5]. Two plasmid constructs, a pSAG1::Cas9-U6::sgRNA*seb1* and a pLIC-YFP-HXGPRT plasmid containing 1kb 3' fragment of the *seb1* gene were generated. Both constructs were used to transfect the Type I RHΔ*hxgprt*Δ*ku80* parasite strain which favors homologous recombination [6]. To ensure proper integration into the endogenous locus of *seb1*, the transfected parasites were analyzed by Immunofluorescence assay (IFA) and confirmed to have proper SEB1 localization to the parasite's Golgi apparatus of intracellular parasites within infected human foreskin fibroblast

(HFF) (Figure 3.2A). Additionally, a transgenic clonal population of TY-FLAG-epitopes tagged parasites (SEB1-TY-FLAG) were utilized along with an organellar marker to establish co-localization analysis with the αTY labeled parasites. SEB1 co-localizes with the Golgi reassembly stacking protein marker GRASP55 (Figure 3.2B). This co-localization was also confirmed via IFA with the *T. gondii* Golgi marker TgSORTLR and migrates at about 160 kDa, contrary to its unpredicted size ~144 kDa (Figures 3.2C and 3.2D, toxodb.org). Together, these results show SEB1 is a Golgi resident protein.

SEB1 interacts with multiple proteins of the parasite secretory pathway.

SEB1 interactors, including several known GRAs and ROPs (rhoptry proteins), were identified using an IP followed by MS (data not shown). To further study this association robustly, we firstly confirmed that the FLAG-epitope was properly expressing in SEB1-TY-FLAG tagged parasites and utilized these parasites to find SEB1 interactors. A western blot (WB) of the FLAG-epitope showed a similar migration pattern as the TY-epitope WB (αTY) of the SEB1-TY-FLAG strain, which migrates at about 160 kDa (Figure 3.3A). We next used the TgSEB1-Ty-FLAG-epitope tagged strain and wild type untagged RHΔ*hxgprt*Δ*ku80* parasites (control) to identify proteins that coprecipitate with anti-FLAG beads nonspecifically with SEB1 followed by MS analysis. The IP and MS analyses demonstrated that SEB1 co-precipitates with a myriad of known GRA proteins, hypothetical proteins and, surprisingly, with known ER to Golgi machinery (Figures 3.3B, 3.3C and 3.3D and Supplemental Table S3.1). Interestingly, this collection of precipitated proteins from the ER to Golgi trafficking pathway are highly conserved among eukaryotes (Figure 3.3D). We further identified and categorized the remaining interactors based on their fitness conferring scores in *Toxoplasma* (CRISPR-fit score) and domain organization criteria such as presence and absence of signal sequence and transmembrane domain (data not

shown) [7]. Altogether, this suggests that SEB1 may play a role in the trafficking machinery of protein within the parasite.

Conditional ablation of SEB1 in tachyzoites compromises parasite replication.

Initially, we failed to generate *seb1*-knockout parasites using our CRISPR-Cas9 based gene deletion strategy, suggesting the essentiality of SEB1, which is also consistent with the fitness score of -4.35 for SEB1 obtained by Sidik *et al.,* 2016 [7]. While the roles of various essential genes have been characterized using the anhydrotetracycline (ATc-controlled SEB1 expression) or the auxin-inducible degron (Indole-3-Acetic-Acid 'IAA' or Auxin- controlled SEB1 expression) knockdown methods, neither of these systems were able to be used to generate a successful knockdown strain [8-10]. Transfection of parasites with a modified *seb1* sequence to attempt these approaches resulted in complete lethality, suggesting that SEB1 might be refractory of certain genetic changes. Therefore, we successfully adopted a LoxP/U1 RNA destabilization strategy in a dimerizable Cre-mediated recombinase DiCre-expressing strain to knockdown the expression level of SEB1 upon rapamycin addition. To do this, we used the RHΔ*ku80*-Dicre:KRed$_{flox}$YFP as the parental strain [11-13]. An HA-epitope was simultaneously engineered in the endogenous locus of *seb1,* hereafter this strain is termed SEB1-KD (Figure 3.4A). Correct localization of SEB1 was assayed via IFA and its correct migration in WB was found at the expected size of 160 kDa as previously observed (Figures 3.4B and 3.4C). Moreover, we observed a significant downregulation of SEB1 starting at 48 hours of rapamycin treatment via WB (Figures 3.4D, 3.4E and Supplemental Figure 3.4). Parasites conditionally depleted of SEB1 were unable to form plaques on human foreskin fibroblast (HFF) monolayer cells, suggesting the inability of the SEB1 mutant to efficiently complete the life cycle compared to the parental DiCre strain parasite (Figures 3.5A and 3.5B). Because the replicative cycle of the parasite consists of a series

of events such as host cell attachment, invasion, parasite replication, and egress, we sought to determine specific aspect of the parasite's life cycle affected by the loss of SEB1. During our routine parasite culturing, we observed a clear invasion process after knockdown of SEB1. To determine the impact of loss of SEB1 on the parasites, we conducted a two-color IF-based intracellular invasion study using pre-treated parasites that were allowed to infect HFFs for approximately 48 hours. We used freshly lysed parasites to infect new HFF cell monolayers as described in the schematic Figure 3.5C to assess the invasion process [14, 15]. It is noteworthy to mention the limitation of the color choice for this proposed assay because it is slightly different than the original Red/Green assay [16]. We initially chose RHΔ*ku80*-Dicre:KRed$_{flox}$YFP as the parental strain, therefore, these parasites are simultaneously changing color from red to green in the presence of rapamycin as the constitutive p5RT70 promoter drives the Killer red (KRed) expression [11]. Therefore, we resorted to using a red and blue two-color invasion IF-based assay. We took advantage of the outer surface of the plasma membrane of uninvaded parasites, which is fully exposed, and labelled it directly using an antibody against the surface antigen protein 1 (SAG1). Conversely, invaded parasites can only be labelled after the host cell permeabilization utilizing another antibody against SAG1 from a different animal. SEB1-KD parasites revealed a mild invasion defect in comparison to the wild type DiCre strain (Figures 3.5D and 3.5E). To continue with the investigation on the impact of SEB1 in the lytic cycle of the parasite, we next assessed its impact upon depletion on parasite replication. For this, we followed the same pre-treatment protocol described on Figure 3.5C and let the parasites invade HFF cell monolayers on coverslips for follow-up parasite replication studies. Interestingly, for the SEB1-KD strain, the percentage of vacuoles containing 2 parasites after treatment with rapamycin in HFFs was significantly higher than the other strains (untreated SEB1-KD parasites, the parental treated and

untreated strains). Concomitantly, the percentage of vacuoles containing 8 parasites for SEB1-KD treated with rapamycin line was considerably lower than all the other conditions (Figure 3.5F). This suggests that there is an early block of parasite replication in mother cells, with vacuoles containing 2 mothers being unable to undergo endodyogeny properly. These results strongly imply a replication defect in parasites lacking SEB1.

Depletion of SEB1 expression level shows a disorganization of the endomembranes of *T. gondii*.

Following 72 hours of rapamycin treatment, the intracellular growth of SEB1-deficient tachyzoites led to a severe impairment in parasites vacuoles containing 2 mothers, (Figure 3.5F). A parasite sample preparation was obtained as described in Figure 3.6A and intracellular tachyzoites were subjected to a morphological analysis using transmission electron microscopy (TEM). Multiple ultrathin sections of SEB1-KD parasites exhibited a significant disorganization of their vesicles compared to wild type parasites (Figure 3.6B). Because SEB1 is a Golgi-resident protein, we noted what appeared to be "collapsed or disturbed" Golgi in SEB1-KD parasites (Figure 3.6B), potentially explaining why KD parasites failed to replicate (Figure 3.5F). This overall observed disruption of the parasite endomembranes, especially the impairment of the Golgi apparatus, could be the cause of the lethal phenotype. Therefore, we next investigated the dynamic nature of parasite vesicles during endodyogeny. We took advantage of the morphological markers, IMC1 and IMC3, capable of tracking the cell cycle during daughter parasite formation [17-19]. Additionally, it has been demonstrated that the development of the daughter IMC begins with the encapsulation of centrioles and Golgi, followed by the apicoplast, nucleus, and ER, to ultimately acquire the plasma membrane of the mother while leaving all the unencapsulated materials as a residual body [19, 20]. Thus, we used IFA to characterize Golgi duplication and distribution in

daughter-forming SEB1-KD tachyzoites at 72 hours post rapamycin treatment. Although it appears that these parasites featured some mis-segregation or odd partition of the Golgi during earlier replication of daughter parasite elongation (data not shown), a quantitative analysis of SEB1-KB treated and untreated fluorescence parasites stained with IMC and Golgi markers confirmed no significant difference between the two strains (data not shown). This apparent mis-segregation of the Golgi seems to be normal and a rare morphological anomaly that has also been seen in the previous report by Dinkorma T. Ouologuem and David S. Roos in 2014 during their observation of daughter parasite elongation while investigating the IMC membrane dynamics during parasite replication [21]. However, the authors did not mention any Golgi distribution abnormality after binary fission, as after about 4 hours post-initiation it was seen that some mother cells contained their Golgi while developing daughters received theirs after their emergence from the mother parasite [21]. To be specific, a total of three Golgi apparati was identified: one in the mother and one in each emerging daughter [21]. We therefore concluded that there was no aberrant Golgi organelle division nor its partition when comparing both SEB1-KB treated and untreated parasites. Moreover, using IFA, we assayed the duplication of the centriole, the nucleus, and the Golgi apparatus of parasite undergoing endodyogeny and noticed that these structures were unperturbed (Figures 3.6C and 3.6D). Concomitantly, the effect of SEB1-KO on the localization of secretory proteins, which are dependent on Golgi trafficking, was investigated in intracellular and extracellular SEB1-KD tachyzoites. We examined the localization of transmembrane protein MIC2 to the micronemes, GRA2 to the dense granules, and ROP7 to the rhoptries in presence and absence of rapamycin and they showed no trafficking disruption upon the downregulation of SEB1 (Supplemental Figures S3.6A, S3.6B, S3.6C). We also showed that trafficking of ATrx1 to its destination membrane-bound apicoplast organelle not affected (Supplemental Figure S3.6D).

ATrx1 is a protein that does not required Golgi-trafficking to reach its final destination. In sum, although we noticed a clear disorganization of the endomembranes of *T. gondii* in downregulated SEB1 parasites using a TEM approach, we were unable to observe a phenotype via immunofluorescence assay after knockdown of SEB1.

3.3 DISCUSSION

This work reports our continuing progress in characterizing novel Golgi resident protein, termed SEB1, that we found to be essential for *T. gondii* lytic cycle. Using an in silico bioinformatic approach, we determined that SEB1 contained an amino acid sequence which is preserved within the apicomplexan group, and specifically to the coccidian branch. That sequence may be important for the function of this protein and so far, remains uncharacterized. To identify the phenotypic consequences of SEB1 knockdown, we used a Cre-mediated recombinase system to regulate *seb1* expression. Downregulation of the *seb1* gene inhibited parasite replication in the PV and induced a disorganization of the endomembranes of *T. gondii* as it has been demonstrated by TEM. This insinuated that SEB1 may be important for maintaining the endomembrane structures in *T. gondii*. Importantly, at the moment we cannot verify through additional observation the defect in morphology that we observed in TEM in downregulated SEB1 parasite. Uncovering the SEB1 mechanism(s) promoting the survival of *T. gondii* remains an important goal. Failure of *T. gondii* to maintain its physiology can cause the parasite death, especially if the Golgi is compromised which can eventually lead to multiple effect such as a dysregulation of protein trafficking. Initial studies by IFA did not detect any defects in the gross morphology of *T. gondii* secretory vesicles. Surprisingly, in these studies, the Golgi apparatus was able to partition correctly in daughter parasites subsequent to their emergence from the mother in SEB1 knockdown

parasites. In sum, our IFA approach was unable to explain the observed TEM phenotype; nonetheless, our goal remains to understand the contribution of SEB1 for parasite survival and the defective endomembranes in SEB1-KD parasite. Chapter 4 of this dissertation presents future approaches that will be taken to continue deciphering the role of SEB1.

3.4 MATERIALS AND METHODS

Parasite and Cell Culture

Both human telomerase reverse transcriptase (hTERT) and human foreskin fibroblast (HFF) cells are used in this research. *T. gondii* tachyzoites were maintained in these two cell line monolayers by serial passage in and were grown in complete Dulbecco's modified Eagle's medium (DMEM) containing 4.5 g/L glucose, 4 mM L-glutamine, 1X penicillin-streptomycin solution (Corning) with either 10% or 1% (when necessary) cosmic calf serum (CCS) at 37°C in 5% CO_2. Primer sets are listed in Table S3.2. Stable transgenic parasites were selected in 50 μg/mL mycophenolic acid (MPA) and 50 μg/mL xanthine (Xa), 3mM pyrimethamine (Pyr), (Sigma).

Alignment analysis of selected SEB1 homologs

The homologs of SEB1 were found using toxoDB and a blast search tool (https://toxodb.org/toxo/app and https://blast.ncbi.nlm.nih.gov/Blast.cgi). Protein sequences for the homologs of SEB1 were aligned using the bioinformatics software platform Geneious Prime (https://www.geneious.com).

Cloning of plasmids and parasite cloning

To generate SEB1-TY-FLAG parasite strain, the CRISPR-Cas9 system was similarly used as on chapter 2. The vector pSAG1::Cas9-U6::sgRNA was used with *seb1* gene specific guide RNA. Primer set 1 and 2 was used to generate this construct. Next, an 1kb of *seb1* gene was

amplified from the parental genomic DNA via PCR using primers 3 (forward) and 4 (reverse). A PCR fragment of pLIC vector was amplified using primers 5 (forward) and 6 (reverse). The resulting PCR fragments were used to construct a pLIC-SEB1-TY-FLAG vector. Both constructs were used for co-transfection hTERTs cells with parental parasites TgRH Δ*ku80,* Δ*hxgprt*, and parasites were selected with the 50 μg/mL mycophenolic acid (MPA) and 50 μg/mL xanthine (Xa) for HXGPRT [22]. The parasites were then single-cloned into 96-well plates by limiting dilution, screened for endogenous integration at the correct locus via IFA (immunofluorescence imaging) as described on chapter 2. Correct C-terminal tags were confirmed by IFAs and western blots.

To generate the SEB1 knockdown strain (SEB1-KD), we used the RHΔku80::KRedflox-YFP DiCre generated strain from Pieperhoff *et al.,* 2015 as parental strain [11]. In absence of rapamycin the constitutive p5RT70 promoter drives Killer Red (KRed) expression and SAG1 drives HXGPRT expression. Upon addition of rapamycin, in one hand, the floxed open reading frame of kred and HXGPRT are excised by Cre/loxP site specific recombination and replaced by YFP and 4U1 respectively. The same vector pSAG1::Cas9-U6::sgRNA above was used with *seb1* gene specific guide RNA to target *seb1*. We next inserted 1 kb of *seb1* into a U1 LoxP knockdown vector to generate the plasmid pSEB1-HA-(3'UTR$_{SAG1}$-5'UTR$_{DHFR}$-HXGPRT-3'UTR$_{DHFR}$)$_{floxLoxP}$-4xU1. Primers 7, 8, 9, 10 were used to generate this plasmid. The parental line was stably transfected with both plasmids (50μg each) into the parental strain. Transfectants were selected for HXGPRT with 50 μg/mL mycophenolic acid (MPA) and 50 μg/mL xanthine (Xa) for HXGPRT and were subsequently cloned using limiting dilution [22]. Integration was confirmed by IFAs and western blots.

Parasite immunofluorescence assay and microscopy Immunofluorescence Assays

For intracellular tachyzoites:

HFF cells were grown on 12mm glass coverslips to confluency and then infected. Samples were fixed with 4% paraformaldehyde in PBS for 10 minutes, then permeabilized with 0.5% Triton X-100 in PBS for 10 minutes and blocked in 5% cosmic calf serum (CCS) in PBS for 30 minutes. Cells were incubated with primary antibodies for 60 minutes and then washed three times in PBS (see Table S3.3 for primary antibodies used). Secondary antibodies, goat anti-mouse IgG Alexa fluor 488 and goat anti-rabbit IgG Alexa fluor 594 (Life Technologies) as well as DAPI were added for 60 minutes followed by a PBS wash. Coverslips were mounted with Fluoro-Gel (Electron Microscopy Sciences) and images were acquired with the Lionheart™ FX Automated Microscope (BioTek Instruments, Inc.).

For extracellular tachyzoites:

Freshly lysed tachyzoites were collected, centrifuged and washed with Buffer A with glucose (BAG: 116 mM NaCl, 5.4 mM KCl, 0.8 mM MgSO4, 50 mM HEPES, and 5.5 mM Glucose). The extracellular parasites were fixed to pre-coated coverslips with polylysine-L and fixed in 4% paraformaldehyde in PBS for 15 min. After fixation, the extracellular parasites were similarly treated as the intracellular parasites (see above paragraph).

Plaque Assay

Plaque assays were performed using protocols in our laboratory as previously described with some modifications (referred to chapter 2 this thesis). A total of 100 freshly egressed tachyzoites, pre-treated with rapamycin or untreated was added to each well of a 6-well plate containing confluent HFF cells monolayer. Plates were incubated undisturbed at 37˚C with 5% CO^2 for 7 days. The pre-treated parasites were incubated with corresponding incubation medium supplemented with the 50nM of rapamycin concentration while the untreated parasites were incubated with medium without rapamycin. On day 7, the wells were washed once with PBS,

incubated in 100% ethanol for 5 minutes followed by staining with crystal violet (CV). Plates were washed with deionized (DI) water, air-dried and were visualized using the ChemiDoc^{TM} MP Imaging System (Biorad).

Red/Blue Invasion assay

The Red/Blue invasion assay was performed following the well-established Red/Green colorimetric immunofluorescence-based (IF-based) invasion assay developed by Leung *et al.,* 2017 with a few modifications [16]. SEB1-KD and the DiCre parental (RHΔKu80-DiCre:KRed$_{flox}$YFP) line in presence and absence of rapamycin were used for this experiment. The parasites were prepared as described in Figure 3.5C. Freshly lysed parasites were used to assess the invasion process in HFF monolayers. All parasites were cultured to be at the same stage at the time of harvest and infection. The parasites were filtered to remove any host cell debris, were resuspended in ice-cold invasion media (3% cosmic calf serum 'CCS' and 10 mM HEPES in DMEM-HG) and were kept at 4°C on ice to allow them to settle on the host cell monolayer that was pre-chilled on ice. The media from the pre-chilled 24 well plate was aspirated and replaced with 300 µl of invasion media plus 200 µl of the parasite suspension (suspension stock: 1 x 10^8 parasites in 1 ml) and the plate was incubated on ice for 20 minutes. Furthermore, the 24 well plate was transferred to a 37°C water bath and parasites were allowed to invade host cells for 5 minutes. The invasion was stopped by washing each well with PBS twice, immediately fixed with 4% paraformaldehyde, and blocked in 5% CCS in PBS for 30 minutes. Extracellular parasites are labeled with rabbit anti-SAG1 polyclonal antibody (1:1000) (a generous gift from Silvia Moreno lab at University of Georgia Athens) for 60 minutes at room temperature. Wells were washed with PBS 3 times to remove antibody (5 minutes incubation at room temperature between each wash) and were permeabilizated with 0.5% Triton X-100 in PBS for 10 minutes and washed 3 times with

PBS. Parasites were then probed with mouse anti-SAG1 monoclonal antibody (1:1000) (ATCC: NR50255) for 60 minutes at room temperature. Cells were washed with PBS 3 times to remove antibody. Secondaries against rabbit (blue; 1,1000) and mouse (red; 1:1000) were used to distinguish invasion from attachment. Secondaries were incubated for 60 minutes at room temperature and washed with PBS 3 times. Counting of red and blue labeled parasites was compiled from three independent experiments via fluorescence microscopy by counting 15 fields of view selected at random and Graph Pad Prism Software was used to make the graph.

Immunofluorescence assay for intracellular replication assay

The intracellular replication assays were performed as previously described above in the "Parasite immunofluorescence assay and microscopy Immunofluorescence Assays" for intracellular tachyzoites section. In addition to that, parasites were prepared in a similarly fashion to the "Red/Blue invasion assay" where they were first cultured for 48 hours in T25 cm^2 flask containing HFF monolayers in presence and absence of rapamycin as depicted in Figure 3.5C. Next, freshly lysed parasites were used to inoculate coverslips with HFF monolayers for 24 hours in presence and absence of rapamycin. Then, the infected cells were processed for immunofluorescence as described above, using antibodies for marker of the parasite surface (SAG1 and the fluorescent nucleic acid stain (DAPI) to count the number of parasites per vacuole and to assess the percentage of replication defects. The number of parasites per vacuole was determined as 2, 4, 8, ≥16; (the number of parasites that was not an integral power of 2 was not part of the counting process). Vacuoles numbers were assessed for each parasite line and condition in each of three independent biological replicates. The data were analyzed using two-way ANOVA multiple comparisons tests with GraphPad Prism v7. Statistically significant, multiplicity adjusted *P* values for comparisons are indicated with asterisks. Other antibodies such as marker

for parasite surface (SAG1), for the mother and daughter cortex (IMC1 and IMC3), centrioles (CEN1), apicoplast (Atrx1), GRA2, MIC2, ROP7 were used to assess intracellular parasite protein secretion.

Transmission Electron Microscopy.

Transmission electron microscopy was done using SEB1-KD and the Dicre parental line in presence and absence of rapamycin. The parasites were prepared as described Figure 3.6A. The flasks were incubated in 1% cosmic calf serum (CCS) in DMEM media at 37°C in 5% CO_2. Host infected HHF monolayers were gently and manually scraped post 24 hours of infection for a total of 72 hours of rapamycin incubation. Furthermore, parasites were fixed for 1 hour at room temperature with 2.5% glutaraldehyde in 0.1 M Cacodylate-HCl buffer, pH 7.2 and the samples were sent to the Department of Molecular Microbiology, Washington University School of Medicine, St. Louis, MO 63110. Sample preparation and images were lastly performed by Dr. Wandy Beatty.

3.6 ACKNOWLEDGMENTS

We are thankful for Silvia Moreno, Christopher West, Vern Carruthers, Garry Ward, Peter Bradley and Markus Meissner for respectively providing us the SAG1 (surface antigen protein 1), HA, TgSORTLR (SORTILIN), IMC1 (Inner Membrane Complex), Atrx1 (apicoplast) antibodies and the parental parasite DiCre expressing strain (RHΔ*ku80*-Dicre:KRed$_{flox}$YFP).

This study was supported by the National Institutes of Health (NIH:T32), The Center for Tropical and Emerging Global Diseases (CTEGD) *at* the University of Georgia and Office of the Vice President for Research (NIH:T32/CTEGD-OVPR; NIH/NIAID (R21AI142431)

FIGURES

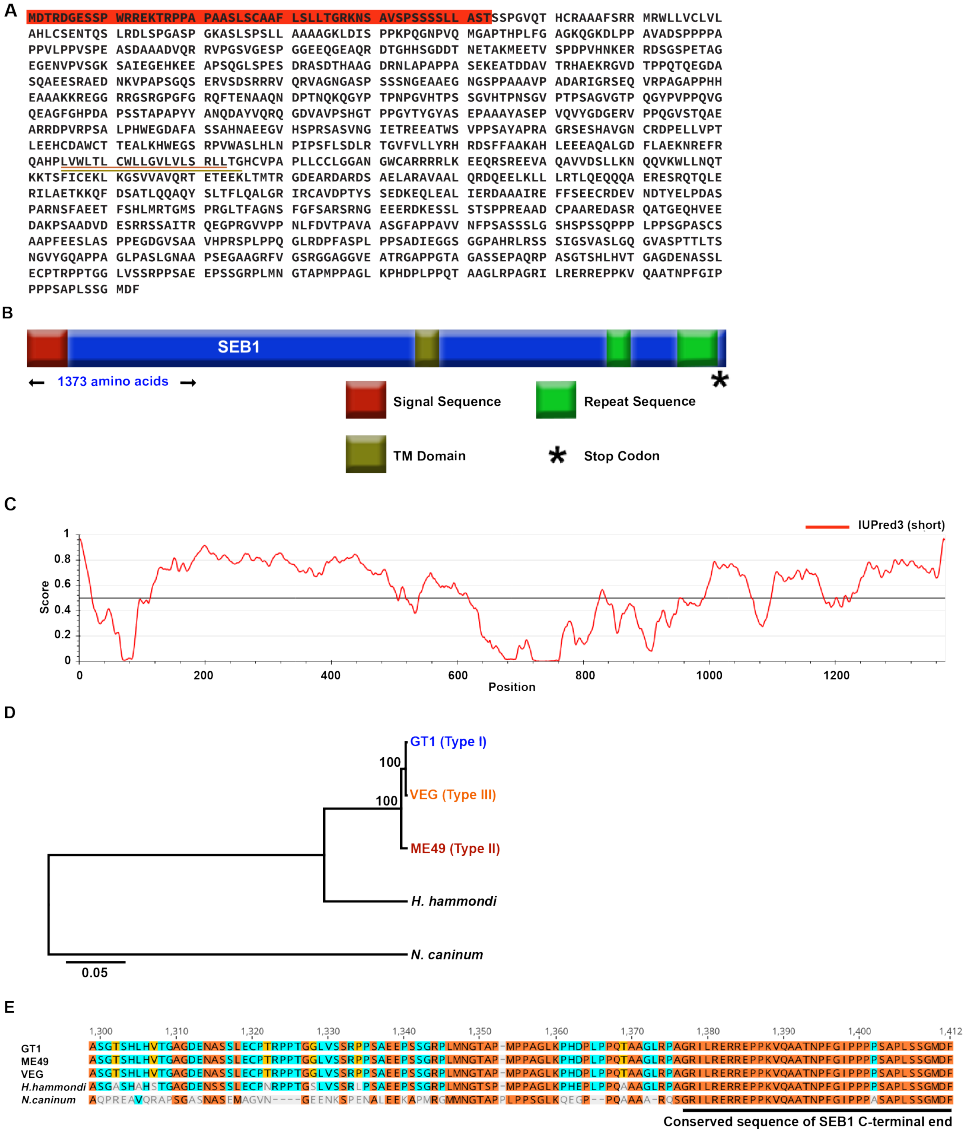
A
MDTRDGESSP WRREKTRPPA PAASLSCAAF LSLLTGRKNS AVSPSSSSLL ASTSSPGVQT HCRAAAFSRR MRWLLVCLVL
AHLCSENTQS LRDLSPGASP GKASLSPSLL AAAAGKLDIS PPKPQGNPVQ MGAPTHPLFG AGKQGKDLPP AVADSPPPPA
PPVLPPVSPE ASDAAADVQR RVPGSVGESP GGEEQGEAQR DTGHHSGDDT NETAKMEETV SPDPVHNKER RDSGSPETAG
EGENVPVSGK SAIEGEHKEE APSQGLSPES DRASDTHAAG DRNLAPAPPA SEKEATDDAV TRHAEKRGVD TPPQTQEGDA
SQAEESRAED NKVPAPSGQS ERVSDSRRRV QRVAGNGASP SSSNGEAAEG NGSPPAAAVP ADARIGRSEQ VRPAGAPPHH
EAAAKKREGG RRGSRGPGFG RQFTENAAQN DPTNQKQGYP TPNPGVHTPS SGVHTPNSGV PTPSAGVGTP QGYPVPPQVG
QEAGFGHPDA PSSTAPAPYY ANQDAYVQRQ GDVAVPSHGT PPGYTYGYAS EPAAAYASEP VQVYGDGERV PPQGVSTQAE
ARRDPVRPSA LPHWEGDAFA SSAHNAEEGV HSPRSASVNG IETREEATWS VPPSAYAPRA GRSESHAVGN CRDPELLVPT
LEEHCDAWCT TEALKHWEGS RPVWASLHLN PIPSFLSDLR TGVFVLLYRH RDSFFAAKAH LEEEAQALGD FLAEKNREFR
QAHPLVWLTL CWLLGVLVLS RLLTGHCVPA PLLCCLGGAN GWCARRRRLK EEQRSREEVA QAVVDSLLKN QQVKWLLNQT
KKTSFICEKL KGSVVAVQRT ETEEKLTMTR GDEARDARDS AELARAVAAL QRDQEELKLL LRTLQEQQQA ERESRQTQLE
RILAETKKQF DSATLQQAQY SLTFLQALGR IRCAVDPTYS SEDKEQLEAL IERDAAAIRE FFSEECRDEV NDTYELPDAS
PARNSFAEET FSHLMRTGMS PRGLTFAGNS FGFSARSRNG EEERDKESSL STSPPREAAD CPAAREDASR QATGEQHVEE
DAKPSAADVD ESRRSSAITR QEGPRGVVPP NLFDVTPAVA ASGFAPPAVV NFPSASSSLG SHSPSSQPPP LPPSGPASCS
AAPFEESLAS PPEGDGVSAA VHPRSPLPPQ GLRDPFASPL PPSADIEGGS GGPAHRLRSS SIGSVASLGQ GVASPTTLTS
NGVYGQAPPA GLPASLGNAA PSEGAAGRFV GSRGGAGGVE ATRGAPPGTA GASSEPAQRP ASGTSHLHVT GAGDENASSL
ECPTRPPTGG LVSSRPPSAE EPSSGRPLMN GTAPMPPAGL KPHDPLPPQT AAGLRPAGRI LRERREPPKV QAATNPFGIP
PPPSAPLSSG MDF
B
SEB1
1373 amino acids
Signal Sequence
Repeat Sequence
TM Domain
Stop Codon
C
IUPred3 (short)
Score
Position
D
GT1 (Type I)
VEG (Type III)
ME49 (Type II)
H. hammondi
N. caninum
100
100
0.05
E
GT1
ME49
VEG
H.hammondi
N.caninum
Conserved sequence of SEB1 C-terminal end

Figure 3.1. Identification of a TgIST secreted effector binding protein 1 (SEB1).

(A) Amino acid sequence of TGGT1_221870. The predicted signal peptide is highlighted in red (Signal-3L prediction), while the predicted transmembrane domains are indicated by underlines (Orange – Phobius prediction, Olive green – SMART prediction). **(B)** Schematic representation of the SEB1 protein with SMART predicted domains. The transmembrane domain (TM domain) is shown in olive green, and two internal repeat sequences are shown in green. The putative signal sequence is shown in red (as predicted by Signal-3L). **(C)** Results from IUPred3 short disorder prediction of TGGT1_221870 protein intrinsic disorder is displayed using medium smoothing. The score indicates regions of low and high disorder. **(D)** Phylogenetic tree showing the relationship of the Type I (GT1), II (ME49), III (VEG) strains of *Toxoplasma gondii* amino acid sequences with SEB1 homologues in Apicomplexans. The tree was constructed using Geneious. **(E)** An alignment of C-terminal end of SEB1 with the three clonal lineages of *T. gondii* (*T.g.*), *Hammondia h.* (*H.h.*) and *Neospora c.* (*N.c*.) depicts high conservation at the C-terminal end of the protein. The alignment was done using Geneious.

Supplemental Figure 3.1

(A) SEB1 amino acid sequence alignment. The alignment was done using Geneious with the predicted amino acid sequence for the primary translation product of the SEB1 gene for the three clonal lineages of *T. gondii* Type I (GT1), II (ME49) and III (VEG), *Hammondia h.* (*H.h.*) and Neospora c. (*N.c.*); and two internal repeat sequences are underlined in black

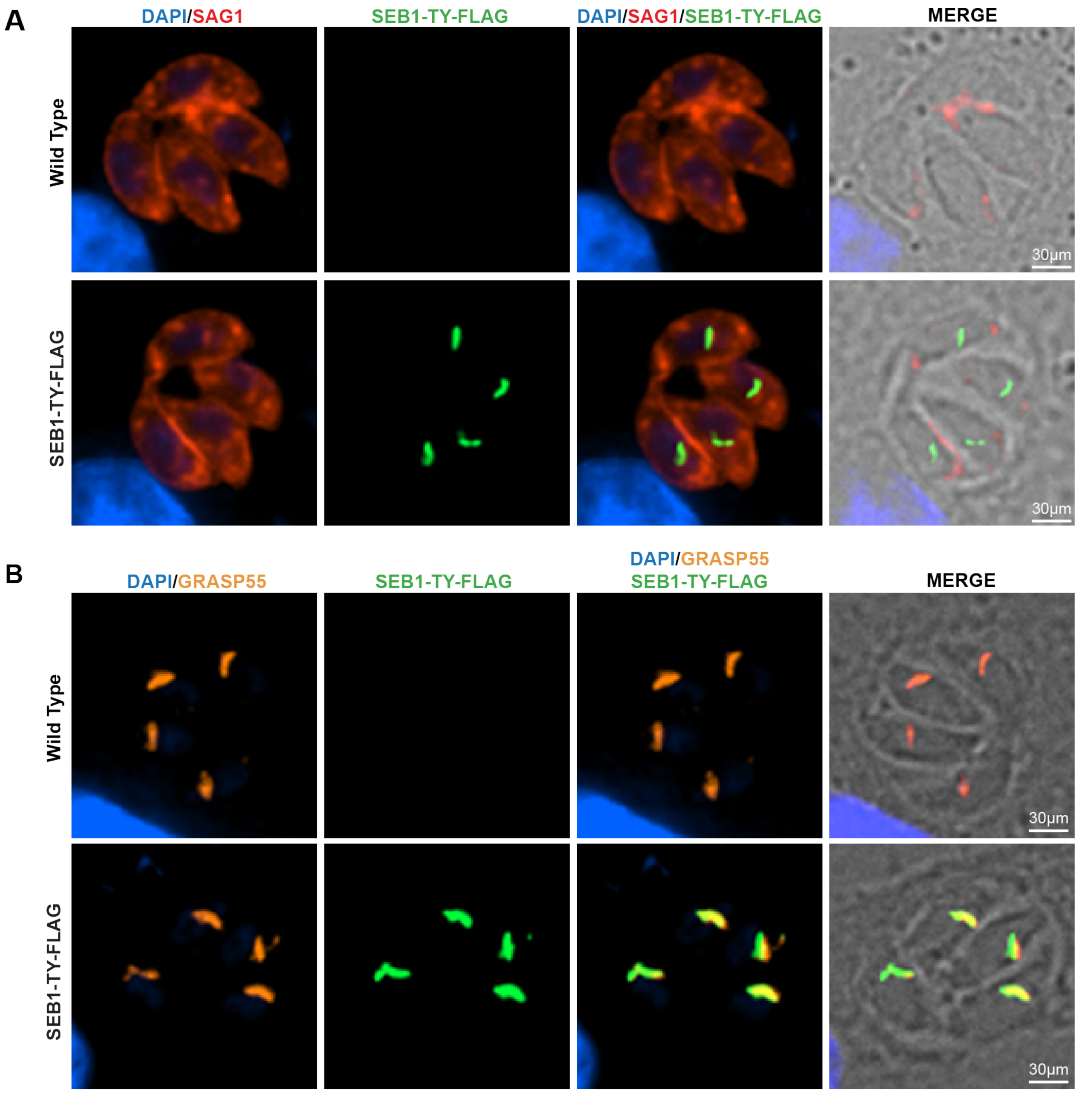
A
DAPI/SAG1
SEB1-TY-FLAG
DAPI/SAG1/SEB1-TY-FLAG
MERGE
Wild Type
SEB1-TY-FLAG
30µm
30µm
B
DAPI/GRASP55
SEB1-TY-FLAG
DAPI/GRASP55
SEB1-TY-FLAG
MERGE
Wild Type
SEB1-TY-FLAG
30µm
30µm

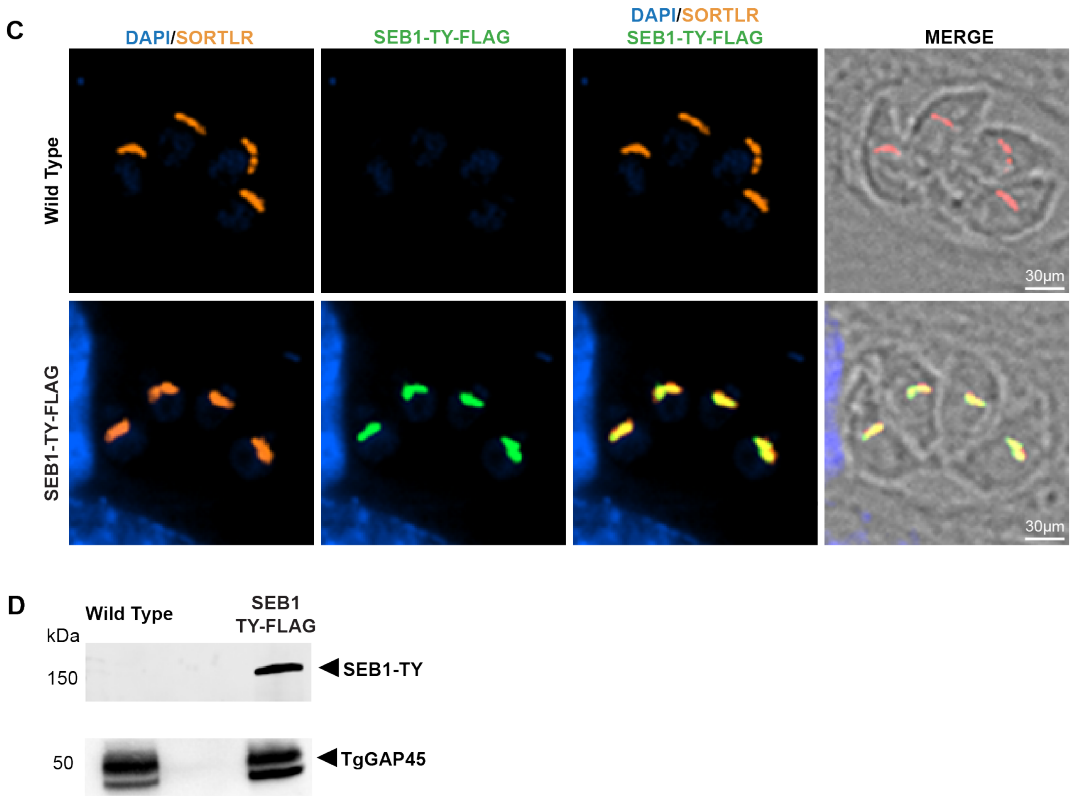

Figure 3.2. SEB1 is a parasite Golgi apparatus resident protein.

(A) HFF cells infected (24hrs) with wild type and SEB1-TY-FLAG expressing *T. gondii* (Red). rabbit monoclonal anti-SAG1 for parasite surface marker (red), mouse monoclonal anti-TY antibody TY-tagged parasites (green) and DAPI nuclei (blue). Scale 30µm. Right = merge with bright field. **(B)** HFF cells infected (24hrs) with tachyzoites (wild type and SEB1-TY-FLAG expressing *T. gondii*) transiently expressing GRASP55-RFP and mouse monoclonal anti-TY antibody. GRASP55 (red), mouse monoclonal anti-TY antibody TY-tagged parasites (green) and DAPI nuclei (blue). Scale 30µm. Right = merge with bright field. **(C)** HFF cells infected (24hrs) with wild type and SEB1-TY-FLAG. mouse monoclonal anti-TgSORTLR antibody TgSORTLR (red), rabbit monoclonal anti-FLAG antibody FLAG-tagged parasites (green) and DAPI nuclei (blue). Scale 30µm. Right = merge with bright field. **(D)** Western blot comparing parental strain

(wild type) and SEB1-TY-FLAG expressing parasites: mouse monoclonal anti-TY antibody was used to detect the tagged line and rabbit monoclonal anti-GAP45 was used as control.

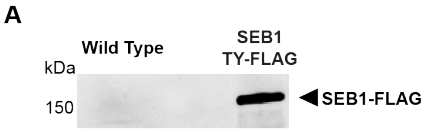

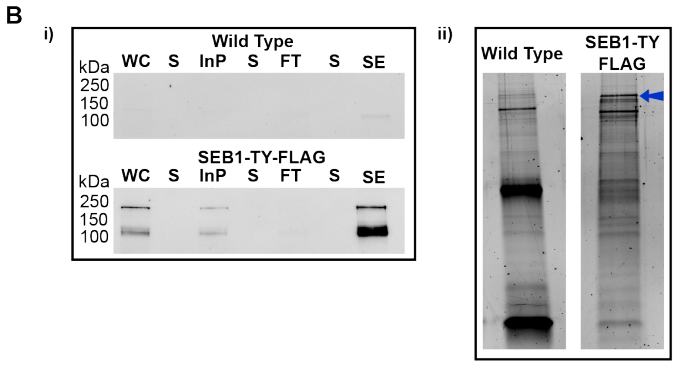

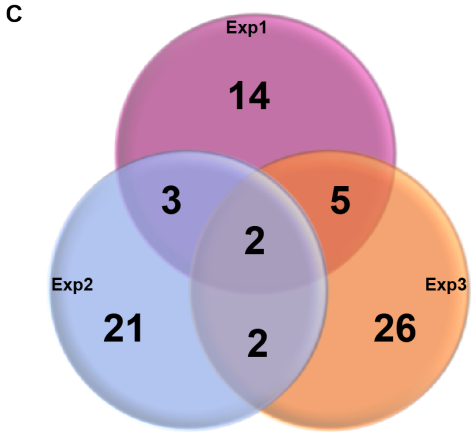

D

Identified Protein	Gene ID	MW (kDa)
BiP	TGGT1_311720	73
Sec24	TGGT1_277000	108
Sec23/Sec24	TGGT1_291680	88
WD domain	TGGT1_320210	56
Rab1	TGGT1_214770	23
Rab11A	TGGT1_289680	25
Toxofilin	TGGT1_214080	27
TgSRTLR	TGGT1_290160	114
GRA2	TGGT1_227620	20
GRA5	TGGT1_286450	13
GRA6	TGGT1_275440	23
GRA12	TGGT1_288650	48
ROP1	TGGT1_309590	50
ROP4	TGGT1_295125	40
ROP5	TGVEG_442220	61
ROP7	TGGT1_295110	63
IMC4	TGGT1_231630	53
LDH1	TGGT1_232350	36
SPM1	TGGT1_263520	39
HSP90	TGGT1_288380	82
GAPDH1	TGGT1_289690	53

Figure 3.3. SEB1 interacts with multiple proteins of the parasite secretory pathway and trafficking.

(A) Western blot comparing parental strain (Wild Type) and SEB1-TY-FLAG expressing parasites: mouse monoclonal anti-FLAG antibody was used to detect the tagged line and rabbit monoclonal anti-GAP45 was used as control. **(B)** Western blot (i) and oriole stain (ii) analyses of total nuclear lysates confirming FLAG-epitope tagging of SEB1, SEB1 is indicated with blue arrow (WC: Whole Cell Lysate; InP: Input; FT: Flow Through; SE: Specific Elution; S: Empty Space). **(C)** Venn diagram showing 3 independents pull down Mass Spectrometry results of the number of proteins and their commonality within the experiments. Those proteins are presented in a table format on supplemental figure 3S and the proteins were identified by two or more peptides with a confidence above 95 % (Scaffold) from the analysis. **(D)** Known *Toxoplasma gondii* proteins that interact with SEB1, identified by mass spectrometry analysis. Proteins were identified by two or more peptides with a confidence above 95 % (Scaffold) from the analysis.

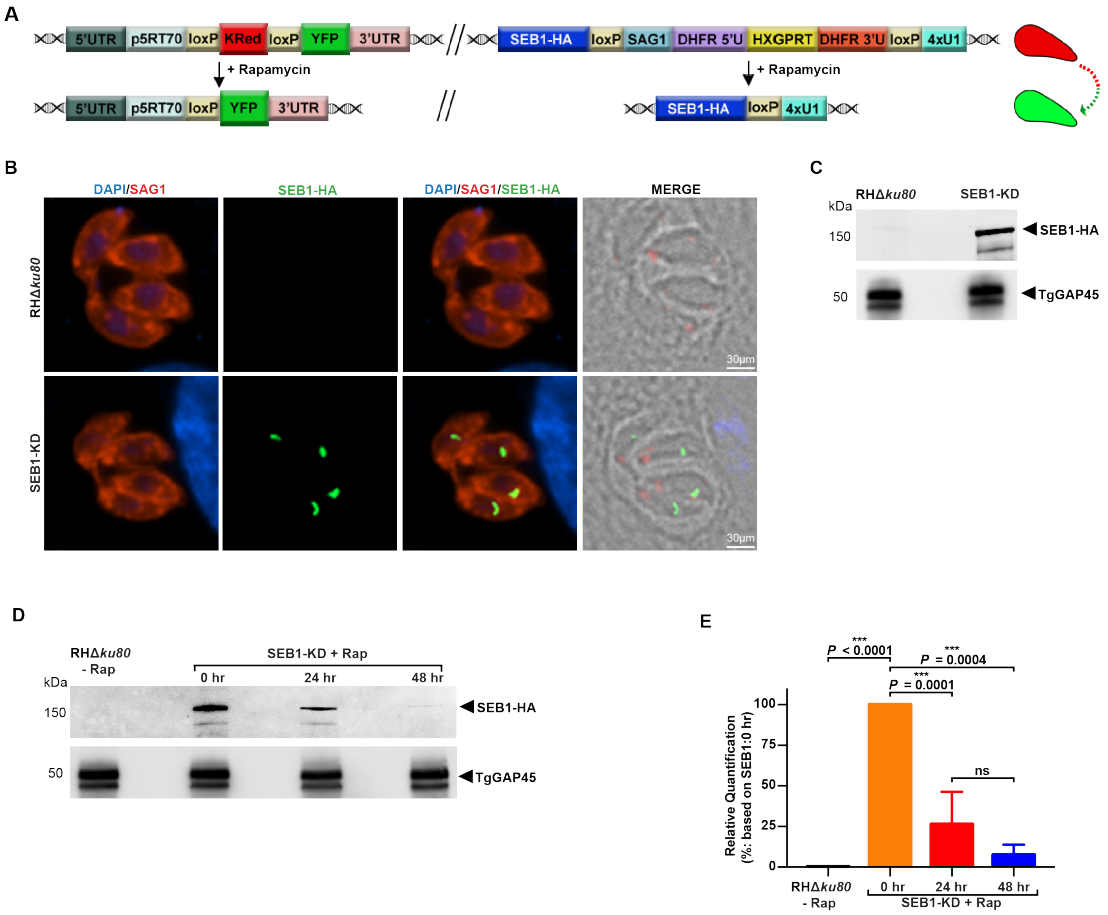

Figure 3.4. Conditional ablation of SEB1 gene in *T. gondii*.

(A) Schematic of SEB1 knockdown line (SEB1-KD) using the RHΔku80::KRedflox-YFP DiCre generated strain from Pieperhoff *et al.,* 2015. In absence of rapamycin the constitutive p5RT70 promoter drives Killer Red (KRed) expression and SAG1 drives HXGPRT expression. Upon addition of rapamycin, the floxed open reading frame of kred and HXGPRT are excised by Cre/loxP site specific recombination and then replaced by YFP and 4U1 respectively. The snRNP U1 mediates adjacent to the termination codon of SEB1 leading to its conditional knockdown in presence of rapamycin-induction. **(B)** HFF cells infected (24hrs) with wild type RHΔku80 DiCre strain and SEB1-KD expressing *T. gondii*: rabbit monoclonal anti-SAG1 for parasite surface

marker (red), mouse monoclonal anti-HA hemagglutinin antibody (green) and DAPI nuclei (blue). Scale 30μm. Right = merge with bright field. **(C)** Western blot comparing parental strain RHΔku80 DiCre strain and SEB1-KD expressing parasites: mouse monoclonal anti-HA hemagglutinin antibody was used to detect the tagged line and rabbit monoclonal anti-GAP45 was used as control. **(D)** Western blot time course displaying the decrease expression level of SEB1 upon rapamycin treatment: mouse monoclonal anti-HA hemagglutinin antibody was used to detect the tagged line and rabbit monoclonal anti-GAP45 was used as control. **(E)** Quantification of western blot of 3 biological replicates and each densitometry RHΔku80 DiCre strain and SEB1-KD expressing *T. gondii* was compared with two-way ANOVA test, ***P < 0.0001, ***P = 0.0004 and ***P = 0.0001. Mouse monoclonal anti-HA hemagglutinin antibody was used to detect the tagged line.

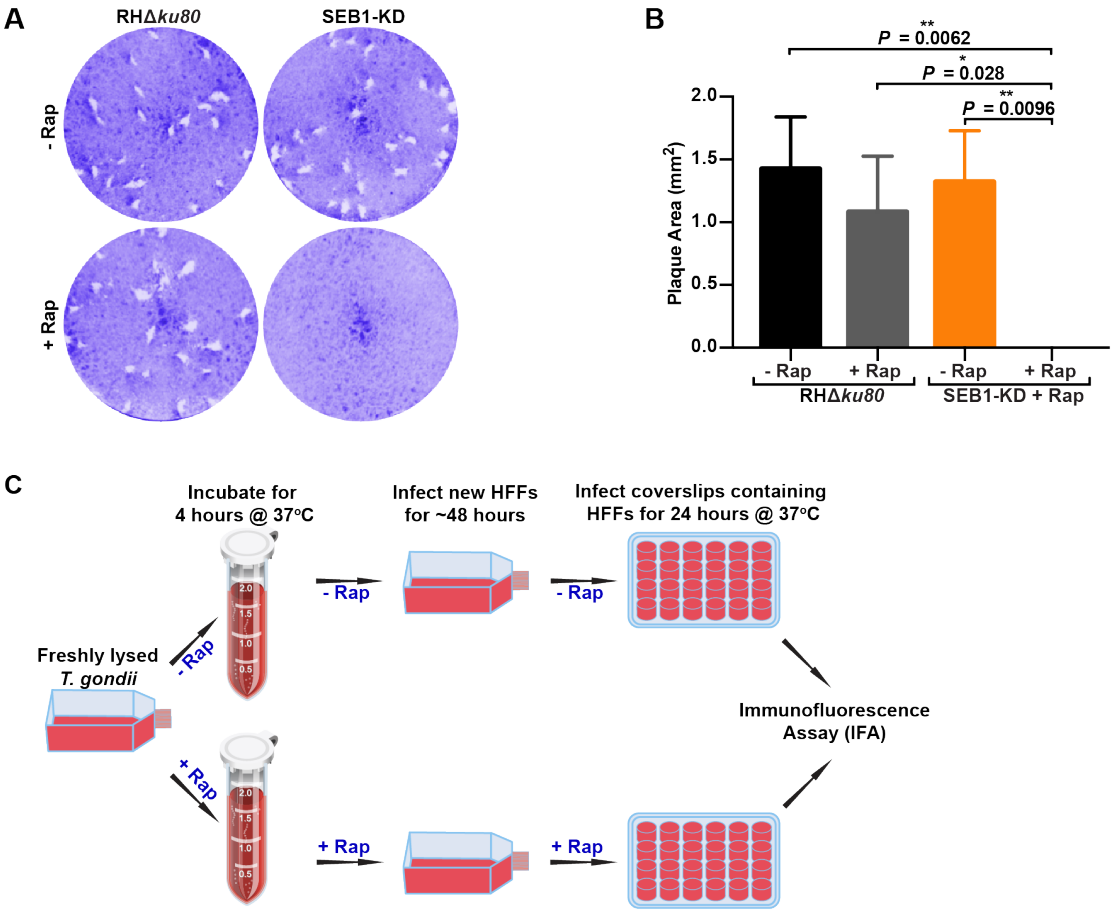
A
RHΔku80
SEB1-KD
- Rap
+ Rap
B
P = 0.0062
P = 0.028
P = 0.0096
Plaque Area (mm2)
2.0
1.5
1.0
0.5
0.0
- Rap
+ Rap
- Rap
+ Rap
RHΔku80
SEB1-KD + Rap
C
Incubate for
4 hours @ 37°C
Infect new HFFs
for ~48 hours
Infect coverslips containing
HFFs for 24 hours @ 37°C
Freshly lysed
T. gondii
- Rap
+ Rap
- Rap
+ Rap
+ Rap
Immunofluorescence
Assay (IFA)

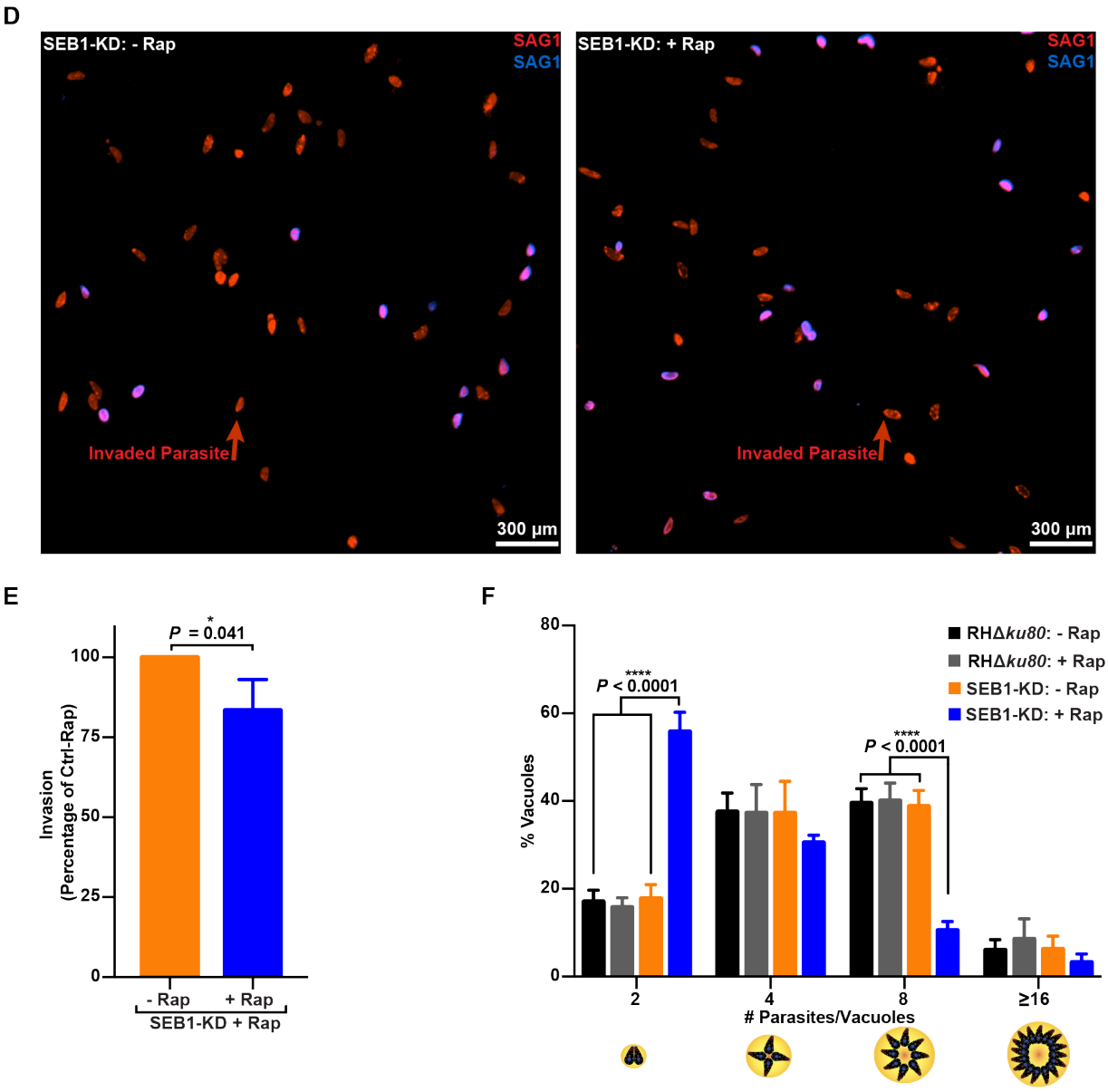

Figure 3.5. SEB1 downregulation affects parasite replication.

(A) Plaque assay of SEB1-KD (SEB1 knockdown line) and RHΔku80 (DiCre ku80::KRedflox-YFP generated strain from Pieperhoff et al., 2015) tachyzoites on HFF monolayers in presence and absence of rapamycin. Each well was infected with 100 parasites and the monolayers were fixed seven days post-infection and stained with crystal violet. **(B)** Plaque assay quantification of the size of plaque area. Multiple comparisons were performed using one-way ANOVA test, **P =

0.0096, **P = 0.0062 and *P = 0.028. **(C)** Schematic displaying the procedure for the invasion and replication assays. **(D)** Representative wide-field fluorescence images of invasion by SEB1-KD parasites in presence and absence of rapamycin. **(E)** Quantification of the mean±s.e.m. number of invaded parasites per field for SEB1-KD parasites in presence and absence of rapamycin, n=3, *P = 0.041. **(F)** Comparison of intracellular growth of SEB1-KD and RHΔku80 parasites in presence and absence of rapamycin: percentage (mean±s.e.m.) of vacuoles containing number of parasites with a replication defect, 4 biological replicates were compared with two-way ANOVA test, ***P < 0.0001

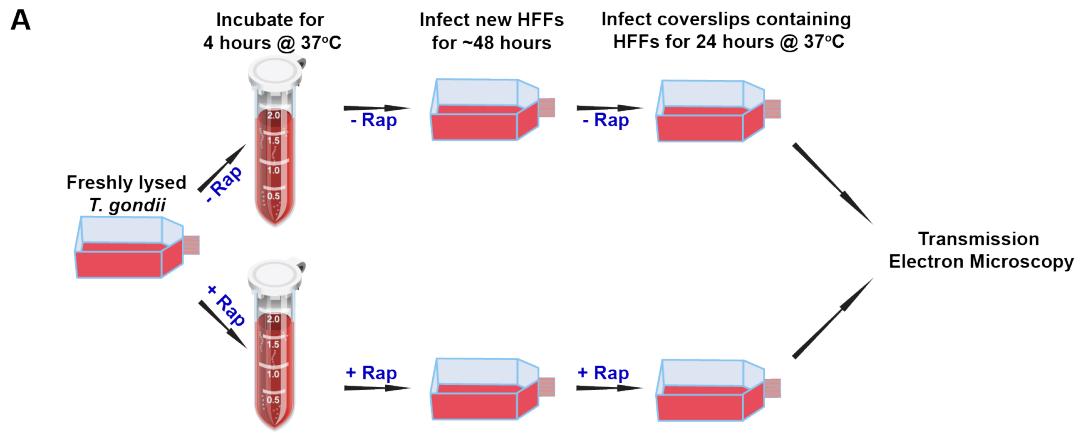
A
Incubate for
4 hours @ 37°C
Infect new HFFs
for ~48 hours
Infect coverslips containing
HFFs for 24 hours @ 37°C
Freshly lysed
T. gondii
- Rap
+ Rap
- Rap
+ Rap
- Rap
+ Rap
Transmission
Electron Microscopy

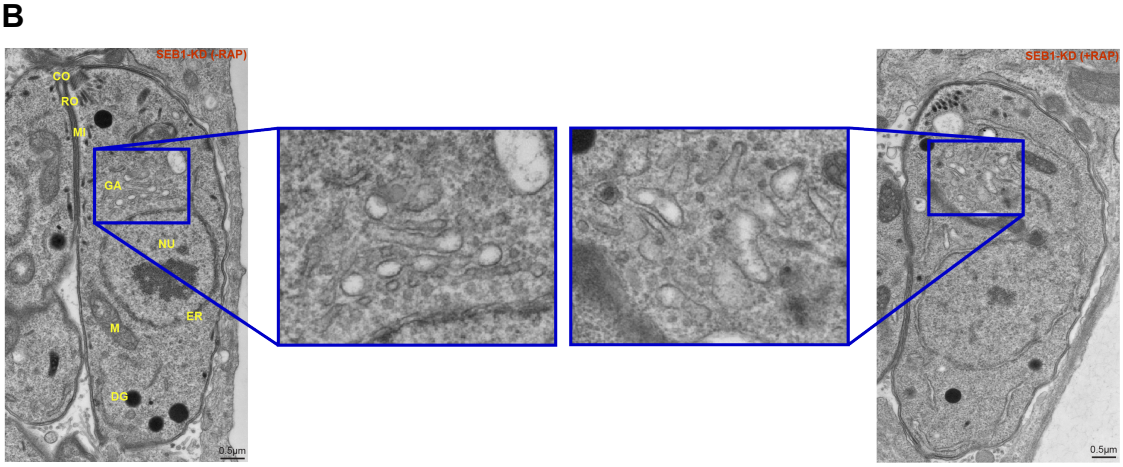
B
SEB1-KD (-RAP)
OO
RO
M
GA
NU
ER
M
OG
0.5µm
SEB1-KD (+RAP)
0.5µm

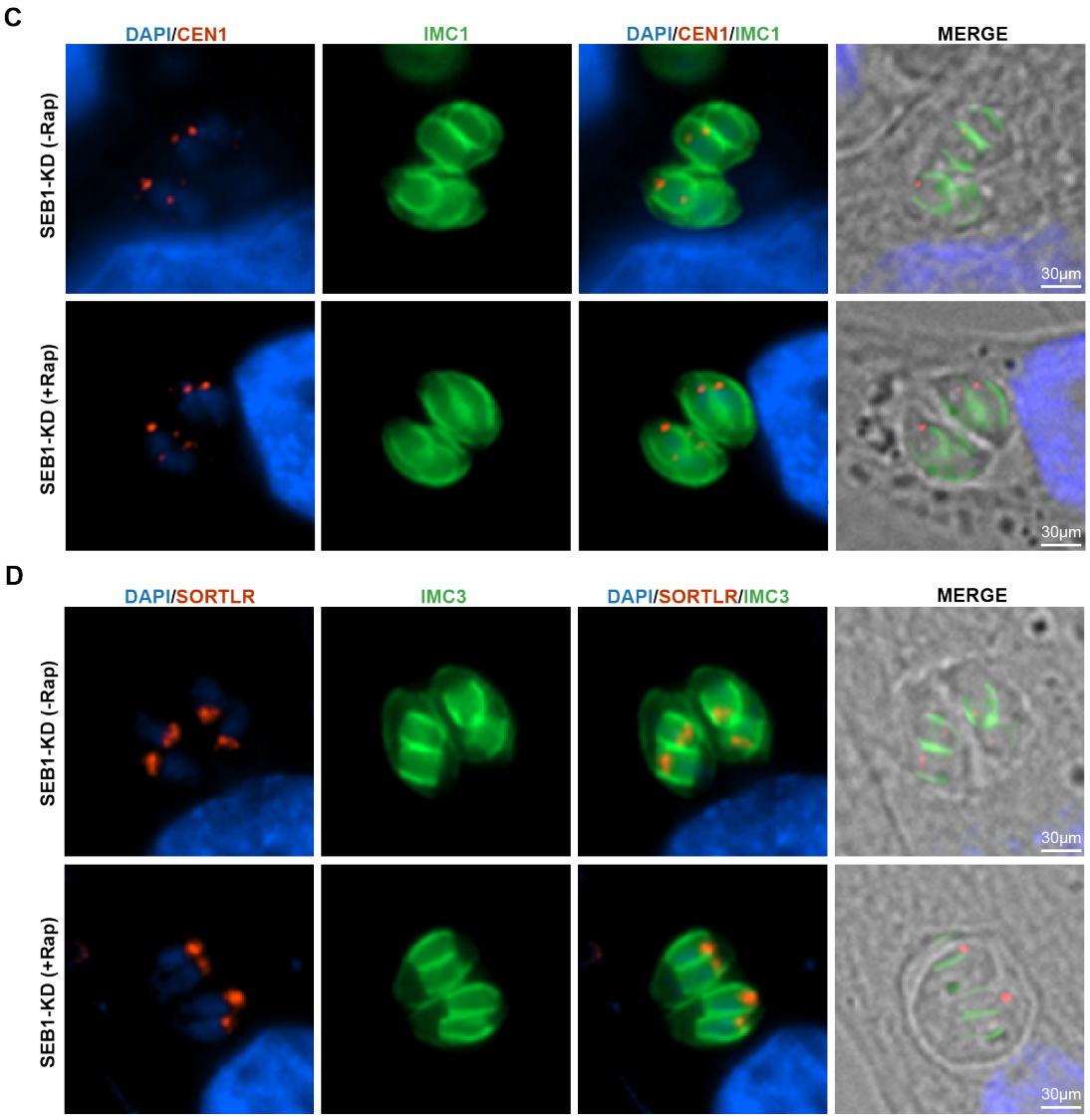

Figure 3.6. Depletion of SEB1 expression level shows a disorganization of the endomembranes of *T. gondii*.

(A) Schematic displaying the procedure for the transmission electron microscopy (TEM) assay. **(B)** Thin Section of electron micrographs of *T. gondii* tachyzoites comparing SEB1-KD line in absence of rapamycin 'SEB1-KD (-Rap)' and presence of rapamycin 'SEB1-KD (+Rap)': CO, conoid; RO, rhoptries; MI, micronemes; DG, dense granules; GA, Golgi apparatus, M, mitochondrion; ER, endoplasmic reticulum; NU, nucleus. Scale bar, 0.5µm. **(C)** HFF cells infected (24hrs) with SEB1-KD line in absence of rapamycin 'SEB1-KD (-Rap)' and presence of

rapamycin ‘SEB1-KD (+Rap)’ expressing *T. gondii* (Green): mouse monoclonal anti-IMC1 for parasite inner membrane complex marker (green), rabbit monoclonal anti-CEN1 antibody for parasite centrin1 (red) and DAPI nuclei (blue). Scale 30µm. Right = merge with bright field. **(D)** HFF cells infected (24hrs) with SEB1-KD line in absence of rapamycin ‘SEB1-KD (-Rap)’ and presence of rapamycin ‘SEB1-KD (+Rap)’ expressing *T. gondii* (Green): rabbit monoclonal anti-IMC3 for parasite inner membrane marker (green), mouse monoclonal anti-TgSORTLR antibody for parasite Golgi apparatus (red) and DAPI nuclei (blue). Scale 30µm. Right = merge with bright field.

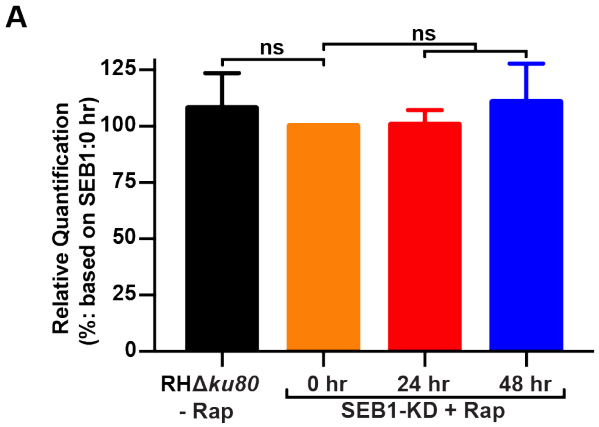

Supplemental Figure 3.4. Conditional ablation of SEB1 gene in *T. gondii*.

(A) Quantification of western blot of 3 biological replicates and each densitometry RHΔku80 DiCre strain and SEB1-KD expressing *T. gondii* was compared with two-way ANOVA test, ns: non-significant p. value. Rabbit monoclonal anti-GAP45 was used for this experiment as control.

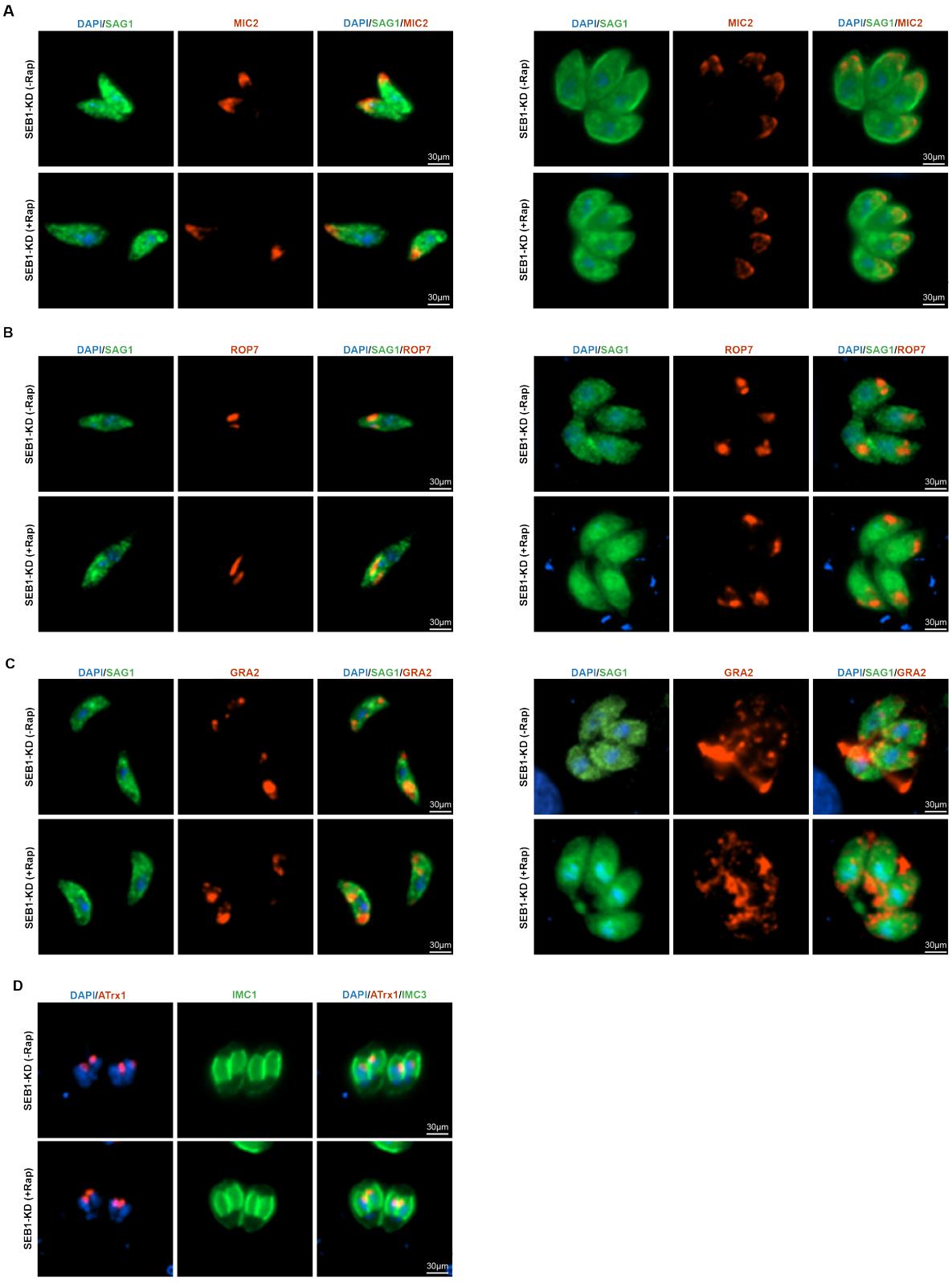
A
DAPI/SAG1
MIC2
DAPI/SAG1/MIC2
SEB1-KD (-Rap)
SEB1-KD (+Rap)
30μm
B
DAPI/SAG1
ROP7
DAPI/SAG1/ROP7
C
DAPI/SAG1
GRA2
DAPI/SAG1/GRA2
D
DAPI/ATrx1
IMC1
DAPI/ATrx1/IMC3

Supplemental Figure 3.6. Depletion of SEB1 expression level does not affect protein trafficking of the secretory organelles of *T. gondii.*

(A) HFF cells infected (24hrs) with SEB1-KD line in absence of rapamycin 'SEB1-KD (-Rap)' and presence of rapamycin 'SEB1-KD (+Rap)' expressing *T. gondii*: mouse monoclonal anti-MIC2 for parasite micronemes marker (red), rabbit monoclonal anti-SAG1 antibody for parasite surface (green) and DAPI nuclei (blue). Scale 30µm. Left = Extracellular parasites; Right = Intracellular parasites. **(B)** HFF cells infected (24hrs) with SEB1-KD line in absence of rapamycin 'SEB1-KD (-Rap)' and presence of rapamycin 'SEB1-KD (+Rap)' expressing *T. gondii* (Green): mouse monoclonal anti-ROP7 for parasite rhoptries marker (red), rabbit monoclonal anti-SAG1 antibody for parasite surface (green) and DAPI nuclei (blue). Scale 30µm. Left = Extracellular parasites; Right = Intracellular parasites. **(C)** HFF cells infected (24hrs) with SEB1-KD line in absence of rapamycin 'SEB1-KD (-Rap)' and presence of rapamycin 'SEB1-KD (+Rap)' expressing *T. gondii* (Green): mouse monoclonal anti-GRA2 for parasite dense granules marker (red), rabbit monoclonal anti-SAG1 antibody for parasite surface (green) and DAPI nuclei (blue). Scale 30µm. Left = Extracellular parasites; Right = Intracellular parasites. **(D)** HFF cells infected (24hrs) with SEB1-KD line in absence of rapamycin 'SEB1-KD (-Rap)' and presence of rapamycin 'SEB1-KD (+Rap)' expressing *T. gondii* (Green): rabbit monoclonal anti-IMC3 for parasite inner membrane complex marker (green), mouse monoclonal anti-ATrx1 antibody for parasite apicoplast (red) and DAPI nuclei (blue). Scale 30µm.

TABLE

Table S3.1. Number of peptides found for all proteins identified by mass spectrometry with two or more peptides with a confidence above 95 %(Scaffold) from the analysis.

				Total unique spectrum count					
				Exp.1	**Exp. 1**	**Exp.2**	**Exp. 2**	**Exp.3**	**Exp. 3**
Identified Protein	**Gene annotation**	**Accession Number[b]**	**MW (kDa)**	**SEB1-TY-Flag**	**WT**	**SEB1-TY-Flag**	**WT**	**SEB1-TY-Flag**	**WT**
SEB1	hypothetical protein	TGGT1_221870	144	110	0	113	0	85	0
Sec24	putative transport protein Sec24	TGGT1_277000	108	3	0	4	0	3	0
–	ribosomal protein RPL13	TGGT1_263050	40	4	0	2	0	2	0

ROP5	rhoptry protein ROP5	TGVEG_442220	61	18	0	16	0	0	0
Rab1	putative small GTP binding protein rab1a	TGGT1_214770	23	2	0	2	0	0	0
–	hypothetical protein	TGGT1_301250	96	4	0	2	0	0	0
GRA2	dense granule protein GRA2	TGGT1_227620	20	8	0	0	0	0	0
WD domain	WD domain, G-beta repeat domain containing protein	TGGT1_320210	56	2	0	0	0	2	0
–	ribosomal protein RPL3	TGGT1_227360	44	5	0	0	0	2	0
–	protein phosphatase 2C domain-containing protein	TGGT1_237500	97	2	0	0	0	2	0

–	ribosomal protein RPL14	TGGT1_267060	18	3	0	0	0	4	0
Sec23/Sec24	Sec23/Sec24 trunk domain-containing protein	TGGT1_291680	88	0	0	5	0	4	0
–	ribosomal protein RPL10	TGGT1_288720	25	0	0	2	0	3	0
–	hypothetical protein | location	TGGT1_209210	167	2	0	0	0	0	0
–	DnaJ domain-containing protein	TGGT1_267430	49	4	0	0	0	0	0
–	hypothetical protein	TGGT1_269710	170	4	0	0	0	0	0
–	ribosomal protein RPS6	TGGT1_210690	29	4	0	0	0	0	0

GRA12	dense granule protein GRA12	TGGT1_288650	48	3	0	0	0	0	0
–	putative ATPase synthase subunit alpha	TGGT1_204400	62	6	0	0	0	0	0
–	RNA recognition motif-containing protein	TGGT1_304760	147	4	0	0	0	0	0
ROP1	rhoptry protein ROP1	TGGT1_309590	50	3	0	0	0	0	0
BiP	chaperonin protein BiP	TGGT1_311720	73	4	0	0	0	0	0
–	hypothetical protein	TGGT1_313350	47	4	0	0	0	0	0
–	RNA recognition motif-containing protein	TGGT1_262620	32	14	0	0	0	0	0

–	hypothetical protein	TGVEG_212955	64	2	0	0	0	0	0
–	putative DNA replication licensing factor	TGGT1_214970	117	2	0	0	0	0	0
–	beta-tubulin	TGGT1_266960	50	4	**0**	0	0	0	0
SPM1	microtubule associated protein SPM1	TGGT1_263520	39	0	0	2	0	0	0
TgSRTLR	putative sortilin	TGGT1_290160	114	0	0	3	0	0	0
IMC4	alveolin domain containing intermediate filament IMC4	TGGT1_231630	53	0	0	3	0	0	0
ROP4	ROP4	TGGT1_295125	40	0	0	2	0	0	0

ROP7	ROP7	TGGT1_295110	63	0	0	4	0	0	0
GRA6	GRA6	TGGT1_275440	23	0	0	3	0	0	0
GAPDH1	glyceraldehyde-3-phosphate dehydrogenase GAPDH1	TGGT1_289690	53	0	0	2	0	0	0
–	ribosomal protein RPS16	TGGT1_263040	24	0	0	4	0	0	0
–	ribosomal protein RPS8	TGGT1_245460	23	0	0	2	0	0	0
–	ribosomal protein RPL8	TGGT1_204020	28	0	0	5	0	0	0
–	hypothetical protein	TGGT1_279100	48	0	0	4	0	0	0

–	hypothetical protein	TGGT1_215220	55	0	0	6	0	0	0
–	putative eukaryotic initiation factor-4A	TGGT1_250770	47	0	0	2	0	0	0
LDH1	lactate dehydrogenase LDH1	TGGT1_232350	36	0	0	4	0	0	0
–	cAMP-dependent protein kinase regulatory subunit	TGGT1_242070	43	0	0	2	0	0	0
–	ribosomal protein RPS7	TGGT1_239100	23	0	0	3	0	0	0
–	ribosomal protein RPL30	TGGT1_232230	12	0	0	2	0	0	0
–	hypothetical protein	TGGT1_262935	77	0	0	2	0	0	0

–	FUSE-binding protein 2	TGGT1_216670	100	0	0	2	0	0	0
–	hypothetical protein	TGGT1_297430	25	0	0	3	0	0	0
–	hypothetical protein	TGGT1_240060	89	0	0	2	0	0	0
GRA5	dense granule protein GRA5	TGGT1_286450	13	0	0	0	0	3	0
Rab11	Ras-related protein Rab11	TGGT1_289680	25	0	0	0	0	2	0
Toxofilin	Toxofilin	TGGT1_214080	27	0	0	0	0	2	0
HSP90	heat shock protein HSP90	TGGT1_288380	82	0	0	0	0	2	0

–	histone H2Bv	TGGT1_209910	14	0	0	0	0	3	0
–	eukaryotic porin protein	TGGT1_263300	31	0	0	0	0	2	0
–	thioredoxin domain-containing protein	TGGT1_247350	34	0	0	0	0	3	0
–	putative eukaryotic translation initiation factor 4A, isoform 3	TGGT1_256770	45	0	0	0	0	3	0
–	hypothetical protein	TGGT1_286580	107	0	0	0	0	3	0
–	14-3-3 protein	TGGT1_263090	37	0	0	0	0	3	0
–	putative protein disulfide isomerase-related protein (provisional)	TGGT1_249270	60	0	0	0	0	2	0

–	ribosomal protein RPL32	TGGT1_267400	16	0	0	0	0	3	0
–	ribosomal protein RPSA	TGGT1_266060	32	0	0	0	0	3	0
–	fructose-1,6-bisphosphate aldolase	TGGT1_236040	47	0	0	0	0	2	0
–	ribosomal protein RPL23A	TGGT1_238010	19	0	0	0	0	2	0
–	ribosomal protein RPL7	TGGT1_314810	30	0	0	0	0	2	0
–	putative eukaryotic initiation factor-4E	TGGT1_223410	26	0	0	0	0	4	0
–	DEAD/DEAH box helicase domain-containing protein	TGME49_284050	282	0	0	0	0	4	0

_	domain K- type RNA binding proteins family protein	TGGT1_235930	64	0	0	0	0	4	0
_	ribosomal protein RPL13A	TGGT1_292130	33	0	0	0	0	3	0
_	splicing factor SF2	TGGT1_319530	54	0	0	0	0	2	0
_	putative transmembrane protein	TGGT1_410370	48	0	0	0	0	4	0
_	RNA recognition motif-containing protein	TGGT1_270640	25	0	0	0	0	2	0
_	ribosomal protein RPL10A	TGGT1_215470	25	0	0	0	0	2	0
_	protein disulfide isomerase	TGGT1_211680	53	0	0	0	0	4	0

–	putative vacuolar ATP synthase subunit A	TGGT1_256970	68	0	0	0	0	2	0

Table S3.2. Primers used in this study.

Primer	Primer Sequence
1	CCAAAATGGACACTCGAGACGTTTTAGAGCTAGAAATAGC
2	AACTTGACATCCCCATTTAC
3	TCCAATTTAATTAAGAACCTCAGCCTTTCGCTGTAGTTGGACAGGAGGAGAGCGCGAGAA
4	TACAGCGAAAGGCTGAGGTTCTTAATTAAATTGGATTGGAAGTAC
5	GAGGTCCACACGAACCAGGACCCGCTCGATGACTATAAAGACGATGACGATAAG
6	ATCGAGCGGGTCCTGGTTCGTGTGGACCTCAAAGTCCATCCCTGAAGAGAGAGGTGCACT
7	CCCTGTACTTCCAATCCAATCAGCGTGCATCAGTCGAGCGCGGGCACAAGCTCAGTTGGA
8	TCTGGAACATCGTATGGGTAAAAGTCCATCCCTGAAGAGAGAGGTGCACTCGGTGGTGGG
9	TACCCATACGATGTTCCAGATTACGCTGCTGACTA
10	ATTGGATTGGAAGTACAGGGTACGATCTCGACGCA

Table S3.3. Antibodies used in this study.

Category	Target (clone)	Species	Source	Diltution	Product #
Immunofluorescence Assays: Primary	Ty-Tag	mouse		1/1000	
	GAP45	rabbit		1/1000	
	HA-Tag	mouse		1/500	
	IMC3	rabbit		1/2000	
	IMC1	mouse		1/1000	
	Cen1	rabbit		1/1000	
	Atrx1	mouse		1/1000	
	SORTLR	mouse		1/1000	
	MIC2	mouse		1/1000	
	ROP7	mouse		1/1000	
	GRA2	mouse		1/1000	
	SAG1	mouse		1/1000	
	SAG1	rabbit		1/1000	
Immunofluorescence Assays: Secondary	Mouse IgG	Goat conjugated to Alexa488	Life Technologies	1/1000	A11029
	Rabbit IgG	Goat conjugated to Alexa594	Life Technologies	1/1000	A11037

Western Blotting: Primary	Ty-Tag	mouse		1/1000	
	GAP45	rabbit		1/1000	
	HA-Tag	mouse	Cell Signaling	1/10000	
Western Blotting: Secondary	Mouse IgG	Goat conjugated to IRDye 680CW	LI-COR Biosciences	1/2000	926-68070 lot#: C80619-05

3.6 REFERENCES

1. Olias, P., et al., *Toxoplasma Effector Recruits the Mi-2/NuRD Complex to Repress STAT1 Transcription and Block IFN-gamma-Dependent Gene Expression.* Cell Host Microbe, 2016. **20**(1): p. 72-82.
2. Rosenberg, A. and L.D. Sibley, *Toxoplasma gondii secreted effectors co-opt host repressor complexes to inhibit necroptosis.* Cell Host Microbe, 2021. **29**(7): p. 1186-1198 e8.
3. Erdős, G., M. Pajkos, and Z. Dosztányi, *IUPred3: prediction of protein disorder enhanced with unambiguous experimental annotation and visualization of evolutionary conservation.* Nucleic Acids Res, 2021. **49**(W1): p. W297-w303.
4. Sidik, S.M., et al., *Efficient genome engineering of Toxoplasma gondii using CRISPR/Cas9.* PLoS One, 2014. **9**(6): p. e100450.
5. Shen, B., et al., *Development of CRISPR/Cas9 for Efficient Genome Editing in Toxoplasma gondii.* Methods Mol Biol, 2017. **1498**: p. 79-103.
6. Huynh, M.H. and V.B. Carruthers, *Tagging of endogenous genes in a Toxoplasma gondii strain lacking Ku80.* Eukaryot Cell, 2009. **8**(4): p. 530-9.
7. Sidik, S.M., et al., *A Genome-wide CRISPR Screen in Toxoplasma Identifies Essential Apicomplexan Genes.* Cell, 2016. **166**(6): p. 1423-1435 e12.
8. Meissner, M., et al., *Modulation of myosin A expression by a newly established tetracycline repressor-based inducible system in Toxoplasma gondii.* Nucleic acids research, 2001. **29**(22): p. e115-e115.
9. Mital, J., et al., *Conditional expression of Toxoplasma gondii apical membrane antigen-1 (TgAMA1) demonstrates that TgAMA1 plays a critical role in host cell invasion.* Molecular Biology of the Cell, 2005. **16**: p. 4341–4349.

10. Long, S., et al., *Calmodulin-like proteins localized to the conoid regulate motility and cell invasion by Toxoplasma gondii.* PLoS Pathog, 2017. **13**(5): p. e1006379.

11. Pieperhoff, M.S., et al., *Conditional U1 Gene Silencing in Toxoplasma gondii.* PLoS One, 2015. **10**(6): p. e0130356.

12. Andenmatten, N., et al., *Conditional genome engineering in Toxoplasma gondii uncovers alternative invasion mechanisms.* Nat Methods, 2013. **10**(2): p. 125-7.

13. Hunt, A., et al., *Differential requirements for cyclase-associated protein (CAP) in actin-dependent processes of Toxoplasma gondii.* Elife, 2019. **8**.

14. Carey, K.L., et al., *A small-molecule approach to studying invasive mechanisms of Toxoplasma gondii.* Proc Natl Acad Sci U S A, 2004. **101**(19): p. 7433-8.

15. Mital, J. and G.E. Ward, *Current and emerging approaches to studying invasion in apicomplexan parasites.* Subcell Biochem, 2008. **47**: p. 1-32.

16. Leung, J.M., et al., *Stability and function of a putative microtubule-organizing center in the human parasite Toxoplasma gondii.* Mol Biol Cell, 2017. **28**(10): p. 1361-1378.

17. Hu, K., D.S. Roos, and J.M. Murray, *A novel polymer of tubulin forms the conoid of Toxoplasma gondii.* J Cell Biol, 2002. **156**(6): p. 1039-50.

18. Kono, M., et al., *Evolution and architecture of the inner membrane complex in asexual and sexual stages of the malaria parasite.* Mol Biol Evol, 2012. **29**(9): p. 2113-32.

19. Nishi, M., et al., *Organellar dynamics during the cell cycle of Toxoplasma gondii.* J Cell Sci, 2008. **121**(Pt 9): p. 1559-68.

20. Pelletier, L., et al., *Golgi biogenesis in Toxoplasma gondii.* Nature, 2002. **418**(6897): p. 548-552.

21. Ouologuem, D.T. and D.S. Roos, *Dynamics of the Toxoplasma gondii inner membrane complex.* J Cell Sci, 2014. **127**(Pt 15): p. 3320-30.

22. Donald, R.G., et al., *Insertional tagging, cloning, and expression of the Toxoplasma gondii hypoxanthine-xanthine-guanine phosphoribosyltransferase gene. Use as a selectable marker for stable transformation.* J Biol Chem, 1996. **271**(24): p. 14010-9.

CHAPTER 4

CONCLUSIONS AND FUTURE WORK

4.1 INTRODCUTION

Over the past decades, many significant studies have increased our knowledge of the biology of *Toxoplasma gondii* and how it dramatically remodels a myriad of important cell pathways including the cell cycle. However, many aspects of this host-parasite interaction are unresolved, such as the lack of identified parasite molecules responsible for altering the host cell cycle phase. Dissecting the molecular function of a protein responsible for modulating the host cell cycle was partially the aim of the work presented in this dissertation. Herein we describe the role of HCE1 in cyclin E upregulation. HCE1 is responsible for driving host cell to transit from G1 phase to S-Phase. We further validate that there was a block in S-phase progression and host cell DNA synthesis in many cell lines normally used in the study of *Toxoplasma*. Over the course of these studies we found, among the cell types tested, only infected primary mouse fibroblasts were able to synthesize their genome and could do so only when contact inhibition was removed. Additionally, we also present an essential Golgi resident protein termed SEB1 that is required for parasite replication. As shown by electron microscopy, loss of SEB1 leads to a disorganization of the vesicles in *T. gondii* such as the micronemes, rhoptries, dense granules, and Golgi apparatus. Altogether, this work helps to address the specificity of a discharged molecular weapon regulating the host cell cycle progression as well as the importance of a unique coccidian protein for the parasite lytic cycle and lays the foundation for further characterization of SEB1.

4.2 THE MODULATION OF THE HOST CELL CYCLE BY *TOXOPLASMA GONDII*

HCE1*: a sharp inducer of the cell cycle.*

Among the diverse groups of pathogenic microorganisms, intracellular invaders have evolved distinct ways of promoting their survival within the host cell by controlling multiple processes. An eminent example of this is the regulation of host cell cycle progression in different means by many infectious agents, such as viruses (human cytomegalovirus 'HCMV' and chicken anemia virus 'CAV' apoptin) and parasites (*Toxoplasma gondii and Theileria annulata*) [1-9]. This often results in an array of effects, including abnormal proliferation of the host cell and inhibition of the growth of the host cell by affecting its cellular DNA synthesis. This thesis demonstrates that *T. gondii* upregulates expression of the host cyclin E to induce the progression of the infected cell from G0/G1 into S-phase, which also reveals a block in host DNA synthesis in multiple commonly used host cells in the study of *Toxoplasma*. Our observation that infected mouse fibroblast cells initiate DNA synthesis upon the removal of contact inhibition (CI) is, however, far from complete. The cyclin-cdk inhibitors p21 and p27 are usually the proteins involved in CI and DNA damage, however, so far, we show that p21 protein was not responsible for the restoration of the DNA synthesis in infected MF cells as this phenomenon was solely dependent on HCE1. The role of p27 in MF-p27-deficient cells infected with *Toxoplasma*, however, remains unresolved. Hence, identifying host-specific intrinsic factors capable of responding to *Toxoplasma* infection and circumventing the parasite reprogramming highlights significant questions about the parasite and host interaction. It has been demonstrated, in other organisms, that loss of CI in the infected cell can pathologically lead to uncontrolled cell growth resulting to some tumorous characteristics, the aspects of which also need to be unraveled in the context of infection of *Toxoplasma* into primary host cells [10-12]. Additionally, future

investigation using other primary cells, such as primary cells from humans or other warmed-blooded mammals, can also provide valuable information about the role of CI in this process. This could be evaluated by freshly harvesting primary host cells, infecting them with *Toxoplasma*, and assessing their genome synthesis using an EdU incorporation assay upon the removal of CI as was performed on the primary infected mouse fibroblasts (Chapter 2). Also, it is noteworthy to mention that even freshly primary cells if cultured too long may confine some aberrant phenotypes. In fact, cells may continue to proliferate, and as the passage number increases their phenotype and genotype may change. Thus, certain intrinsic acquired mechanism may obscure some analyses. Therefore, further investigation of this specific aspect of host-parasite interaction may increase our understanding about the response of host cell reprogramming by the manipulation of *T. gondii* considering different host cell types.

4.3 SEB1 GOLGI RESIDENT PROTEIN: ITS ROLE IN THE COCCIDIAN

4.3.1 Determining the role of SEB1 in subset of GRA protein translocation:

Data presented in chapter 3 of this dissertation demonstrates that the essential role of SEB1 is not related to protein trafficking, at least considering the subset of proteins for which localization in KD-conditions were tested. Furthermore, in KD conditions, microneme and rhoptry proteins appeared to function normally, as determined in the parasite invasion assay indicating that the invasion machinery was not impaired. Additionally, IFA demonstrated that the canonical proteins from each of the three secretory vesicles were able to properly reach their endomembranes in the parasite. Notably, dense granules proteins can be divided into four classes based on their localization: PV, PVM, host cytosol and host nucleus (Figure 1.4). However, it remains unresolved whether or the nuclear targeted GRAs are able to properly reach their destination in knockdown

parasites. Thus, we speculate that the trafficking of these GRAs may be affected in knockdown parasites. This aforementioned group of GRA proteins translocation experiment in SEB1-KD line should be examined for further characterization of SEB1.

4.3.2 Determining SEB1 topology and orientation:

Based on the predicted structure from the amino acid sequence, we speculate that SEB1 is a type I transmembrane protein. To further investigate membrane localization and orientation, a peptide protease protein assay could be employed, which utilizes the established fluorescence protease protection (FPP) assay [13]. For this approach, C-terminal tagged SEB1-TY-FLAG parasites could be allowed to invade HFF monolayers which would be then be subjected to selective permeabilization using the detergent digitonin. Digitonin is a cholesterol binding drug that has the ability to selectively permeabilize the plasma membrane, while leaving intracellular organelles intact due to their low cholesterol content [14, 15]. A digitonin concentration titration process could be used to establish the optimal conditions for disrupting both the host and parasite plasma membranes, without perturbing the Golgi membrane. A cytosolic-tagged protein and markers of Golgi GRASP or Sortilin 'TgSORTLR' could serve as controls. We would take advantage of the digitonin permeabilization which would also allow the entry of exogenous molecules, such as proteinase K or trypsin, to cleave any peptides present in the cytosol of the host and parasite. Through an immunofluorescence assay, we could then assess if the TY and FLAG peptides cleave off from both cytosolic control and SEB1-TY-FLAG, but not on our control Golgi marker. This could be achieved in the presence of both digitonin permeabilization and proteinase K or trypsin treatment. This would suggest that the C-terminal of SEB1 is in the cytosol while the N-terminal end resides in the lumen of the Golgi of the parasite. In that case, SEB1 would be confirmed as a type I transmembrane topology. If the TY and FLAG peptides are still present after

treatment, this would deduce that the C-terminal of SEB1 is in the lumen of the Golgi while the N-terminal end resides in the cytosol, making SEB1 a type II transmembrane protein.

4.3.3 Carboxyl end (C-terminal) requirement for SEB1 function:

In chapter 3 of this dissertation, I showed that the C-terminal end of SEB1 is conserved across cyst-forming coccidia (Figure 3.3E). We postulate that the C-terminal end of SEB1 plays a role in parasite survival as well as in the observed vesicles disorganization phenotype upon depletion of this protein. Further characterization is needed to investigate the importance of this C-terminal end on parasite survival and its overall function. The SEB1 nucleotide sequence lacks its conserved C-terminal amino acid sequence from *Toxoplasma.* cDNA should be isolated to generate an inducible mutant "SEB1ΔC-terminal-end". This mutant could be used in the TATi system encoding the gene promoter TgSAG4 where SEB1ΔC- terminal-end mutant expression will be controlled in the absence and presence of anhydrotetracycline [16]. This construct could be transfected in TATi-RH *T. gondii* tachyzoites that constitutively express TATi protein (TetR + TATi transactivator) by means of a pT/5Rf70 or p5RT70 promoter [16]. A clonal population could be isolated, and the resulting parasite mutant line would serve as a dominant negative. We should subsequently examine the role of SEB1 using the previous assays discussed in chapter 3 for assessing parasite survival (plaque assay, fitness assays 'invasion, replication, egress, protein secretion), protein trafficking, and EM analysis to examine the biogenesis of parasite key organelles (Golgi, micronemes, rhoptries and dense granules).

4.4 CONCLUSION

In summary, by elucidating the role of HCE1 to modulate the infected host, this dissertation solves a longstanding mystery in the field of *T. gondii* biology. As it has been postulated in the

field that *T. gondii* controls the progression of the cell cycle from G1 to S-phase, direct evidence for a molecular protein responsible for this aspect has remained an enigma. This thesis demonstrates the role of HCE1, a secreted host nuclear targeted effector, responsible for regulating the host cell cycle progression from G0/G1 into S-phase and ultimately blocks DNA synthesis in the infected host cell. Removal of contact inhibition (CI) using recently derived primary infected mouse fibroblast cells plays a critical role in restoring this observed DNA synthesis blockage and is found to be HCE1 dependent. Future investigation in search of mechanical signal for intrinsic key molecules controlling this host CI specificity is therefore left to be unraveled. Additionally, we showed the essential function of the Golgi resident protein, termed SEB1, for parasite replication and viability. However, more studies are needed to dissect the functional role of SEB1 as the key attributes of the observed endomembranes disorganization and parasite replication defects. Moreover, because of its distinct and enthralling conserved C-terminal end found across the cyst forming coccidians, we can speculate that this feature could be a hallmark of evolutionary process employed by the parasite to aid cyst formation. Altogether, I hope that the work presented in this dissertation provides a better understanding of how *Toxoplasma* regulates its host cell cycle and displays the importance of a Golgi resident protein for the physiology of the parasite and survival. How specific host-parasite interact remains a perpetual significance in the biology of *Toxoplasma* and it is imperative to understand for finding ways to control *Toxoplasma* infection in humans. Additional studies are needed to decipher the function of HCE1 in acute and chronic infections. HCE1/TEEGR is suggested to have a positive contribution to *T. gondii* persistence when mice chronically infected with knockout parasites showed a lower number of cysts in their brain when compared to the parental strain. We can speculate that promoting cell cycle progression could efficiently support bradyzoites conversion rate. Furthermore, SEB1 requires a more vigorous

characterization involving its molecular mechanism that could ultimately give rise to novel strategies to limit the parasite's transmission and dissemination.

4.5 REFERENCES

1. Fehr, A.R. and D. Yu, *Control the host cell cycle: viral regulation of the anaphase-promoting complex.* J Virol, 2013. **87**(16): p. 8818-25.
2. Molestina, R.E., N. El-Guendy, and A.P. Sinai, *Infection with Toxoplasma gondii results in dysregulation of the host cell cycle.* Cell Microbiol, 2008. **10**(5): p. 1153-65.
3. Lavine, M.D. and G. Arrizabalaga, *Induction of mitotic S-phase of host and neighboring cells by Toxoplasma gondii enhances parasite invasion.* Mol Biochem Parasitol, 2009. **164**(1): p. 95-9.
4. Laliberte, J. and V.B. Carruthers, *Host cell manipulation by the human pathogen Toxoplasma gondii.* Cell Mol Life Sci, 2008. **65**(12): p. 1900-15.
5. Saeij, J.P., et al., *Toxoplasma co-opts host gene expression by injection of a polymorphic kinase homologue.* Nature, 2007. **445**(7125): p. 324-7.
6. Zeng, X., et al., *Pharmacologic inhibition of the anaphase-promoting complex induces a spindle checkpoint-dependent mitotic arrest in the absence of spindle damage.* Cancer Cell, 2010. **18**(4): p. 382-95.
7. Kramer, E.R., et al., *Mitotic regulation of the APC activator proteins CDC20 and CDH1.* Mol Biol Cell, 2000. **11**(5): p. 1555-69.
8. Mo, M., S.B. Fleming, and A.A. Mercer, *Cell cycle deregulation by a poxvirus partial mimic of anaphase-promoting complex subunit 11.* Proc Natl Acad Sci U S A, 2009. **106**(46): p. 19527-32.
9. Dessauge, F., et al., *c-Myc activation by Theileria parasites promotes survival of infected B-lymphocytes.* Oncogene, 2005. **24**(6): p. 1075-83.
10. Hanahan, D. and R.A. Weinberg, *The hallmarks of cancer.* Cell, 2000. **100**(1): p. 57-70.

11. Mayor, R. and C. Carmona-Fontaine, *Keeping in touch with contact inhibition of locomotion.* Trends Cell Biol, 2010. **20**(6): p. 319-28.

12. McClatchey, A.I. and A.S. Yap, *Contact inhibition (of proliferation) redux.* Curr Opin Cell Biol, 2012. **24**(5): p. 685-94.

13. White, C., A. Nixon, and N.A. Bradbury, *Determining Membrane Protein Topology Using Fluorescence Protease Protection (FPP).* J Vis Exp, 2015(98).

14. Shah, K., C.E. McCormack, and N.A. Bradbury, *Do you know the sex of your cells?* Am J Physiol Cell Physiol, 2014. **306**(1): p. C3-18.

15. Nixon, A., et al., *Determination of the membrane topology of lemur tyrosine kinase 2 (LMTK2) by fluorescence protease protection.* Am J Physiol Cell Physiol, 2013. **304**(2): p. C164-9.

16. Soldati, D. and J.C. Boothroyd, *A selector of transcription initiation in the protozoan parasite Toxoplasma gondii.* MOLECULAR AND CELLULAR BIOLOGY, 1995. **15**(1): p. 87-93.

APPENDIX

A MASS SPECTROMETRY DATA OF SEB1 IMMUNOPRECIPITATION ASSAYS.

Data from mass spectrometry analysis of three replicates of SEB1 immunoprecipitation assays. To validate mass spectrometry analyses based on peptide and protein identifications for the overall result, the accepted peptides were established when they are greater than 99% probability using Scaffold (version Scaffold_4.10.0, Proteome Software Inc., Portland, OR) [1]. The list of proteins presented in the tables was identified by peptides count with a confidence above 95% (Scaffold) and an abundance of one peptide minimum. Determining interacting partners of SEB1 is described as proteins that are present in SEB1-TY-FLAG strain and absent in wild type strain. These interactors were identified using the abundance ratio of presence of two or more peptides with a confidence above 95% and are highlighted in bold.

Mass spectrometry data analysis: experiment 1

Protein name	**Gene ID**	**Molecular Weight (kDa)**	**SEB-TY-FLAG**	**Wild Type**
Hypothetical protein	TGGT1_221870	144	110	0
Hypothetical protein	TGGT1_233220	160	42	17

Isoleucyl-tRNA synthetase family protein	TGGT1_207640	141	39	12
RNA recognition motif-containing protein	TGGT1_262620	32	14	10
Rhoptry protein ROP5	TGVEG_442220	61	18	0
Sjogren's syndrome/scleroderma autoantigen 1 (Autoantigen p27) protein	TGGT1_212260	38	17	7
SAG-related sequence SRS29B	TGGT1_233460	35	14	5
Ribosomal protein RPL4	TGGT1_309120	46	10	4
Splicing factor SF2	TGGT1_319530	54	12	3
Alveolin domain containing intermediate filament IMC4	TGGT1_231630	50	9	7
Glyceraldehyde-3-phosphate dehydrogenase GAPDH1	TGGT1_289690	53	6	1
Putative ATPase synthase subunit alpha	TGGT1_204400	62	6	1
Putative eukaryotic initiation factor-4E	TGGT1_223410	26	8	4

Hypothetical protein	TGGT1_263320	42	7	2
Hypothetical protein	TGGT1_269710	170	4	1
Dense granule protein GRA2	TGGT1_227620	20	8	0
Ribosomal protein RPS14	TGGT1_263700	16	4	4
RecName: Full=Ig kappa chain C region	P01837.1	12	1	0
Dense granule protein GRA7	TGGT1_203310	26	7	3
Ribosomal protein RPL3	TGGT1_227360	44	5	0
DnaJ domain-containing protein	TGGT1_267430	49	4	0
Chaperonin protein BiP	TGGT1_311720	73	4	0
RNA recognition motif-containing protein	TGGT1_304760	147	4	1
Actin	TGGT1_411760	32	4	3
Ribosomal protein RPL5	TGGT1_320050	35	1	0

Ribosomal protein RPL13	TGGT1_263050	40	4	0
Dense granule protein GRA12	TGGT1_288650	48	3	2
Rhoptry protein ROP8	TGGT1_363030	64	1	0
Putative heat shock protein 90	TGGT1_244560	98	1	0
3xFLAG-MCS-3xFLAG [Expression vector pQF]	AGU99855.1	8	1	1
Ribosomal protein RPL12	TGGT1_254440	18	2	2
Actin ACT1	TGGT1_209030	42	1	0
Hypothetical protein	TGGT1_220950	36	5	0
Dense granule protein GRA8	TGGT1_254720	29	3	1
Beta-tubulin	TGGT1_266960	50	4	0
Rribosomal protein RPS6	TGGT1_210690	29	3	0

Rypothetical protein	TGGT1_313350	47	4	0
Ribosomal protein RPP0	TGGT1_218410	34	3	0
Subtilisin SUB1	TGGT1_204050	85	2	0
Ribosomal protein RPS2	TGGT1_305520	29	3	2
Ribosomal protein RPL10A	TGGT1_215470	25	1	1
Ribosomal protein RPL19	TGGT1_289530	22	2	1
Hypothetical protein	TGGT1_301250	96	4	0
Ribosomal protein RPL14	TGGT1_267060	18	3	1
WD domain, G-beta repeat domain containing protein	TGGT1_320210	56	2	0
Ribosomal protein RPS25	TGGT1_231140	19	1	2
Ribosomal protein RPL18A	TGGT1_262670	21	2	1

Putative transmembrane protein	TGGT1_410360	38	1	0
RNA recognition motif-containing protein	TGGT1_306600	21	2	2
CorA family Mg2+ transporter protein	TGGT1_235402	128	2	0
Hypothetical protein	TGGT1_248160	122	1	1
Hypothetical protein	TGVEG_212955	64	2	1
Desmoglein 1 preproprotein [Homo sapiens]	NP_001933.2	114	1	1
Rhoptry protein ROP1	TGGT1_309590	50	3	0
Putative eukaryotic translation initiation factor 4A, isoform 3	TGGT1_256770	45	1	0
Junction plakoglobin [Homo sapiens]	NP_002221.1	82	3	3
RNA recognition motif-containing protein	TGGT1_209850	171	1	0
Ribosomal protein RPS24 | location	TGGT1_215460	30	1	0

Putative phosphate carrier	TGGT1_278990	53	1	0
Heat shock protein HSP70	TGGT1_273760	72	1	0
Elongation factor 1-alpha (EF-1-ALPHA), putative	TGME49_286420	49	2	1
Ribosomal protein RPL22 | location	TGGT1_239760	15	1	1
Ribosomal protein RPS26	TGGT1_243570	13	2	2
Putative sortilin	TGGT1_290160	114	2	2
Ribosomal protein RPS15	TGGT1_316110	74	1	2
Histone H2A1	TGGT1_261250	20	1	0
Nuclear factor NF2	TGGT1_286790	36	1	0
Hypothetical protein	TGGT1_209210	167	2	0
Putative transport protein Sec24	TGGT1_277000	108	3	0

Protein disulfide-isomerase domain-containing protein	TGGT1_238040A	126	1	0
Putative small GTP binding protein rab1a	TGGT1_214770	23	2	0
Putative mago nashi family protein 2	TGGT1_267420	24	1	1
Ribosomal protein RPL26	TGGT1_248390	16	1	0
Ribosomal protein RPL7A	TGGT1_261570	31	2	0
Ribosomal protein RPS11	TGGT1_226970	19	2	0
Microtubule associated protein SPM1	TGGT1_263520	39	1	2
Myb family DNA-binding domain-containing protein	TGGT1_275480	99	2	1
Small nuclear ribonucleoprotein	TGGT1_209690	25	1	1
Ribosomal protein RPS18	TGGT1_225080	18	2	1
Nuclear factor NF7	TGGT1_248810	54	2	0

Rhoptry neck protein RON5	TGGT1_311470	187	1	1
Dense granule protein GRA6	TGGT1_275440	23	1	1
Protein phosphatase 2C domain-containing protein	TGGT1_237500	97	2	0
Putative DNA replication licensing factor	TGGT1_214970	117	2	0
Pre-mRNA processing splicing factor PRP8	TGGT1_231970	292	1	0
SKIP/SNW domain-containing protein	TGGT1_233190	62	1	0
Splicing factor, CC1 family protein	TGGT1_312530	69	1	0
Ribosomal protein RPS3A	TGGT1_232710	29	1	0
Domain K- type RNA binding proteins family protein	TGGT1_235930	64	1	0
Product=toxofilin	TGGT1_214080	27	1	0
Rhoptry protein ROP7	TGGT1_295110	63	1	0

Amylo-alpha-1,6-glucosidase	TGGT1_226910	208	1	0
Putative vacuolar ATP synthase subunit b	TGGT1_219800	57	1	0
Rhoptry neck protein RON4	TGGT1_229010	107	1	0
Ribosomal protein RPL9	TGGT1_284560	21	1	0
Dermcidin preproprotein [Homo sapiens]	NP_444513.1	11	2	2
Sec61beta family protein	TGGT1_211040	10	1	1
Hypothetical protein	TGGT1_254570	224	1	0
SAG-related sequence SRS34A	TGGT1_271050	19	1	0
Alpha tubulin TUBA1	TGGT1_316400B	48	2	0
DEAD/DEAH box helicase domain-containing protein	TGGT1_284050	281	2	0
Hypothetical protein	TGGT1_263080	14	1	0

CBS domain-containing protein	TGGT1_307580	126	1	1
Sec23/Sec24 trunk domain-containing protein	TGGT1_291680	88	1	0
Desmoplakin isoform II [Homo sapiens]	NP_001008844.1	260	1	1
Hypothetical protein	TGGT1_206670	218	1	0
Alba 2	TGGT1_218820	15	1	0
Hypothetical protein	TGGT1_222300	159	1	0
Putative activating signal cointegrator 1 complex subunit 3 family 1 ASCC3L1	TGGT1_223390	248	1	0
Sec23/Sec24 trunk domain-containing protein	TGGT1_226510	165	1	0
Inner membrane complex protein IMC2A	TGGT1_228170	182	1	0
Myosin A	TGGT1_235470	93	1	0
Surp module domain-containing protein	TGGT1_246500	72	1	0

Hypothetical protein	TGGT1_308870	75	1	0
Putative DnaJ family chaperone	TGGT1_311240	47	1	0
Helicase associated domain (ha2) protein	TGGT1_318440	237	1	0
Hypothetical protein	TGGT1_208350	40	1	0
DEAD (Asp-Glu-Ala-Asp) box polypeptide DDX3X	TGGT1_226250	79	1	0
Putative RNA binding protein	TGGT1_203540	119	1	0
Hypothetical protein	TGGT1_313070	36	1	0
Rhoptry metalloprotease toxolysin TLN1	TGGT1_269885B	62	1	0
Ribosomal protein RPL8	TGGT1_204020	28	1	0
Putative ethylene inducible protein	TGGT1_237140	33	1	0

Mass spectrometry data analysis: experiment 2

Protein name	Gene ID	Molecular Weight (kDa)	SEB-TY-FLAG	Wild Type
Hypothetical protein	TGGT1_221870	144	113	0
IGH1M_MOUSE RecName: Full=Ig gamma-1 chain C region, membrane-bound form	P01869.2	43	41	99
IGKC_MOUSE RecName: Full=Ig kappa chain C region	P01837.1	12	15	40
Isoleucyl-tRNA synthetase family protein	TGGT1_207640	141	32	14
Chaperonin protein BiP	TGGT1_311720	73	26	18
Hypothetical protein	TGGT1_233220	160	31	22
Rhoptry protein ROP5	TGGT1_308090	61	20	21
Putative ATPase synthase subunit alpha	TGGT1_204400	62	25	18

SAG-related sequence SRS29B	TGGT1_233460	35	19	22
Putative heat shock protein 90	TGGT1_244560	98	14	17
ATP synthase beta subunit ATP-B	TGGT1_261950	60	11	13
Dense granule protein GRA7	TGGT1_203310	26	11	16
RNA recognition motif-containing protein	TGGT1_262620	32	11	13
Alpha tubulin TUBA1	TGGT1_316400B	48	11	10
Beta-tubulin	TGGT1_266960	50	9	8
SAG-related sequence SRS34A	TGGT1_271050	19	11	12
Ribosomal protein RPL3	TGGT1_227360	44	6	5
Actin	TGGT1_411760	32	9	7
Dense granule protein GRA12	TGGT1_288650	48	9	6

Elongation factor 1-alpha (EF-1-ALPHA), putative	TGME49_286420	49	6	7
Sjogren's syndrome/scleroderma autoantigen 1 (Autoantigen p27) protein	TGGT1_212260	38	6	9
Ribosomal protein RPS14	TGGT1_263700	16	9	7
Putative vacuolar ATP synthase subunit b	TGGT1_219800	57	9	6
Heat shock protein HSP70	TGGT1_273760	72	8	5
Actin ACT1	TGGT1_209030	42	7	7
Dense granule protein GRA2	TGGT1_227620	20	4	5
Ribosomal protein RPS6	TGGT1_210690	29	3	4
Ribosomal protein RPL10A	TGGT1_215470	25	3	4
Histone H2Bb	TGGT1_251870	13	6	2
Ribosomal protein RPL4	TGGT1_309120	46	7	8

Ribosomal protein RPL18A	TGGT1_262670	21	2	3
Hypothetical protein	TGGT1_263320	42	7	3
DnaJ domain-containing protein	TGGT1_267430	49	4	7
Dense granule protein GRA3	TGGT1_227280	24	0	2
Putative eukaryotic translation initiation factor 4A, isoform 3	TGGT1_256770	45	5	5
Toxofilin	TGGT1_214080	27	5	4
Ribosomal protein RPS16	TGGT1_263040	24	4	1
Rhoptry protein ROP7	TGGT1_295110	63	4	2
Ribosomal protein RPS8	TGGT1_245460	23	2	1
Hypothetical protein	TGGT1_263080	14	3	3
Ribosomal protein RPS2	TGGT1_305520	29	5	3

Putative polyadenylate binding protein	TGGT1_224850	83	3	3
Rhoptry protein ROP1	TGGT1_309590	50	6	2
Rhoptry protein ROP8	TGGT1_363030	64	2	3
Dense granule protein GRA6	TGGT1_275440	23	3	2
Dense granule protein GRA8	TGGT1_254720	29	8	1
Hypothetical protein	TGGT1_220950	36	3	4
Myosin A	TGGT1_235470	93	4	5
Hypothetical protein	TGGT1_313350	47	3	2
Protein disulfide isomerase	TGGT1_211680	53	2	4
Acid phosphatase GAP50	TGGT1_219320	47	5	3
Putative vacuolar ATP synthase subunit A	TGGT1_256970	68	4	3

Ribosomal protein RPL13A	TGGT1_292130	33	4	2
DEAD/DEAH box helicase domain-containing protein	TGGT1_284050	281	4	4
Ribosomal protein RPP0	TGGT1_218410	34	2	5
Ribosomal protein RPL14	TGGT1_267060	18	3	3
Dense granule protein GRA5	TGGT1_286450	13	1	3
WD domain, G-beta repeat domain containing protein	TGGT1_320210	56	4	3
Ribosomal protein RPL7A	TGGT1_261570	31	3	2
Hypothetical protein	TGGT1_215220	55	6	0
RNA recognition motif-containing protein	TGGT1_270640	25	0	3
Ribosomal protein RPL8	TGGT1_204020	28	5	1
Hypothetical protein	TGGT1_279100	48	4	0

Ribosomal protein RPL5	TGGT1_320050	35	0	1
Lactate dehydrogenase LDH1	TGGT1_232350	36	4	1
Putative eukaryotic initiation factor-4A	TGGT1_250770	47	2	1
Ribosomal protein RPL24 (RPL24)	TGME49_244320	33	3	1
Ribosomal protein RPL11	TGGT1_309820	20	2	1
Subtilisin SUB1	TGGT1_204050	85	2	2
RNA recognition motif-containing protein	TGGT1_217540	38	3	3
Ribosomal protein RPS7	TGGT1_239100	23	3	0
Sec23/Sec24 trunk domain-containing protein	TGGT1_291680	88	5	0
Microneme protein MIC4	TGGT1_208030	63	3	2
Splicing factor SF2	TGGT1_319530	54	1	2

Hypothetical protein	TGGT1_269710	170	1	0
Sec61beta family protein	TGGT1_211040	10	2	2
Putative mago nashi family protein 2	TGGT1_267420	24	2	4
Putative translation elongation factor 2 family protein	TGGT1_205470	93	1	1
Product=ribosomal protein RPS11	TGGT1_226970	19	3	2
RNA recognition motif-containing protein	TGGT1_321500	51	3	3
Glyceraldehyde-3-phosphate dehydrogenase GAPDH1	TGGT1_289690	53	2	2
Nuclear factor NF2	TGGT1_286790	36	0	1
Histone H2A1	TGGT1_261250	20	2	2
Myosin light chain MLC1	TGGT1_257680	24	2	2
Ribosomal protein RPL13	TGGT1_263050	40	2	1

Alba 2	TGGT1_218820	15	2	3
Hypothetical protein	TGGT1_230160	16	2	3
Nuclear factor NF7	TGGT1_248810	54	3	2
RNA recognition motif-containing protein	TGGT1_209850	171	2	1
Ribosomal protein RPS20	TGGT1_223050	26	0	4
Ribosomal protein RPS26	TGGT1_243570	13	2	3
Putative sortilin	TGGT1_290160	114	3	0
Vacuolar atp synthase subunit e, putative	TGME49_305290	39	2	2
RNA recognition motif-containing protein	TGGT1_236540	53	1	0
Ribosomal protein RPS25	TGGT1_231140	19	1	1
Ribosomal protein RPS3	TGGT1_232300	29	1	1

Putative phosphate carrier	TGGT1_278990	53	0	1
Ribosomal protein RPL19	TGGT1_289530	22	2	1
Ribosomal protein RPS13	TGGT1_270380	17	1	0
RNA recognition motif-containing protein	TGGT1_306600	21	2	2
ATPase/histidine kinase/DNA gyrase B/HSP90 domain-containing protein	TGGT1_297780	148	1	0
Putative transport protein Sec24	TGGT1_277000	108	4	0
cAMP-dependent protein kinase regulatory subunit	TGGT1_242070	43	2	0
Rhoptry neck protein RON3	TGGT1_223920	223	2	2
Hypothetical protein	TGGT1_297430	25	3	1
Putative small GTP binding protein rab1a	TGGT1_214770	23	2	2
Fructose-1,6-bisphosphate aldolase	TGGT1_236040	47	1	2

Protein phosphatase 2C domain-containing protein	TGGT1_237500	97	1	0
Cyclophilin precursor	TGGT1_205700	38	0	1
Rhoptry neck protein RON4	TGGT1_229010	107	1	0
CorA family Mg2+ transporter protein	TGGT1_235402	128	2	0
Actin depolymerizing factor ADF	TGGT1_220400	13	2	1
Putative eukaryotic initiation factor-4E	TGGT1_223410	26	2	2
Ribosomal protein RPL23A	TGGT1_238010	19	2	2
Alveolin domain containing intermediate filament IMC4	TGGT1_231630	50	3	0
RNA recognition motif-containing protein	TGGT1_305850	39	1	2
Hypothetical protein	TGGT1_240060	89	2	0
Ribosomal protein RPL30	TGGT1_232230	12	2	1

Heat shock protein	TGGT1_251780	78	1	2
Microtubule associated protein SPM1	TGGT1_263520	39	2	1
Ribosomal protein RPL10	TGGT1_288720	25	2	1
Heat shock protein	TGGT1_324600	20	0	2
FUSE-binding protein 2 / KH-type splicing regulatory protein	TGGT1_216670	100	2	1
GAP45 protein (GAP45)	TGGT1_223940	27	0	2
Hypothetical protein	TGGT1_262935	77	2	1
Hypothetical protein	TGGT1_215980	24	0	1
Asparaginyl-tRNA synthetase (NOB+tRNA synthase)	TGGT1_270510	75	0	1
Ribosomal protein RPL7	TGGT1_314810	30	1	0
Alveolin domain containing intermediate filament IMC1	TGGT1_231640	70	0	1

Hypothetical protein	TGGT1_212960B	43	2	1
Domain K- type RNA binding proteins family protein	TGGT1_235930	64	1	1
Rhoptry neck protein RON5	TGGT1_311470	187	1	1
Ribosomal protein RPS15	TGGT1_316110	74	2	1
Ribosomal protein RPL22	TGGT1_239760	15	1	0
Dynein, axonemal, heavy chain 2 family protein	TGGT1_235920	514	0	1
Hypothetical protein	TGGT1_301250	96	2	0
Redoxin domain-containing protein	TGGT1_286630	31	1	0
Peptidase M16, alpha subunit, putative	TGME49_202680	62	0	1
Hypothetical protein	TGGT1_306400	152	1	0
Enolase 2	TGGT1_268850	52	1	0

Hypothetical protein	TGGT1_264040	25	1	0
Ribosomal protein RPS3A	TGGT1_232710	29	1	1
Putative ubiquinol cytochrome c oxidoreductase	TGVEG_320220	55	1	1
Hypothetical protein	TGGT1_268835	76	0	1
Chain C, Porcine E-Trypsin	1EPT_C	10	1	1
Ribosomal protein RPS17	TGGT1_207840	15	1	1
SKIP/SNW domain-containing protein	TGGT1_233190	62	1	1
Heat shock protein HSP60	TGGT1_247550	61	1	1
Ribosomal protein RPL12	TGGT1_254440	18	1	1
Putative myosin heavy chain	TGGT1_258060	23	1	1
Profilin PRF	TGGT1_293690 (	18	1	1
Putative DnaJ family chaperone	TGGT1_311240	47	1	1

Plakophilin 1 isoform 1b [Homo sapiens]	NP_000290.2	83	1	0
Keratin 80 isoform b [Homo sapiens]	NP_001074961.1	47	1	0
Protein disulfide-isomerase domain-containing protein	TGGT1_238040A	126	1	0
Ribosomal protein RPL35A	TGGT1_249250	13	1	0
Casein alpha s1 [Bos taurus]	NP_851372.1	25	1	0
Ribosomal protein RPS18	TGGT1_225080	18	1	0
Ribosomal protein RPS24	TGGT1_215460	30	0	1
DEAD (Asp-Glu-Ala-Asp) box polypeptide 17	TGGT1_236650	60	1	0
Splicing factor, CC1 family protein	TGGT1_312530	69	0	1
Hypothetical protein	TGGT1_308870	75	1	0
Hypothetical protein	TGGT1_306650	31	0	1

3xFLAG-MCS-3xFLAG [Expression vector pQF]	AGU99855.1	8	0	1
Desmocollin 1 isoform Dsc1b preproprotein [Homo sapiens]	NP_004939.1	94	0	1
cAMP-dependent protein kinase	TGGT1_209985	30	0	1
Hypothetical protein	TGGT1_215430	28	0	1
Putative ATP synthase	TGGT1_226000	19	0	1
Nuclease and tudor domain-containing protein	TGGT1_238050	114	0	1
Ribosomal protein RPP1	TGGT1_260260	19	0	1
RNA recognition motif-containing protein	TGGT1_264610	45	0	1
Glyceraldehyde-3-phosphate dehydrogenase GAPDH2	TGGT1_269190	105	0	1
Hypothetical protein	TGGT1_282180	35	0	1
SAG-related sequence SRS20A	TGGT1_285870	35	0	1

SAG-related sequence SRS52A	TGGT1_315320	34	0	1
Splicing factor U2AF family SnRNP auxilary factor large subunit, RRM domain-containing protein	TGGT1_319850	52	0	1
Putative alternative splicing type 3	TGGT1_210980	65	1	0
Dihydrolipoyllysine-residue succinyltransferase component of oxoglutarate dehydrogenase	TGGT1_219550	50	1	0
Sarco/endoplasmic reticulum Ca2+-ATPase	TGGT1_230420	119	1	0
Hypothetical protein	TGGT1_237015	29	1	0
Putative ethylene inducible protein	TGGT1_237140	33	1	0
Hypothetical protein	TGGT1_246580	43	1	0
Hypothetical protein	TGGT1_247770	19	1	0
Dense granule protein GRA9	TGGT1_251540	35	1	0

Parasite porphobilinogen synthase PBGS	TGGT1_253900	71	1	0
Hypothetical protein	TGGT1_254570	224	1	0
Putative DnaJ protein	TGGT1_258390	45	1	0
Myb family DNA-binding domain-containing protein	TGGT1_275480	99	1	0
Emp24/gp25L/p24 family protein	TGGT1_310750	65	1	0
Hypothetical protein	TGGT1_229470	45	0	1
Hypothetical protein	TGGT1_229920	35	1	0
LSM domain-containing protein	TGGT1_300280	18	0	1
Hypothetical protein	TGME49_257430	239	1	0
Hypothetical protein	TGGT1_315570	9	1	0
Hypothetical protein	TGGT1_226380	43	1	0

Hypothetical protein	TGGT1_310790	25	0	1

Mass spectrometry data analysis: experiment 3. The asterisk sign * indicates that this sample was a non-specific elution.

Protein name	**Gene ID**	**Molecular Weight (kDa)**	**SEB-TY-FLAG**	***SEB-TY-FLAG**	**Wild Type**
Hypothetical protein	TGGT1_221870	144	85	40	0
Isoleucyl-tRNA synthetase family protein	TGGT1_207640	141	28	28	42
Hypothetical protein	TGGT1_233220	160	21	24	31
Rhoptry protein ROP5	TGGT1_308090	61	8	24	20
SAG-related sequence SRS29B	TGGT1_233460	35	8	23	24
Beta-tubulin	TGGT1_266960	50	15	13	23
Ribosomal protein RPS20	TGGT1_223050	26	0	15	17

DnaJ domain-containing protein	TGGT1_267430	49	7	10	13
Alpha tubulin TUBA1 (TUBA1)	TGME49_316400	50	9	14	15
ATP synthase beta subunit ATP-B	TGGT1_261950	60	6	12	14
Putative ATPase synthase subunit alpha	TGGT1_204400	62	6	13	10
Sjogren's syndrome/scleroderma autoantigen 1 (Autoantigen p27) protein	TGGT1_212260	38	5	11	13
Chaperonin protein BiP	TGGT1_311720	73	10	10	6
Elongation factor 1-alpha (EF-1-ALPHA), putative	TGME49_286420	49	5	15	11
Actin ACT1	TGGT1_209030	42	5	8	10
RNA recognition motif-containing protein	TGGT1_262620	32	10	7	7
Glyceraldehyde-3-phosphate dehydrogenase GAPDH1	TGGT1_289690	53	1	5	9
SAG-related sequence SRS34A	TGGT1_271050	19	6	8	8

Actin	TGGT1_411760	32	2	5	8
Putative vacuolar ATP synthase subunit b	TGGT1_219800	57	5	7	6
Dense granule protein GRA12	TGGT1_288650	48	2	7	6
Myosin A	TGGT1_235470	93	1	7	8
Putative heat shock protein 90	TGGT1_244560	98	4	5	7
Dense granule protein GRA7	TGGT1_203310	26	5	7	5
Heat shock protein HSP70	TGGT1_273760	72	5	4	2
Alveolin domain containing intermediate filament IMC4	TGGT1_231630	50	3	8	6
Histone H2Ba	TGGT1_305160	13	4	2	0
Ribosomal protein RPP0	TGGT1_218410	34	2	5	5
Putative transmembrane protein	TGGT1_410360	38	5	5	4

Alveolin domain containing intermediate filament IMC1	TGGT1_231640	70	1	6	3
Putative sortilin	TGGT1_290160	114	4	2	6
Dense granule protein GRA2	TGGT1_227620	20	0	4	1
Histone H4	TGGT1_239260	11	1	4	5
Ribosomal protein RPS18	TGGT1_225080	18	1	5	3
Ribosomal protein RPS14	TGGT1_263700	16	3	3	4
Ribosomal protein RPS13	TGGT1_270380	17	2	3	4
Microtubule associated protein SPM1	TGGT1_263520	39	1	4	7
Ribosomal protein RPS25	TGGT1_231140	19	3	2	4
Rhoptry protein ROP1	TGGT1_309590	50	2	6	5
Ribosomal protein RPS6	TGGT1_210690	29	2	3	2

Ribosomal protein RPS11	TGGT1_226970	19	1	4	2
Myosin light chain MLC1	TGGT1_257680	24	1	6	5
Ribosomal protein RPL4	TGGT1_309120	46	6	2	3
Heat shock protein	TGGT1_324600	20	1	4	4
Putative transmembrane protein	TGGT1_410370	48	0	4	1
Ribosomal protein RPL3	TGGT1_227360	44	2	3	2
Histone H3.3	TGGT1_218260	15	0	1	0
Hypothetical protein	TGGT1_215980	24	3	2	2
Putative polyadenylate binding protein	TGGT1_224850	83	1	2	4
Hypothetical protein	TGGT1_263320	42	1	3	2
Putative eukaryotic translation initiation factor 4A, isoform 3	TGGT1_256770	45	3	2	1

ATP synthase F1, delta subunit protein	TGGT1_284540	28	0	0	2
Sec23/Sec24 trunk domain-containing protein	TGGT1_291680	88	4	3	0
Putative vacuolar ATP synthase subunit A	TGGT1_256970	68	2	2	1
Ribosomal protein RPS4	TGGT1_207440	36	1	1	2
Ribosomal protein RPL10A	TGGT1_215470	25	1	2	0
RNA recognition motif-containing protein	TGGT1_270640	25	0	2	1
Ribosomal protein RPL9	TGGT1_284560	21	1	2	0
Histone H2Bv	TGGT1_209910	14	3	3	1
Histone H2AZ	TGGT1_300200	16	0	3	4
Protein disulfide isomerase	TGGT1_211680	53	0	4	1
Rhoptry protein ROP7	TGGT1_295110	63	1	3	3

Putative vacuolar atp synthase subunit e	TGGT1_305290	39	1	2	4
NAC domain-containing protein	TGME49_257090	39	0	2	4
Ribosomal protein RPS3A	TGGT1_232710	29	0	2	2
Ribosomal protein RPL23A	TGGT1_238010	19	2	1	1
PDI family protein	TGGT1_232410	25	2	4	2
CorA family Mg2+ transporter protein	TGGT1_235402	128	3	3	3
Ribosomal protein RPS17	TGGT1_207840	15	1	2	2
Acid phosphatase GAP50	TGGT1_219320	47	2	3	3
Ribosomal protein RPS23	TGGT1_229670	16	1	1	3
Hypothetical protein	TGGT1_230160	16	2	3	3
Dense granule protein GRA8	TGGT1_254720	29	0	2	3

Ribosomal protein RPL14	TGGT1_267060	18	1	4	1
Enolase 2	TGGT1_268850	52	1	3	4
Ribosomal protein RPS3	TGGT1_232300	29	2	3	3
Ribosomal protein RPL8	TGGT1_204020	28	1	2	2
Ribosomal protein RPS19	TGGT1_212290	35	2	1	2
Ribosomal protein RPL7	TGGT1_314810	30	2	1	0
Ribosomal protein RPL10	TGGT1_288720	25	3	2	1
Dense granule protein GRA3	TGGT1_227280	24	1	2	2
Ribosomal protein RPL13	TGGT1_263050	40	1	2	1
Ribosomal protein RPL18A	TGGT1_262670	21	2	0	0
Putative eukaryotic initiation factor-4E	TGGT1_223410	26	4	2	1

Leucyl aminopeptidase LAP	TGGT1_290670	83	1	3	2
Hypothetical protein	TGGT1_313350	47	1	2	3
Splicing factor SF2	TGGT1_319530	54	2	2	1
Ribosomal protein RPL6 (RPL6)	TGME49_313390	31	0	1	1
NAC domain-containing protein	TGGT1_205558	21	0	2	4
Putative translation elongation factor 2 family protein	TGGT1_205470	93	0	2	3
Hypothetical protein	TGGT1_231410	65	0	2	3
DEAD/DEAH box helicase domain-containing protein	TGME49_284050	282	4	1	1
GAP45 protein (GAP45)	TGGT1_223940	27	0	1	2
Ribosomal protein RPS24	TGGT1_215460	30	1	2	2
Hypothetical protein	TGGT1_269710	170	0	0	2

Ribosomal protein RPS7	TGGT1_239100	23	1	1	2
Ribosomal protein RPL17	TGGT1_299050	22	0	0	1
Ribosomal protein RPS16	TGGT1_263040	24	1	0	1
Ribosomal protein RPL27	TGGT1_262690	16	0	1	1
Putative phosphate carrier	TGGT1_278990	53	0	1	1
Domain K- type RNA binding proteins family protein	TGGT1_235930	64	4	1	0
Putative transport protein Sec24	TGGT1_277000	108	3	0	0
Ribosomal protein RPL13A	TGGT1_292130	33	3	0	0
Thioredoxin domain-containing protein	TGGT1_247350	34	0	3	0
RNA recognition motif-containing protein	TGGT1_209850	171	0	1	2
Eukaryotic porin protein	TGGT1_263300	31	0	2	1

Ribosomal protein RPS5	TGGT1_242330	22	0	0	1
Ribosomal protein RPL11	TGGT1_309820	20	1	2	2
Putative adenine nucleotide translocator	TGGT1_249900	35	0	1	0
Rhoptry protein ROP8	TGGT1_363030	64	0	1	1
Toxofilin	TGGT1_214080	27	0	2	0
14-3-3 protein	TGGT1_263090	37	0	3	0
Hypothetical protein	TGGT1_286580	107	0	3	1
SAG-related sequence SRS25	TGGT1_213280	21	0	0	1
Ribosomal protein RPL32	TGGT1_267400	16	0	3	1
WD domain, G-beta repeat domain containing protein	TGGT1_320210	56	2	0	1
Heat shock protein HSP90	TGGT1_288380	82	1	2	1

Putative DnaJ protein	TGGT1_258390	45	1	1	2
Putative protein disulfide isomerase-related protein (provisional)	TGGT1_249270	60	0	2	1
Putative small GTP binding protein rab1a	TGGT1_214770	23	0	2	2
Ribosomal protein RPSA	TGGT1_266060	32	0	3	1
Alba 2	TGGT1_218820	15	1	1	1
ENO1_YEAST Enolase 1 - Saccharomyces cerevisiae (Baker's yeast)	P00924.2	46	1	0	0
MAG1 protein (MAG1)	TGGT1_270240	49	1	1	0
Ribosomal protein RPL12	TGGT1_254440	18	1	1	1
RNA recognition motif-containing protein	TGGT1_305850	39	0	1	1
Glutaredoxin domain-containing protein	TGGT1_238070	26	0	1	0
Ribosomal protein RPS26	TGGT1_243570	13	0	1	1

Ribosomal protein RPL24 (RPL24)	TGME49_244320	33	0	1	1
Dense granule protein GRA5	TGGT1_286450	13	0	3	0
SAG-related sequence SRS57	TGGT1_308020	42	0	0	2
SAG-related sequence SRS51	TGGT1_308840	38	0	0	2
Fructose-bisphospatase II	TGGT1_247510	42	0	1	0
GTP-binding nuclear protein ran/tc4	TGGT1_248340	26	0	1	2
Ras-related protein Rab11	TGGT1_289680	25	0	2	1
Hypothetical protein	TGGT1_201800	29	0	0	2
Photosensitized INA-labeled protein PHIL1	TGGT1_258410	19	0	1	0
Rhoptry protein ROP18	TGGT1_205250	62	1	0	0
Putative polyubiquitin UbC	TGGT1_219820	34	1	0	1

Dense granule protein GRA6	TGGT1_275440	23	0	0	1
Rhoptry neck protein RON1	TGGT1_310010	128	0	0	1
Casein alpha-S2 [Bos taurus]	NP_776953.1	35	1	0	1
Rhoptry kinase family protein ROP39	TGGT1_262050	65	0	1	1
Hypothetical protein	TGGT1_312150	61	0	0	1
Ribosomal protein RPL19	TGGT1_289530	22	2	1	0
SAG-related sequence SRS52A	TGGT1_315320	34	0	0	2
Protein phosphatase 2C domain-containing protein	TGGT1_237500	97	0	2	0
Ribosomal protein RPP2	TGGT1_309810	12	0	1	0
Putative DnaJ family chaperone	TGGT1_311240	47	0	1	0
Heat shock protein	TGGT1_251780	78	1	0	0

cAMP-dependent protein kinase regulatory subunit	TGGT1_242070	43	0	1	1
Putative alternative splicing type 3 and	TGGT1_210980	65	0	1	1
Hypothetical protein	TGGT1_286600	43	0	0	1
Rhoptry neck protein RON8	TGGT1_306060	329	0	0	1
Hypothetical protein	TGGT1_231160	18	0	1	1
Hypothetical protein	TGGT1_240060	89	0	1	1
Cytochrome c1, heme protein	TGGT1_246540	46	0	0	1
Hypothetical protein	TGGT1_249780	36	0	1	1
RNA recognition motif-containing protein	TGGT1_217540	38	0	1	1
Phosphofructokinase PFKII	TGGT1_226960	131	0	1	0
Ribosomal protein RPL26	TGGT1_248390	16	0	1	1

Putative myosin heavy chain	TGGT1_258060	23	1	1	0
Hypothetical protein	TGGT1_297430	25	1	1	0
Ribosomal protein RPS2	TGGT1_305520	29	1	1	0
RNA recognition motif-containing protein	TGGT1_321500	51	0	1	0
Putative eukaryotic initiation factor-4A	TGGT1_250770	47	1	1	0
Putative DNA replication licensing factor	TGGT1_214970	117	1	0	0
Ribosomal protein RPL5	TGGT1_320050	35	1	0	0
Subtilisin SUB1	TGGT1_204050	85	0	0	1
Translation initiation factor 3 subunit	TGGT1_294670	32	0	1	1
RNA recognition motif-containing protein	TGGT1_306600	21	0	0	1
Hypothetical protein	TGGT1_315610	16	0	1	0

Ribosomal protein RPL21	TGGT1_245680	18	0	0	1
Rhoptry neck protein RON2	TGGT1_300100	166	0	1	1
Alveolin domain containing intermediate filament IMC10	TGGT1_230210	61	0	1	0
Fructose-1,6-bisphosphate aldolase	TGGT1_236040	47	0	2	0
Tryptophanyl-tRNA synthetase (TrpRS2)	TGGT1_288360	77	0	1	0
Ribosomal protein RPS15	TGGT1_316110	74	0	1	0
Putative ethylene inducible protein	TGGT1_237140	33	1	0	0
Putative citrate synthase	TGGT1_263130	69	0	0	1
Peroxiredoxin PRX3	TGGT1_230410	30	0	1	0
Hypothetical protein	TGGT1_221510	18	0	0	1
PDI family protein	TGGT1_225790	22	0	0	1

Putative ATP synthase	TGGT1_226000	19	0	0	1
DnaJ domain-containing protein	TGGT1_226068	50	0	0	1
Hypothetical protein	TGGT1_254570	224	0	0	1
Splicing factor, CC1 family protein	TGGT1_312530	69	0	0	1
Amylo-alpha-1,6-glucosidase	TGME49_226910	208	0	0	1
Hypothetical protein	TGGT1_214575	10	0	1	0
Lactate dehydrogenase LDH1	TGGT1_232350	36	0	1	0
Putative prohibitin	TGGT1_243950	30	0	1	0
Putative importin alpha	TGGT1_252290	59	0	1	0
Hypothetical protein	TGGT1_258870B	52	0	1	0
Hypothetical protein	TGGT1_267500	26	0	1	0

Hypothetical protein	TGGT1_313380	32	0	1	0
Chain C, Porcine E-Trypsin	1EPT_C	?	1	0	0
ATP synthase F1 gamma subunit	TGGT1_231910	35	1	0	0
RNA-binding protein 8A family protein	TGGT1_233230	18	1	0	0
Ribosomal protein RPL35A	TGGT1_249250	13	1	0	0
cAMP-dependent protein kinase	TGVEG_209985	44	1	0	0
Sec61beta family protein	TGGT1_211040	10	1	0	0
Dehydrogenase E1 component family protein	TGGT1_239490	64	1	0	0
Nuclease and tudor domain-containing protein	TGGT1_238050	114	1	0	0
Dihydropteroate synthase	TGGT1_259550	83	0	0	1

REFERENCE

1. Keller, A., et al., *Empirical statistical model to estimate the accuracy of peptide identifications made by MS/MS and database search.* Anal Chem, 2002. **74**(20): p. 5383-92.